



THESIS APPROVAL

GRADUATE SCHOOL, KASETSART UNIVERSITY

Master of Engineering (Materials Engineering)

DEGREE

Materials Engineering

FIELD

Materials Engineering

DEPARTMENT

TITLE: Development of Mica-Based Glass-Ceramics with Fluorapatite Variation for Restorative Dental Applications

NAME: Miss Kanungnuch Keawsupsak

THIS THESIS HAS BEEN ACCEPTED BY

THESIS ADVISOR

(Assistant Professor Duangrudee Chaysuwan, Ph.D.)

THESIS CO-ADVISOR

(Mrs. Tepiwan Jitwatcharakomol, Dr.Ing.)

THESIS CO-ADVISOR

(Mrs. Chutima Eamchotchawalit, Ph.D.)

DEPARTMENT HEAD

(Mr. Patiphan Juijerm, Dr.Ing.)

APPROVED BY THE GRADUATE SCHOOL ON _____

DEAN

(Associate Professor Gunjana Theeragool, D.Agr.)

THESIS

DEVELOPMENT OF MICA-BASED GLASS-CERAMICS WITH
FLUORAPATITE VARIATION FOR RESTORATIVE DENTAL
APPLICATIONS



KANUNGNUCH KEAWSUPSAK

A Thesis Submitted in Partial Fulfillment of
the Requirements for the Degree of
Master of Engineering (Materials Engineering)
Graduate School, Kasetsart University
2010

Kanungnuch Keawsupsak 2010: Development of Mica-Based Glass-Ceramics with Fluorapatite Variation for Restorative Dental Applications. Master of Engineering (Materials Engineering), Major Field: Materials Engineering, Department of Materials Engineering. Thesis Advisor: Assistant Professor Duangrudee Chaysuwan, Ph.D. 149 pages.

The purpose of this research was to study the effect of fluorapatite variation on thermal behaviors, crystalline phases, microstructures, mechanical properties, machinability and chemical solubility of the mica-based glass-ceramics. The glass-ceramics in the glass system of $\text{SiO}_2\text{-Al}_2\text{O}_3\text{-MgO-MgF}_2\text{-SrCO}_3\text{-CaCO}_3\text{-CaF}_2$ and P_2O_5 were produced by variation of fluorapatite content between 3.0-5.0 mol% and called GCF3.0-5.0, respectively.

The results were found that the higher the fluorapatite content, the lower the glass transition and peak crystallization temperatures. Furthermore, the increasing fluorapatite content influences to the crystalline structures of both calcium-mica and fluorapatite. All of the glass-ceramics revealed mainly plate-like calcium-mica and needle-like fluorapatite structures on surfaces whereas the plate-like structure was mainly shown in bulks. Mechanical properties such as biaxial flexural strength, Vickers hardness and fracture toughness in each of glass-ceramics heated at different temperatures were presented that almost all of heat-treated glass-ceramics of T_{p1} gave the values higher than those of T_{p2} . The biaxial flexural strength, fracture toughness and chemical solubility values of all glass-ceramics would be suitable as core ceramics for dental restorations according to International Standard ISO 6872:2008(E). In addition, the coefficient of thermal expansion of the glass-ceramics was found close to that of the restorative materials. In this research, the most suitable type of glass-ceramics as a dental restorative material was GCF3.5 heat-treated at T_{p1} . However, its appearance for more aesthetic is required.

Student's signature

Thesis Advisor's signature

ACKNOWLEDGEMENTS

This thesis will not successfully complete without my advisor, Assistant Professor Dr. Duangrudee Chaysuwan who always gives good recommendations, great inspirations and constant encouragements.

I am grateful for all helps of staff at Department of Materials Engineering, Faculty of Engineering, Kasetsart University in providing facilities for my thesis experiments.

The research was provided funding grants by Department of Science Service, Ministry of Science and Technology and Kasetsart University Research and Development Institute, Kasetsart University. Furthermore, it was supported by the research grant of The King Prajadhipok and Queen Rambhai Barni Memorial Foundation of years 2009 and The Graduate School Kasetsart University for publication on international journals.

Finally, my graduation will not be achieved without best wishes from my family to support for everything and always gives me greatest love, willpower and financial support until this study completion. Also, I would like to gratefully expression to my relations and my friends for their helps and encouragements.

Kanungnuch Keawsupsak

April 2010

TABLE OF CONTENTS

	Page
TABLE OF CONTENTS	i
LIST OF TABLES	ii
LIST OF FIGURES	v
LIST OF ABBREVIATIONS	xv
INTRODUCTION	1
OBJECTIVES	3
LITERATURE REVIEW	4
MATERIALS AND METHODS	26
Materials	26
Methods	28
RESULTS AND DISCUSSION	39
CONCLUSION AND RECOMMENDATION	65
Conclusion	65
Recommendation	65
LITERATURE CITED	66
APPENDICES	71
Appendix A Optimum nucleation temperature and time results	72
Appendix B Crystalline phase results	112
Appendix C Biaxial flexural strength, Vickers microhardness and fracture toughness results	117
Appendix D Coefficient of thermal expansion results	121
Appendix E Chemical solubility results	127
Appendix F Conferences	130
CIRRICULUM VITAE	149

LIST OF TABLES

Table	Page
1 Core materials for dental restorations	7
2 Classification of ceramics for dental restoration as ISO 6872:2008(E) with recommended mechanical and chemical properties	25
3 Varied fluorapatite composition of the glasses	28
4 Thermal behaviors of all the glasses	41
5 Optimum nucleation temperatures of all glass-ceramics	42
6 Optimum nucleation times of all glass-ceramics	42
7 Mechanical properties of all-ceramic for dental restoration	57
8 Coefficient of thermal expansion of restorative materials	61
 Appendix Table	
A1 Data of optimum nucleation temperature determination of heated GCF3.0 at T_{p1}	98
A2 Data of optimum nucleation temperature determination of heated GCF3.0 at T_{p2}	98
A3 Data of optimum nucleation temperature determination of heated GCF3.5 at T_{p1}	98
A4 Data of optimum nucleation temperature determination of heated GCF3.5 at T_{p2}	99
A5 Data of optimum nucleation temperature determination of heated GCF4.0 at T_{p1}	99
A6 Data of optimum nucleation temperature determination of heated GCF4.0 at T_{p2}	99
A7 Data of optimum nucleation temperature determination of heated GCF4.5 at T_{p1}	100

LIST OF TABLES (Continued)

Appendix Table	Page
A8 Data of optimum nucleation temperature determination of heated GCF4.5 at T_{p2}	100
A9 Data of optimum nucleation temperature determination of heated GCF5.0 at T_{p1}	100
A10 Data of optimum nucleation temperature determination of heated GCF5.0 at T_{p2}	101
A11 Data of optimum nucleation time determination of heated GCF3.0 at T_{p1}	101
A12 Data of optimum nucleation time determination of heated GCF3.0 at T_{p2}	101
A13 Data of optimum nucleation time determination of heated GCF3.5 at T_{p1}	102
A14 Data of optimum nucleation time determination of heated GCF3.5 at T_{p2}	102
A15 Data of optimum nucleation time determination of heated GCF4.0 at T_{p1}	102
A16 Data of optimum nucleation time determination of heated GCF4.0 at T_{p1}	103
A17 Data of optimum nucleation time determination of heated GCF4.5 at T_{p1}	103
A18 Data of optimum nucleation time determination of heated GCF4.5 at T_{p2}	103
A19 Data of optimum nucleation time determination of heated GCF5.0 at T_{p1}	104
A20 Data of optimum nucleation time determination of heated GCF5.0 at T_{p2}	104

LIST OF TABLES (Continued)

Appendix Table		Page
B1	ICDD Powder Diffraction file No.03-0559.	113
B2	ICDD Powder Diffraction file No.25-0155	113
B3	ICDD Powder Diffraction file No.46-0744	114
B4	ICDD Powder Diffraction file No.48-1477	114
B5	ICDD Powder Diffraction file No.71-1083	115
B6	ICDD Powder Diffraction file No. 80-0573	115
B7	ICDD Powder Diffraction file No. 82-1556	116
B8	ICDD Powder Diffraction file No. 82-1646	116
B9	ICDD Powder Diffraction file No. 83-0557	116
C1	The biaxial flexural strength of the glass-ceramics	118
C2	The Vickers microhardness of the glass-ceramics	119
C3	The fracture toughness of the glass-ceramics	120
E1	Chemical solubility of all glass-ceramics in 4% (v/v) acetic acid	128
E2	Chemical solubility of all glass-ceramics in distilled water	128
E3	Chemical solubility of all glass-ceramics in 0.1 M sodium hydroxide	129

LIST OF FIGURES

Figure		Page
1	Schematic of dental restoration: (a) inlay, (b) onlay, (c) crown, (d) bridge	4
2	Clinical application for inlay and onlay restorations with amalgam fillings	5
3	Representation of veneer restoration with porcelain	8
4	Crystal structure of fluorophlogopite ($K/NaMg_3AlSi_3O_{10}F_2$) mica	9
5	Clinical application for inlay and onlay restorations with IPS Empress fillings	10
6	Three-unit dental bridge consisting of a lithium disilicate framework (IPS Empress2) veneered with fluoroapatite containing glass-ceramic	11
7	Scheme representation of (a) restorative material design with Computer Aided Design (CAD) and (b) machining of a restorative material with Computer Aided Machine (CAM)	12
8	Schematic representation Ceramics blocks	13
9	Schematics of (a) random network glassy form and (b) ordered crystalline form	13
10	Schematic of the structure of a sodium silicate glass	14
11	Specific volume-temperature relationship of liquid, glass and crystal	15
12	Relationship between the nucleation rate and temperature of $Li_2O-2SiO_2$ glass	19
13	Crystallization peak of $Li_2O-2SiO_2$ glass detected by DTA	20
14	$T_p^* - T_p$ plotted as a function of temperature of heat treatment of $Li_2O-2SiO_2$ glass	22
15	$T_p^* - T_p$ plotted as a function of time of heat treatment of $Li_2O-2SiO_2$ glass	22
16	Schematic of heat-treated profile of glass-ceramic	23
17	Differential thermal analyzer	29

LIST OF FIGURES (Continued)

Figure		Page
18	Definition of the most frequently used conventional quantities for characterization of the glass transition	30
19	Determination of the optimum nucleation temperature of glass-ceramics	31
20	Determination of the optimum nucleation time of glass-ceramics	32
21	Universal testing machine	33
22	Vickers microhardness tester	34
23	Schematic indentation of Vickers hardness	35
24	Schematic representation of Vickers indent fracture system, showing characteristic c and a dimensions of crack	36
25	Scanning electron microscope	36
26	X-rays diffractometer	37
27	DTA curves of the glasses: (a) GCF3.0, (b) GCF3.5, (c) GCF4.0, (d) GCF4.5, (e) GCF5.0	40
28	Representatives of (a) a glass rod, (b) a glass-ceramic heat-treated at T_{p1} and (c) a glass-ceramic heat-treated at T_{p2} of GCF4.0	43
29	XRD patterns of heat-treated glass-ceramics at T_{p1} of GCF: (a) 3.0, (b) 3.5, (c) 4.0, (d) 4.5, (e) 5.0	45
30	XRD patterns of heat-treated glass-ceramics at T_{p2} of GCF: (a) 3.0, (b) 3.5, (c) 4.0, (d) 4.5, (e) 5.0	45
31	XRD patterns of GCF3.0: (a) as-received glass, (b) heat-treated glass-ceramic at T_{p1} , (c) heat-treated glass-ceramic at T_{p2}	46
32	XRD patterns of GCF3.5: (a) as-received glass, (b) heat-treated glass-ceramic at T_{p1} , (c) heat-treated glass-ceramic at T_{p2}	46
33	XRD patterns of GCF4.0: (a) as-received glass, (b) heat-treated glass-ceramic at T_{p1} , (c) heat-treated glass-ceramic at T_{p2}	47
34	XRD patterns of GCF4.5: (a) as-received glass, (b) heat-treated glass-ceramic at T_{p1} , (c) heat-treated glass-ceramic at T_{p2}	47

LIST OF FIGURES (Continued)

Figure		Page
35	XRD patterns of GCF5.0: (a) as-received glass, (b) heat-treated glass-ceramic at T_{p1} , (c) heat-treated glass-ceramic at T_{p2}	48
36	Bulk microstructures of GCF3.0 heat-treated at T_{p1} (a) no etching and (b) etching with HF, 5,000X	50
37	Bulk microstructures of GCF3.0 heat-treated at T_{p2} (a) no etching and (b) etching with HF, 5,000X	50
38	Bulk microstructures of GCF3.5 heat-treated at T_{p1} (a) no etching and (b) etching with HF, 5,000X	50
39	Bulk microstructures of GCF3.5 heat-treated at T_{p2} (a) no etching and (b) etching with HF, 5,000X	51
40	Bulk microstructures of GCF4.0 heat-treated at T_{p1} (a) no etching and (b) etching with HF, 5,000X	51
41	Bulk microstructures of GCF4.0 heat-treated at T_{p2} (a) no etching and (b) etching with HF, 5,000X	51
42	Bulk microstructures of GCF4.5 heat-treated at T_{p1} (a) no etching and (b) etching with HF, 5,000X	52
43	Bulk microstructures of GCF4.5 heat-treated at T_{p2} (a) no etching and (b) etching with HF, 5,000X	52
44	Bulk microstructures of GCF5.0 heat-treated at T_{p1} (a) no etching and (b) etching with HF, 5,000X	52
45	Bulk microstructures of GCF5.0 heat-treated at T_{p2} (a) no etching and (b) etching with HF, 5,000X	53
46	Surface microstructures of etched with HF GCF3.0 heat-treated at (a) T_{p1} and (b) T_{p2} , 20,000X	53
47	Surface microstructures of etched with HF GCF3.5 heat-treated at (a) T_{p1} and (b) T_{p2} , 20,000X	53
48	Surface microstructures of etched with HF GCF4.0 heat-treated at (a) T_{p1} and (b) T_{p2} , 20,000X	54

LIST OF FIGURES (Continued)

Figure		Page
49	Surface microstructures of etched with HF GCF4.5 heat-treated at (a) T_{p1} and (b) T_{p2} , 20,000X	54
50	Surface microstructures of etched with HF GCF5.0 heat-treated at (a) T_{p1} and (b) T_{p2} , 20,000X	54
51	Biaxial flexural strength of all glass-ceramics	56
52	Vickers hardness of all glass-ceramics	56
53	Fracture toughness of all glass-ceramics	57
54	Drilling test for the glass-ceramics after heat-treated at T_{p1} (on the above) and at T_{p2} (on the below): (a) and (f) GCF3.0, (b) and (g) GCF3.5, (c) and (h) GCF4.0, (d) and (i) GCF4.5, (e) and (j) GCF5.0	59
55	Coefficient of thermal expansion of all glass-ceramics	60
56	Chemical solubility of all glass-ceramics in 4% (V/V) acetic acid	62
57	Chemical solubility of all glass-ceramics in distilled water	62
58	Chemical solubility of all glass-ceramics in 0.1 M sodium hydroxide	63
59	Schematic of dental restorative material	64
Appendix Figure		
A1	Crystallized GCF3.0 hold on T_g-30 °C for 1.0 hour	73
A2	Crystallized GCF3.0 hold on T_g-15 °C for 1.0 hour	73
A3	Crystallized GCF3.0 hold on T_g °C for 1.0 hour	73
A4	Crystallized GCF3.0 hold on T_g+15 °C for 1.0 hour	74
A5	Crystallized GCF3.0 hold on T_g+30 °C for 1.0 hour	74
A6	Crystallized GCF3.0 hold at optimum nucleation temperature of T_{p1} for 0.5 hours	74
A7	Crystallized GCF3.0 hold at optimum nucleation temperature of T_{p1} for 1.0 hours	75

LIST OF FIGURES (Continued)

Appendix Figure	Page
A8 Crystallized GCF3.0 hold at optimum nucleation temperature of T_{p1} for 2.0 hours	75
A9 Crystallized GCF3.0 hold at optimum nucleation temperature of T_{p1} for 4.0 hours	75
A10 Crystallized GCF3.0 hold at optimum nucleation temperature of T_{p1} for 10.0 hours	76
A11 Crystallized GCF3.0 hold at optimum nucleation temperature of T_{p2} for 0.5 hours	76
A12 Crystallized GCF3.0 hold at optimum nucleation temperature of T_{p2} for 1.0 hours	76
A13 Crystallized GCF3.0 hold at optimum nucleation temperature of T_{p2} for 2.0 hours	77
A14 Crystallized GCF3.0 hold at optimum nucleation temperature of T_{p2} for 4.0 hours	77
A15 Crystallized GCF3.0 hold at optimum nucleation temperature of T_{p2} for 10.0 hours	77
A16 Crystallized GCF3.5 hold on T_g-30 °C for 1.0 hour	78
A17 Crystallized GCF3.5 hold on T_g-15 °C for 1.0 hour	78
A18 Crystallized GCF3.5 hold on T_g °C for 1.0 hour	78
A19 Crystallized GCF3.5 hold on T_g+15 °C for 1.0 hour	79
A20 Crystallized GCF3.5 hold on T_g-30 °C for 1.0 hour	79
A21 Crystallized GCF3.5 hold at optimum nucleation temperature of T_{p1} for 0.5 hours	79
A22 Crystallized GCF3.5 hold at optimum nucleation temperature of T_{p1} for 1.0 hours	80
A23 Crystallized GCF3.5 hold at optimum nucleation temperature of T_{p1} for 2.0 hours	80

LIST OF FIGURES (Continued)

Appendix Figure	Page
A24 Crystallized GCF3.5 hold at optimum nucleation temperature of T_{p1} for 4.0 hours	80
A25 Crystallized GCF3.5 hold at optimum nucleation temperature of T_{p1} for 10.0 hours	81
A26 Crystallized GCF3.5 hold at optimum nucleation temperature of T_{p2} for 0.5 hours	81
A27 Crystallized GCF3.5 hold at optimum nucleation temperature of T_{p2} for 1.0 hours	81
A28 Crystallized GCF3.5 hold at optimum nucleation temperature of T_{p2} for 2.0 hours	82
A29 Crystallized GCF3.5 hold at optimum nucleation temperature of T_{p2} for 4.0 hours	82
A30 Crystallized GCF3.5 hold at optimum nucleation temperature of T_{p2} for 10.0 hours	82
A31 Crystallized GCF4.0 hold on T_g-30 °C for 1.0 hour	83
A32 Crystallized GCF4.0 hold on T_g-15 °C for 1.0 hour	83
A33 Crystallized GCF4.0 hold on T_g °C for 1.0 hour	83
A34 Crystallized GCF4.0 hold on T_g+15 °C for 1.0 hour	84
A35 Crystallized GCF4.0 hold on T_g+30 °C for 1.0 hour	84
A36 Crystallized GCF4.0 hold at optimum nucleation temperature of T_{p1} for 0.5 hours	84
A37 Crystallized GCF4.0 hold at optimum nucleation temperature of T_{p1} for 1.0 hours	85
A38 Crystallized GCF4.0 hold at optimum nucleation temperature of T_{p1} for 2.0 hours	85
A39 Crystallized GCF4.0 hold at optimum nucleation temperature of T_{p1} for 4.0 hours	85

LIST OF FIGURES (Continued)

Appendix Figure	Page
A40 Crystallized GCF4.0 hold at optimum nucleation temperature of T_{p1} for 10.0 hours	86
A41 Crystallized GCF4.0 hold at optimum nucleation temperature of T_{p2} for 0.5 hours	86
A42 Crystallized GCF4.0 hold at optimum nucleation temperature of T_{p2} for 1.0 hours	86
A43 Crystallized GCF4.0 hold at optimum nucleation temperature of T_{p2} for 2.0 hours	87
A44 Crystallized GCF4.0 hold at optimum nucleation temperature of T_{p2} for 4.0 hours	87
A45 Crystallized GCF4.0 hold at optimum nucleation temperature of T_{p2} for 10.0 hours	87
A46 Crystallized GCF4.5 hold on T_g-30 °C for 1.0 hour	88
A47 Crystallized GCF4.5 hold on T_g-15 °C for 1.0 hour	88
A48 Crystallized GCF4.5 hold on T_g °C for 1.0 hour	88
A49 Crystallized GCF4.5 hold on T_g+15 °C for 1.0 hour	89
A50 Crystallized GCF4.5 hold on T_g+30 °C for 1.0 hour	89
A51 Crystallized GCF4.5 hold at optimum nucleation temperature of T_{p1} for 0.5 hours	89
A52 Crystallized GCF4.5 hold at optimum nucleation temperature of T_{p1} for 1.0 hours	90
A53 Crystallized GCF4.5 hold at optimum nucleation temperature of T_{p1} for 2.0 hours	90
A54 Crystallized GCF4.5 hold at optimum nucleation temperature of T_{p1} for 4.0 hours	90
A55 Crystallized GCF4.5 hold at optimum nucleation temperature of T_{p1} for 10.0 hours	91

LIST OF FIGURES (Continued)

Appendix Figure	Page
A56 Crystallized GCF4.5 hold at optimum nucleation temperature of T_{p2} for 0.5 hours	91
A57 Crystallized GCF4.5 hold at optimum nucleation temperature of T_{p2} for 1.0 hours	91
A58 Crystallized GCF4.5 hold at optimum nucleation temperature of T_{p2} for 2.0 hours	92
A59 Crystallized GCF4.5 hold at optimum nucleation temperature of T_{p2} for 4.0 hours	92
A60 Crystallized GCF4.5 hold at optimum nucleation temperature of T_{p2} for 10.0 hours	92
A61 Crystallized GCF5.0 hold on $T_g - 30$ °C for 1.0 hour	93
A62 Crystallized GCF5.0 hold on $T_g - 15$ °C for 1.0 hour	93
A63 Crystallized GCF5.0 hold on T_g °C for 1.0 hour	93
A64 Crystallized GCF5.0 hold on $T_g - 15$ °C for 1.0 hour	94
A65 Crystallized GCF5.0 hold on $T_g + 30$ °C for 1.0 hour	94
A66 Crystallized GCF5.0 hold at optimum nucleation temperature of T_{p1} for 0.5 hours	94
A67 Crystallized GCF5.0 hold at optimum nucleation temperature of T_{p1} for 1.0 hours	95
A68 Crystallized GCF5.0 hold at optimum nucleation temperature of T_{p1} for 2.0 hours	95
A69 Crystallized GCF5.0 hold at optimum nucleation temperature of T_{p1} for 4.0 hours	95
A70 Crystallized GCF5.0 hold at optimum nucleation temperature of T_{p1} for 10.0 hours	96
A71 Crystallized GCF5.0 hold at optimum nucleation temperature of T_{p2} for 0.5 hours	96

LIST OF FIGURES (Continued)

Appendix Figure	Page
A72 Crystallized GCF5.0 hold at optimum nucleation temperature of T_{p2} for 1.0 hours	96
A73 Crystallized GCF5.0 hold at optimum nucleation temperature of T_{p2} for 2.0 hours	97
A74 Crystallized GCF5.0 hold at optimum nucleation temperature of T_{p2} for 4.0 hours	97
A75 Crystallized GCF5.0 hold at optimum nucleation temperature of T_{p2} for 10.0 hours	97
A76 Analysis optimum nucleation temperature heated GCF3.0 of T_{p1}	98
A77 Analysis optimum nucleation temperature heated GCF3.0 of T_{p2}	98
A78 Analysis optimum nucleation temperature heated GCF3.5 of T_{p1}	98
A79 Analysis optimum nucleation temperature heated GCF3.5 of T_{p2}	99
A80 Analysis optimum nucleation temperature heated GCF4.0 of T_{p1}	99
A81 Analysis optimum nucleation temperature heated GCF4.0 of T_{p2}	99
A82 Analysis optimum nucleation temperature heated GCF4.5 of T_{p1}	100
A83 Analysis optimum nucleation temperature heated GCF4.5 of T_{p2}	100
A84 Analysis optimum nucleation temperature heated GCF5.0 of T_{p1}	100
A85 Analysis optimum nucleation temperature heated GCF5.0 of T_{p2}	101
A86 Analysis optimum nucleation time heated GCF3.0 of T_{p1}	101
A87 Analysis optimum nucleation time heated GCF3.0 of T_{p2}	101
A88 Analysis optimum nucleation time heated GCF3.5 of T_{p1}	102
A89 Analysis optimum nucleation time heated GCF3.5 of T_{p2}	102
A90 Analysis optimum nucleation time heated GCF4.0 of T_{p1}	102
A91 Analysis optimum nucleation time heated GCF4.0 of T_{p2}	103
A92 Analysis optimum nucleation time heated GCF4.5 of T_{p1}	103
A93 Analysis optimum nucleation time heated GCF4.5 of T_{p2}	103
A94 Analysis optimum nucleation time heated GCF5.0 of T_{p1}	104
A95 Analysis optimum nucleation time heated GCF5.0 of T_{p2}	104

LIST OF FIGURES (Continued)

Appendix Figure		Page
D1	Coefficient of thermal expansion of heat-treated GCF3.0 at T_{p1} by dilatometer	122
D2	Coefficient of thermal expansion of heat-treated GCF3.0 at T_{p2} by dilatometer	122
D3	Coefficient of thermal expansion of heat-treated GCF3.5 at T_{p1} by dilatometer	123
D4	Coefficient of thermal expansion of heat-treated GCF3.5 at T_{p2} by dilatometer	123
D5	Coefficient of thermal expansion of heat-treated GCF4.0 at T_{p1} by dilatometer	124
D6	Coefficient of thermal expansion of heat-treated GCF4.0 at T_{p2} by dilatometer	124
D7	Coefficient of thermal expansion of heat-treated GCF4.5 at T_{p1} by dilatometer	125
D8	Coefficient of thermal expansion of heat-treated GCF4.5 at T_{p2} by dilatometer	125
D9	Coefficient of thermal expansion of heat-treated GCF5.0 at T_{p1} by dilatometer	126
D10	Coefficient of thermal expansion of heat-treated GCF5.0 at T_{p2} by dilatometer	126

LIST OF ABBREVIATIONS

a	=	the half diagonal of the indentation
Å	=	Angstrom
Al ₂ O ₃	=	aluminium oxide or alimina
As ₂ O ₅	=	Arsenic oxide
b	=	a constant related to the nucleation mechanism
β	=	the heating rate
BaO	=	barium oxide
BeO	=	bellilium oxide
B ₂ O ₃	=	boron oxide
BOs	=	bridging oxygens
B.S.	=	Biaxial Flexural Strength
c	=	the half distance between the opposite crack tips
C	=	degree Celsius
CaCO ₃	=	calcium carbonate
CAD	=	computer aided design
CaF ₂	=	calcium fluoride
CAM	=	computer aided machining
CaO	=	calcium oxide
CdO	=	cadmium oxide
CeO ₂	=	cerium oxide
CH ₃ COOH	=	acetic acid
cm ²	=	square centimeter
CNC	=	computerized numerical controller
Cu	=	copper
CTE	=	coefficient of thermal expansion
d	=	the mean length of diagonals of the indentation
	=	the specimen thickness at fracture origin
DTA	=	differential thermal analyzer
E _n	=	kinetic barriers to nucleation
F.T.	=	fracture toughness

LIST OF ABBREVIATIONS (Continued)

k	=	rate constant
K	=	degree of Kelvin
KAlSi_2O_6	=	leucite
kg	=	kilogram
K_{IC}	=	fracture toughness
K_2O	=	potassium oxide
$\text{K/NaMg}_3\text{AlSi}_3\text{O}_{10}\text{F}_2$	=	fluorophlogopite
Ga_2O_3	=	gallium oxide
GeO_2	=	germanium oxide
GICs	=	glass ionomers
GPa	=	giga Pascal
HF	=	hydrofluoric acid
H_v	=	Vickers hardness
I	=	rate constant for nucleation in a super-cooled liquid
ICDD	=	International Centre of Diffraction Data
In_2O_3	=	indium oxide
KAlSi_3O_8	=	sanidine
kg	=	kilogram
$\text{KMg}_{2.5}\text{Si}_4\text{O}_{10}\text{F}_2$	=	tetrasilicic fluoromica
α	=	the degree of crystallization
	=	linear coefficient of thermal expansion
La_2O_3	=	lanthanum oxide
LiO_2	=	lithium oxide
Li_3PO_4	=	lithium phosphate
$\text{Li}_2\text{Si}_2\text{O}_5$	=	lithium disilicate
L_0	=	the overall length of material in the direction being measure
ΔL	=	the change in length of material in the direction being measure
m	=	meter
MgF_2	=	magnesium fluoride
min	=	minute

LIST OF ABBREVIATIONS (Continued)

mm	=	millimeter
mg	=	milligram
MgO	=	magnesium oxide
μm	=	micrometer
n	=	parameter correspond to crystallization mechanism and crystal shape
N	=	Newton
	=	the total number of nuclei per unit volume
N_B	=	the bulk nuclei formed during the DTA run
NBOs	=	nonbridging oxygens
NaCaPO_4	=	sodium calcium phosphate
N_H	=	the bulk nuclei formed during the previous heat treatment of nucleation
Na_2O	=	sodium oxide
NaOH	=	sodium hydroxide
N_S	=	the sum of the surface nuclei
P	=	the total load causing fracture
PbO_2	=	lead oxide
P_2O_5	=	phosphorus pentoxide
PMMA	=	polymethylmethacrylate
rpm	=	round per minute
r_1	=	the radius of support circle
r_2	=	the radius of loaded area
r_3	=	the radius of specimen
s	=	second
σ	=	the maximum center tensile stress
SEM	=	scanning electron microscope
SiF_4	=	silicon tetrafluoride
SiO_2	=	silicon oxide
SrCO_3	=	strontium carbonate

LIST OF ABBREVIATIONS (Continued)

t	=	time
T	=	temperature
T_g	=	glass transition temperature
T_m	=	melting temperature
t_n	=	time of the nucleation heat treatment
T_p	=	peak crystallization temperature
T_p^*	=	the peak crystallization temperature of the sample
ThO_2	=	thorium oxide
TiO_2	=	titanium oxide
ΔT	=	the change in temperature over which ΔL is measured
UTM	=	universal testing machine
ν	=	Poisson's ratio
V_2O_5	=	vanadium oxide
w	=	the thermodynamic to nucleation
XRD	=	x-ray diffractometer
Yb_2O_3	=	ytterbium oxide
ZnO	=	zinc oxide
ZrO_2	=	zirconium oxide

DEVELOPMENT OF MICA-BASED GLASS-CERAMICS WITH FLUORAPATITE VARIATION FOR RESTORATIVE DENTAL APPLICATIONS

INTRODUCTION

Biomaterials have been very important for a medication because they have been used for replacement of tissues or organs in the human body. Metals, polymers, ceramics and composites are produced as biomaterials that each material has difference of properties (Hench and Wilson, 1993). Therefore, selection of biomaterials being suitable with applications is necessary.

In dentistry, teeth are an important part for coarse digestion because they play the role in tearing, scraping, and chewing food. In addition, they allow for clear pronunciation. Thus, teeth loss leads to less efficiency of digestive system, low self-esteem and personality (Pinasco *et al.*, 2007). Restorative dental materials were extensively studied in recently to carry out new materials that have suitability on dental applications such as in-lays, on-lays, veneers and crowns. Materials like metals, amalgam alloys, cements, glass ionomers, ceramics and resin composites have been used for dental restorations (Powers and Sakaguchi, 2006). However, glass-ceramics, one type of ceramics, are significant adequate materials for these applications because of their mechanical properties for example high strength and wear resistance. Furthermore, they are biocompatibility with the oral environment, aesthetic near to natural human teeth and appreciated fabrication techniques (Höland and Beall, 2006). According to these advantages, they are developed for marketing such as Ceravital[®] KGS, Cerabone[®] A-W and Bioverit[®] (Liu *et al.*, 2008).

One of the most popular glass-ceramics for dental applications is mica-based glass-ceramics. Mica structure is plate-like structure affecting on excellent machinability which are tailored to be patient of demand and high fracture toughness. Although their advantages are great, they are unfortunately low mechanical properties (Habelitz *et al.*, 1997). Thus, the production of mica-based glass-ceramics for dentistry needs to improve their mechanical properties.

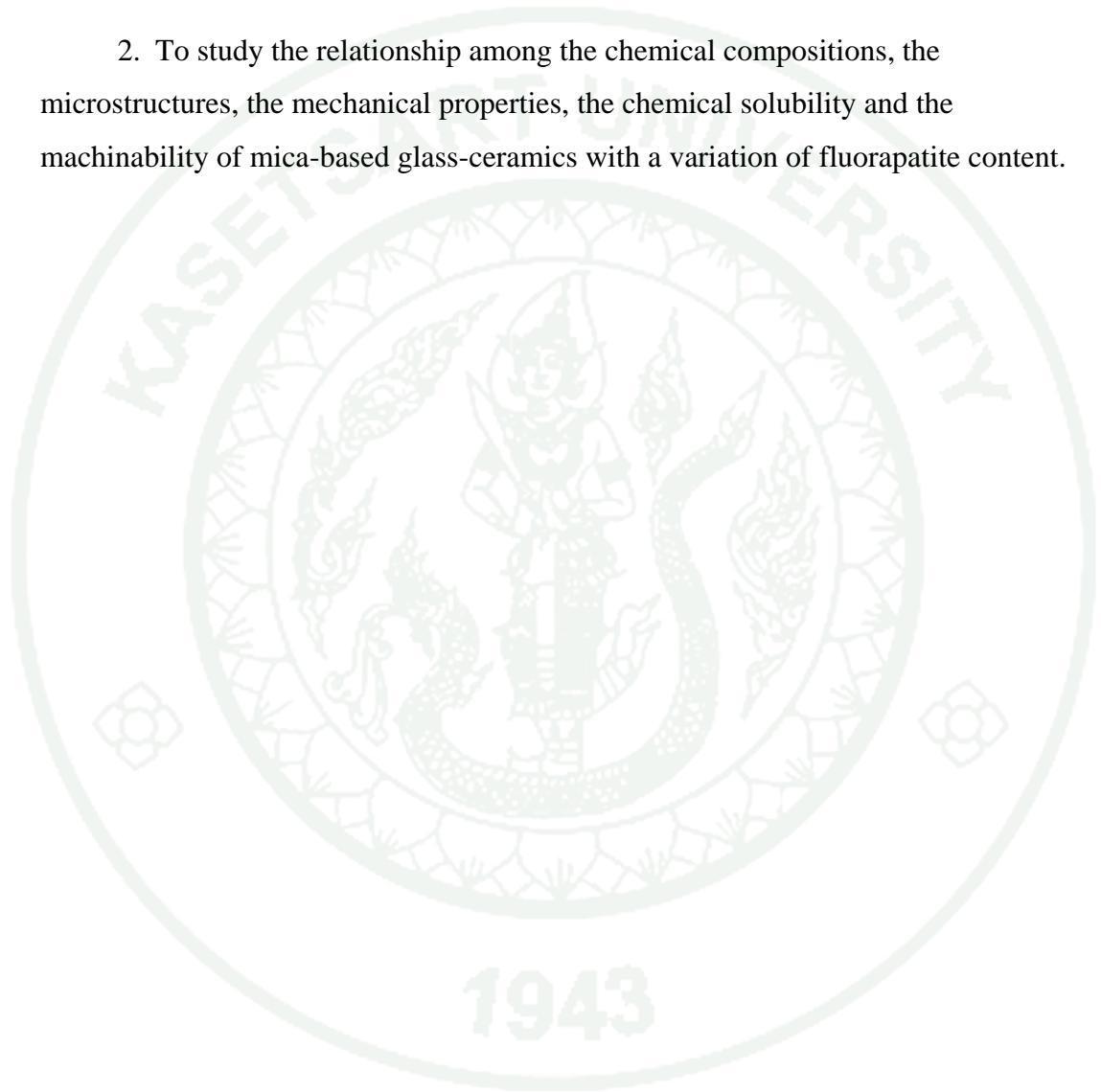
In previous works, fluorapatite crystals always exhibited a particle-like morphology while it was needle-like in human bones and teeth (Liu *et al.*, 2007). Höland described the mechanism for the nucleation and crystallization of needle-like fluorapatite in leucite glass-ceramics that the nucleation of apatite was initiated by a heterogeneous reaction of NaCaPO_4 and an interface reaction of glass droplet-glass matrix and the mechanism of crystal growth of needle-like fluorapatite was diffusion controlled (Höland *et al.*, 1999). The higher amount of needle-like fluorapatite crystals to the glass-ceramics affected to increase mechanical properties owing to their structure like fibres (Xiang *et al.*, 2007). In addition, these crystals are one of compositions of teeth which possessing a good biocompatibility with body (Barth *et al.*, 2007) and a good bioactivity in vivo (Feng *et al.* and Bogdanov *et al.*, 2008). Therefore, it was believed that mica based glass-ceramics were able to be improved by addition of needle-like fluorapatite. The aim of this study is to investigate the effect of fluorapatite on microstructure, mechanical properties, thermal properties, chemical solubility and machinability of mica-based glass-ceramics to develop the glass-ceramics for restorative dental applications.

The results of the research which are the development of the restorative dental material would be contributed to the knowledges and experiences on glasses and glass-ceramics as well as a reduction of imported dental materials from abroad.

1943

OBJECTIVES

1. To develop the mica-based glass-ceramics with variation of fluorapatite contents for restorative dental applications.
2. To study the relationship among the chemical compositions, the microstructures, the mechanical properties, the chemical solubility and the machinability of mica-based glass-ceramics with a variation of fluorapatite content.



LITERATURE REVIEW

1. Restorative dental materials

The dentistry treatment which is allowing biomaterials to replace and reconstruct teeth so that they maintain the original shapes and functions is called a dental restoration (Höland *et al.*, 2006). There are two categories of dental restorations: direct and indirect restorations. For direct restorations or plastic material restorations, they are placed into a prepared oral cavity, gets hard directly and adaptation in the patient's mouth that are consisted of dental amalgam or filling, glass ionomers and resin ionomers or white fillings. On the other hand, indirect restorations which include inlays, onlays, crowns, bridges and veneers are the technique of fabricating the material restoration outside the mouth and then the material is inserted into well prepared cavity in the mouth. However, the indirect restoration consumes more time and more expense than the direct restoration does since the former consists of a more complex layer (Pinasco *et al.*, 2007).

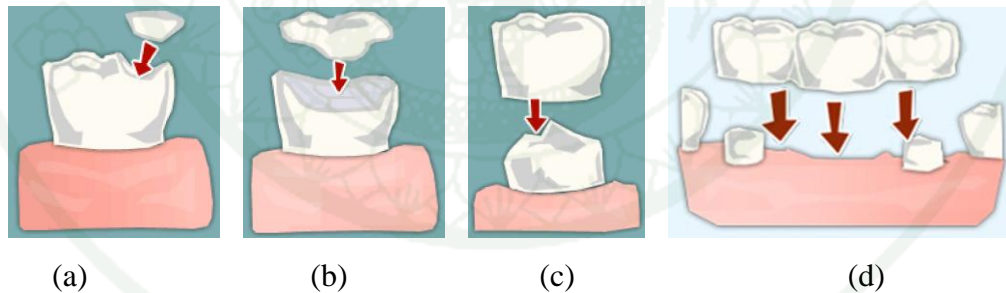


Figure 1 Schematic of dental restoration: (a) inlay, (b) onlay, (c) crown, (d) bridge.

Source: Anonymous (2000)

1.1 Metals and amalgam alloys

Metals are used for restorations because of the ease to polish and to clean for low bacterial plaque, high resistance to brittle fracture and high impact strength.

Most applications of metals can be used as in the dental posterior and roots due to esthetics reasons. The interesting metals of restoration are gold and amalgam which is a complex material of silver (Ag), tin (Sn), copper (Cu), palladium (Pd) and mercury (Hg) for filling. Even though gold possesses high corrosion resistance, it is complexity of preparation, long time consuming and very expensive.



Figure 2 Clinical application for inlay and onlay restorations with amalgam fillings.

Source: Höland *et al.* (2006)

In terms of filling with amalgam, consisting of silver, tin and mercury, it is popular because of high stresses and corrosion, rapid preparation and low cost. Although mercury is one of the components of amalgam, it does not harm the patient, the dentist and the environment. From its advantages mentioned in above, this material has still been used for dental restorations (Powers and Sakaguchi, 2006).

1.2 Composite resins

For soft materials, polymer selected to be used for dental restorative applications is polymethylmethacrylate (PMMA) which is a result from polymerized methylmethacrylate monomers. Owing to shrinkage during the polymerization, it causes gaps between a filling and a tooth. Hence food and bacteria can insert into the gap which cause the decay of teeth. Furthermore, a coefficient of thermal expansion of PMMA is higher than that of dentine ten times. When a patient takes hot and cold food or drink, the filled polymer which contacts the different temperatures will expand more than tooth does. These incidents lead to leakages of interface area

between an enamel and the filling. Because polymers possess low compressive and tensile strengths and poor wear resistance; hence its application for dental restoration is not so interesting (Pinasco *et al.*, 2007).

Subsequently, new materials called composite resins or polymer-ceramics composites were developed by replacement of dimethacrylate monomers. These new materials present low shrinkage, rapid hardening, and high strength but their thermal expansion is much more than that of teeth. Ceramic constituents used in this kind of material are inert such as SiO_2 and Al_2O_3 in order to improve strength and wear resistance as well as to reduce the shrinkage (Whitters *et al.*, 1999). These particles cannot bond to the polymer. Therefore, silane bonding agent is used as a coupling agent to promote bonding between polymer and ceramic particles. Even if degree of shrinkage reduces, it is still limited in clinical dentistry (Pinasco *et al.*, 2007).

1.3 Glass ionomers

Glass ionomers (GICs) or glass-polyalkanoate cements result from the reaction between a glass and an aqueous polyacid such as polyacrylic acid and copolymer of acrylic and maleic acid. The properties of GICs are adhesion, fluoride release, good biocompatibility, sensitivity to moisture and brittleness. In order to improve the compressive and tensile strength, they are added tartaric acid. For restorations, they are applied for a hard tissue repair rather than the dentistry on account of biocompatibility and strength.

The improvement of properties of GICs is practiced by adding metals such as silver-tin alloy or stainless steel to absorb mechanical stress and reduce brittleness. These materials are called cermets or metal-reinforced cements. However, they shrink during the polymerization.

1.4 Ceramics

Materials for all-ceramic restorations use a wide variety of crystalline phases as reinforcing agents. They can be classified according to the processing techniques and the major crystalline phases. Several processing techniques are available for fabricating all-ceramic restorations such as sintering, heat-pressing, slip-casting and machining.

Table 1 Core materials for dental restorations.

Brand name	Main compositions	Processing
IPS Empress	Leucite	Pressing
IPS Empress CAD	Leucite	CAD/CAM
IPS Empress2	Lithiumdisilicate	Pressing
IPS e. max Press	Lithiumdisilicate	Pressing
IPS e. max CAD	Lithiumdisilicate	CAD/CAM
IPS e. max Ceram	Fluorapatite	Sintering
IPS d.SIGN	Leucite and fluorapatite	Sintering
Dicor	Mica	Casting
Dicor MGC	Mica	CAD/CAM

Source: Ban (2008); Höland *et al.* (2006)

1.4.1 Sintered all-ceramic materials

The aluminous core ceramic is a typical example of strengthening by dispersion of a crystalline phase in glassy matrix because alumina has a high modulus of elasticity (350 GPa) and high fracture toughness (3.5 to 4 MPa·m^{0.5}). The core containing alumina is fired on a platinum foil and veneered with matched thermal expansion porcelain. These porcelains have flexural strength of approximately 139 MPa and shear strength of 145 MPa.



Figure 3 Representative of veneer restoration with porcelain.

Source: Höland and Beall (2002)

Porcelain crowns were developed in the early 1900s. They, containing of feldspathic or aluminous, are superior esthetics, resistance to abrasion and excellent shade stability. However, they are limited because of their difficulty of polishing the surface after an occlusal adjustment and resulted in wear of opposing teeth. Furthermore, their thermal expansions are not matching with alloying frameworks which led to failures and fractures during cooling. This problem is solved by addition of high expansion leucite into feldspar glass called a feldspathic porcelain. Feldspathic porcelain consisting of leucite as a reinforcing phase is available for the sintering fabrication. The added leucite leads to increasing of flexural strength and compressive strength of the feldspathic porcelain (Powers and Sakaguchi, 2006).

Glass-ceramics are obtained from a wide variety of compositions, performing a wide range of mechanical and optical properties which depend on the nature of the crystalline phases nucleating and growing within the glass. The major crystalline phases of glass-ceramics interesting of dental restoration are mica, hydroxyapatite, fluorapatite and lithia. Dicor is a mica-based machinable glass-ceramic. The machinability of this glass-ceramic is the presence of a tetrasilicic fluoromica ($\text{KMg}_{2.5}\text{Si}_4\text{O}_{10}\text{F}_2$) as the main phase. In the glass-ceramic, arrangement of the mica crystals is interlocking microstructure effecting on fracture resistance of glass-ceramics and their random orientation makes fracture propagation equally difficult in all directions.

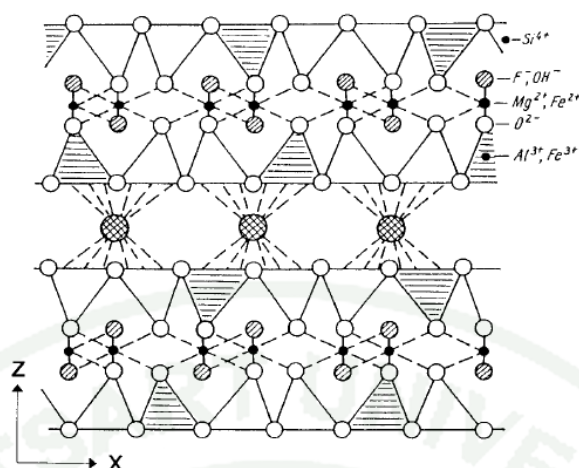


Figure 4 Crystal structure of fluorophlogopite ($\text{K/NaMg}_3\text{AlSi}_3\text{O}_{10}\text{F}_2$) mica.

Source: Habelitz *et al.* (1997)

Hydroxyapatite or fluorapatite phases occurring in glass-ceramics are interesting for dental restorations. Fluorapatite, as a thermally more stable phase in comparison to hydroxyapatite, offers increased possibilities in preparing the glass-ceramics by the convenient melting and crystallization processes. Moreover, fluorapatite is also composition of bones and teeth especially dental enamel (Mojumdar *et al.*, 2004). Höland (Höland *et al.*, 1999) studied the mechanisms of nucleation and controlled crystallization of fluorapatite in glass-ceramics of the SiO_2 - Al_2O_3 - K_2O - CaO - P_2O_5 system. The two mechanisms were important for formation of needle-like fluorapatite in a fluoroapatite-leucite glass-ceramic. The first mechanism was the nucleation by a heterogeneous reaction of primary crystals of NaCaPO_4 and an interface reaction of glass droplet-glass matrix and the second was the crystal growth which was a controlled diffusion process of needle-like apatite. Seiichi (Seiichi *et al.*, 2001) discussed the crystallization process of fluorapatite and calcium-mica glass-ceramics, in which the mica crystals formed interlocking microstructure and fine apatite were dispersed on the surface of the mica crystals. Furthermore, the fluorapatite content influenced on bioactivity in mica-based glass-ceramics (Xiang *et al.*, 2007).

1.4.2 Heat-pressed all-ceramic materials

Heat pressing is also called high temperature injection molding. The technique is an application of external pressure to sinter and shape ceramic at high temperature. Thus, this processing helps avoiding large pores and promoting a good dispersion of crystalline phases within the glassy matrix. However, the main disadvantages are the high cost of the equipment and low strength compared with other all-ceramic processes (Powers and Sakaguchi, 2006).

It was the seventh Mc Lean and O' Brain developed glass-ceramic base on leucite (KAlSi_2O_6 or $\text{K}_2\text{O} \cdot \text{Al}_2\text{O}_3 \cdot 4\text{SiO}_2$) by using this technique which were suitable for single unit restoration such as inlay, onlay and veneering of metal frameworks. IPS Empress is commercial name of this type glass-ceramic being translucency, high strength approximate 150-180 MPa, fracture toughness (K_{IC}) about $1.3 \text{ MPam}^{1/2}$, chemical durability and aesthetic (Conrad *et al.*, 2007). Ceramics are heated between 1150° and 1180°C as well as pressed under 0.3 to 0.4 MPa into a refractory mold made by the lost wax technique in automatic press furnace (Powers and Sakaguchi, 2006).



Figure 5 Clinical application for inlay and onlay restorations with IPS Empress fillings.

Source: Höland *et al.* (2006)

In order to enable glass-ceramics which in fabrication of dental bridges especially three-unit bridges, the strength and toughness of these materials have to be increased. Lithium disilicate ($\text{Li}_2\text{Si}_2\text{O}_5$) glass-ceramics are suitable for the

restorative dental applications presented in IPS Empress2. However, this type of glass-ceramic is not suitable for machining technique including CAD/CAM methods because of both high brittleness and content of crystals which greater than 60 vol% (Höland *et al.*, 2008). A ceramic material that can be heat-pressed on a zirconia endodontic post contains lithium phosphate (Li_3PO_4) as a main crystalline phase. The outstanding property of this glass-ceramic is a good esthetic.



Figure 6 Three-unit dental bridge consisting of a lithium disilicate framework (IPS Empress2) veneered with fluoroapatite containing glass-ceramic.

Source: Höland *et al.* (2006)

1.4.3 Slip-cast all-ceramic materials

Slip casting is a fabrication technique by the condensation of an aqueous slip on a refractory die. The porosity of the refractory die absorbs water from the slip by capillary action after that it is fired at high temperature.

An alumina-based slip is applied into a gypsum refractory die, fired at 1100°C for 4 hours so that the alumina duplicates the die shape and infiltrated during a second firing at 1150°C for 4 hours. The example of the alumina-based ceramic is In-Ceram being slip-cast aluminous porcelain. The flexural strength of the alumina-based material is about 450 MPa. This technique is adequate for dentistry due to the presence of densely packed alumina particles and the lack of porosity (Denry, 1996).

1.4.4 Machinable all-ceramic materials

Machinable ceramics can be milled to form restorations using CAD/CAM (computer aided design/computer aided machining) technology. After the tooth is prepared, it is scanned to computer. The restoration is designed with the aid of computer and then is machined from ceramic blocks by a computer as a milling machine controller. For the whole process of milling, it takes only a few minutes. One of advantages of this technology is for dentists and patients. Although the CAD/CAM system is convenient, it is very expensive and poor marginal accuracy, with gap values of 100 to 150 μm . However, using resin cements to bond with restorations may compensate for poor marginal fit (Powers and Sakaguchi, 2006).

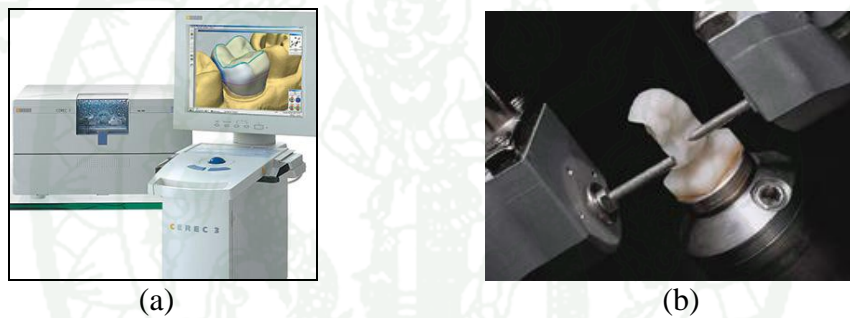


Figure 7 Scheme representation of (a) restorative material design with Computer Aided Design (CAD) and (b) machining of a restorative material with Computer Aid Machine (CAM).

Source: Smyth (2007)

Recently, software of the CAD/CAM known as the Cerec system used with several materials is IPS Empress Pro CAD, Vita Mark II and Dicor MGC. IPS Empress Pro CAD contains the same major crystalline phases as IPS Empress. Vita mark II possesses the sanidine (KAlSi_3O_8) phase as a major crystalline phase within a glassy matrix. The presence of sanidine explains the lack of translucency of this material. Dicor MGC is a machinable glass-ceramic similar to Dicor presenting mica crystals as the main crystalline phase (Denry, 1996).



Figure 8 Representation of ceramics blocks.

Source: Anonymous (2008)

2. Glass

A glass is an anisotropic material made from the melt of inorganic materials at high temperature. When the compositions are melted and cooled, a glass possesses a rigid condition without crystal because its construction is a random network (Happer, 2001) as shown in Figure 9(a). The atomic arrangements in the glass are similar to those in solid except that there is no long-range order.

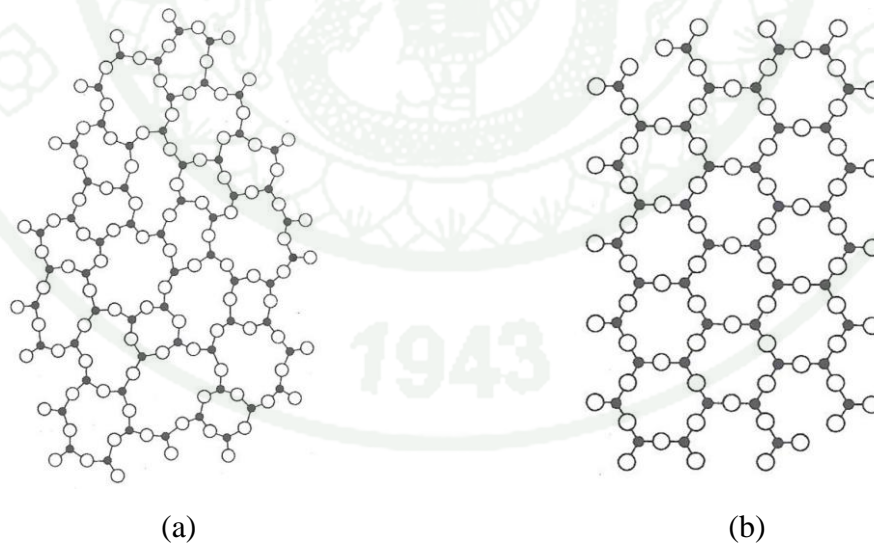


Figure 9 Schematics of (a) random network glassy form and (b) ordered crystalline form.

Source: Kingery *et al.* (1991)

2.1 Oxide form

Criteria for the formation of oxide glasses were developed by W. H. Zacharisen in 1932 who suggested four rules for the formation of an oxide to form a glass as following:-

1. Each oxygen ion is linked to not more than two cations.
2. Cations bonded to four oxygen ions.
3. Oxygen polyhedral share corners, and not edges or faces.
4. At least three corners of each polyhedron are shared.

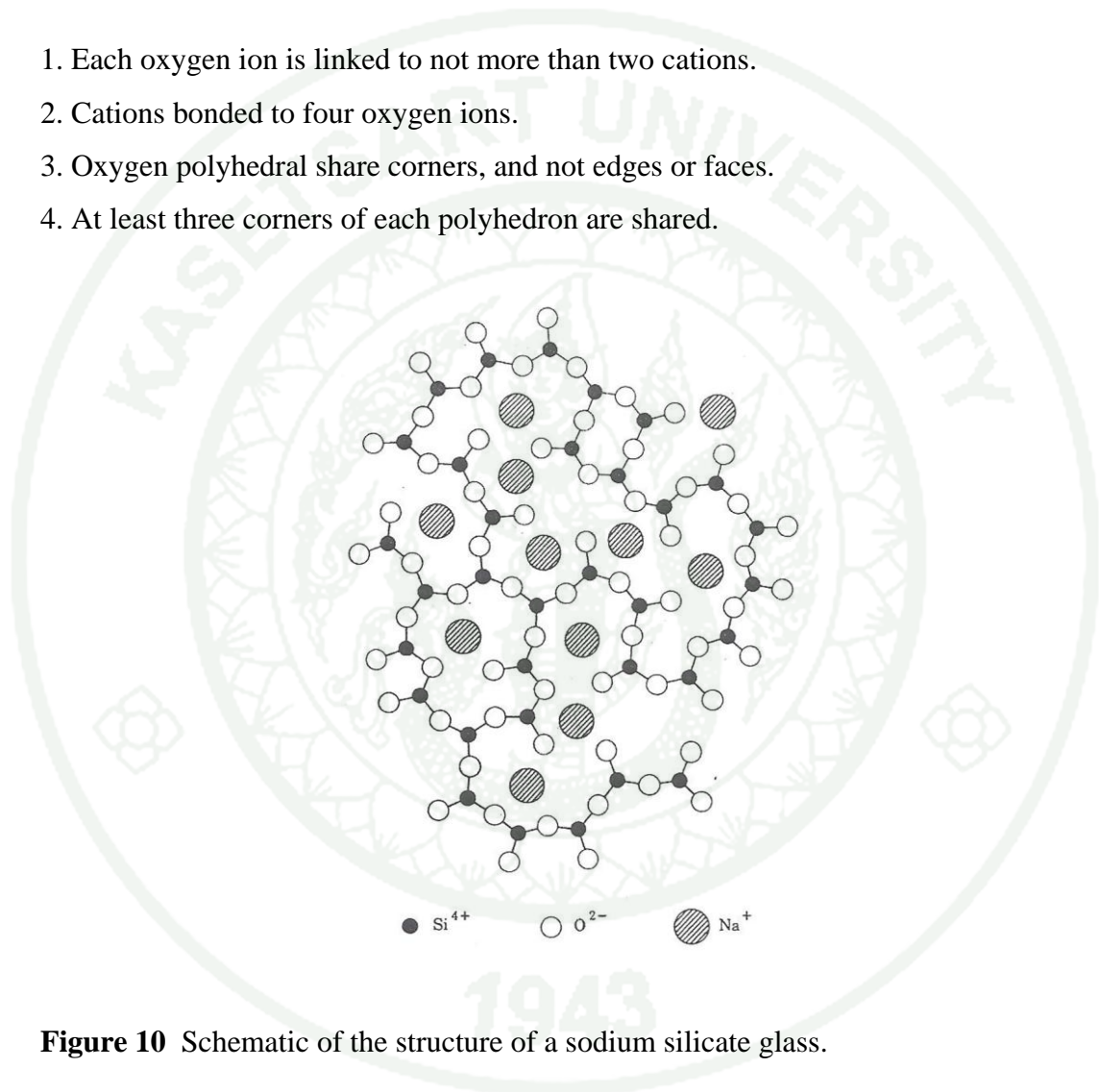


Figure 10 Schematic of the structure of a sodium silicate glass.

Source: Kingery *et al.* (1991)

In practice, a forming of oxides such as SiO_2 , GeO_2 and B_2O_3 is triangles or tetrahedra and cations such as alkali and alkali earth ions forming as coordination of polyhedron have been termed network formers. Alkali ions form with silicate glasses easily and are supposed to occupy random positions distributed through the structure. When oxygen cations connect two silicon tetra hedra at corners, they are

called the bridging oxygens (BOs). Some oxygens linked to only one silicon are called the nonbridging oxygen (NBOs). If oxygens, is a bivalent ions, connect to only one silicon ion resulted in one negative charge, which is satisfied by a univalent positive ion in the spaces.

When considering glass structure, oxides which form glasses classify three types of oxide in terms of their functions in glass structure. Network former oxides are able to build up the continuous skeleton of glass in three-dimensional random network. Examples of this type are B_2O_3 , SiO_2 , GeO_2 , P_2O_5 , V_2O_5 and As_2O_5 . Other oxides such as Li_2O , Na_2O , K_2O , CaO , BaO , ZnO , CdO , Ga_2O_3 , In_2O_3 and PbO_2 play the role network modifiers which cations of these oxides occupied the space in the network formed oxides. Intermediate oxides such as BeO , Al_2O_3 , TiO_2 , ThO_2 and ZrO_2 were termed intermediates. These oxides can take part in glass network which make a high quantities glass.

2.2 Glass formation

Solidification behavior of glass differs from those of crystal solid. This may be understood by examining specific volume-temperature relationship for glass and crystal given as Figure 11.

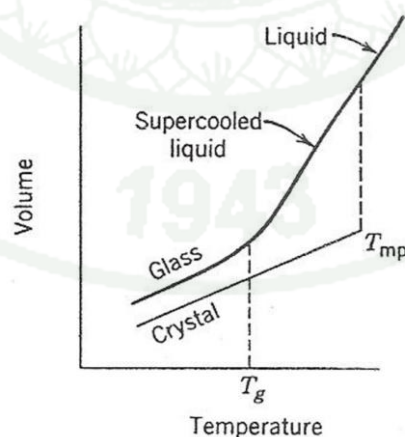


Figure 11 Specific volume-temperature relationship of liquid, glass and crystal.

Source: Kingery *et al.* (1991)

The liquid of glass is formed which is greater volume. On cooling the liquid, it will either recrystallize to form an ordered solid which is the decreased volume called a crystal or produce an amorphous solid called a glass. For the amorphous former, if the liquid is cooled, the viscosity increases. The volume of the liquid decreases at about the same rate as above the melting point until there is a decrease at a range of temperature called the glass transition range. Point on the curve which is initial change of the slope called glass transition temperature (T_g). After the atomic configurations of the liquid affect decreasing of a volume and the liquid becomes solid-like (Harper, 2001). Furthermore, volume depends on the cooling rate. The fast cooling rate is brought to a glass having a volume higher than that of slower rate because a reduced relaxation time generates the high density glass (Kingery *et al.*, 1991).

2.3 Atomic arrangements in glass

2.3.1 Structure of silica glass

The arrangement of silica in glass is tetrahedron comprising a silicon ion bond to four oxygens. Each of the oxygens, one negative charge, satisfies the four positive charges on the silicon which leaves one oxygen to form a corner shared with an adjacent silicon. Thus this acting as a bridging oxygen (BO) is sharing at the corner to allow three angles. The Si-O-Si bond angles are continuously and randomly distributed between 120 and 180° and have a maximum probability at 144°.

2.3.2 Structure of alkali and alkali earth silicate glass

The addition of an alkali oxide such as sodium oxide (Na_2O) and potassium oxide (K_2O) to silica glass breaks up a bond and creates nonbridging oxygens (NBOs) as follows:



when an alkali earth oxide such as CaO is added to silica glass, it plays the role the same as the alkali oxide and produces two NBOs. On account of bivalence of alkali earth, the bridge with alkali earth ion is stronger than that with alkali ion.

2.3.3 Structure of boric oxide, borate and borosilicate glasses

Boric oxide (B_2O_3) is a glass former oxide being better than silica. It is a reactant of producing borate (BO_3^{3-}) triangles in glass. When the addition of alkali or alkali earth oxides to borosilicate glass, they results in the formation of BO_4^- tetrahedra.

2.3.4 Structure of phosphate glasses

Phosphate glasses are composed of oxygen tetrahedral. Since P (phosphorus) is a pentavalent ion, only three of four oxygens are bonded with adjacent tetrahedral. The other oxygen is connected to the P with double bond. With additions of modifier oxides, the molecules break up to form linear chains and sheet-like structures.

3. Glass-ceramics

Glass-ceramic materials developed by S.D. Stookey of Corning glass working in USA are crystalline solids (McMillan, 1979). They are prepared by heat treatment of glass being capable of formation of nuclei and growth of crystalline phases in the glass because there are compositions of nucleating agents. Generally, they consist of a large proportion, typically 95 to 98 vol% of fine crystals which are smaller than 1 micron with a small amount of residual glass phase (Kingery *et al.*, 1991). Due to the amorphous structure of glass, the glass contains nucleating agents to form nuclei and growth crystal. The most commonly used nucleating agents are TiO_2 , ZrO_2 and P_2O_5 .

3.1 Nucleating agents

The role of nucleating agents is a crystallization catalyst and reduces conditions during melting of glass. Crystallization process is divided into two parts: nucleation and crystal growth. In case of the former process, it creates embryos and they are capable of developing spontaneously into particles of the stable phase which are known as nuclei. Nucleation may be homogeneous or heterogeneous. Homogeneous nucleation occurs the nuclei much more difficulty in the interior of a uniform substance. Heterogeneous nucleation occurs much more often than homogeneous nucleation. The oxides used as nucleating agents are, for example, TiO_2 , Yb_2O_3 , La_2O_3 , CeO_2 , V_2O_5 , P_2O_5 and CaF_2 (McMillan, 1984).

3.2 Theoretical of evaluating optimum nucleation temperature and time by Differential Thermal Analysis

It was in 1981 that A. Marotta *et al.* studied to estimate the devitrification of $\text{Li}_2\text{O}-2\text{SiO}_2$ glass by DTA. They said that the total number of nuclei per unit volume (N) was the sum of the surface nuclei (N_S), the bulk nuclei formed during the DTA run (N_B) and the bulk nuclei formed during the previous heat treatment of nucleation (N_H) as following equation:

$$N = N_S + N_B + N_H \quad (2)$$

N_S is the proportional to the specific surface of the sample, N_B is the reciprocal of the heating rate (β) and N_H is related to time of the nucleation heat treatment (t_n) by:

$$N_H = I(t_n)^b \quad (3)$$

where b is a constant related to the nucleation mechanism. The rate constant (I) for nucleation in a super-cooled liquid is given by

$$I = A \exp\left(-\frac{w + E_n}{RT}\right) \quad (4)$$

where w and E_n are the thermodynamic and the kinetic barriers to nucleation, respectively, as well as A is a constant.

Equation 4 is found that the nucleation rate corresponds exponentially to the temperature which this relationship shown in Figure 12.

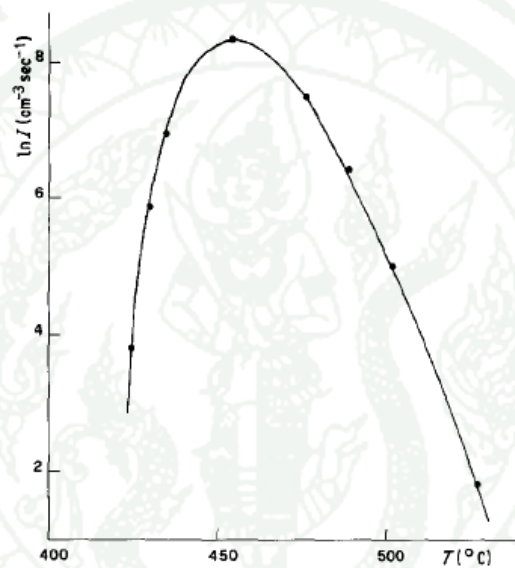


Figure 12 Relationship between the nucleation rate and temperature of $\text{Li}_2\text{O}-2\text{SiO}_2$ glass.

Source: Marotta *et al.* (1981)

The glass heated by DTA appears an exothermic peak on the DTA curve indicated that the formation of crystalline is given in Figure 13. For Johnson-Mehl-Avrami (JMA) equation, it describes a relationship between the degree of crystallization (α) and time (t) as given in

$$\alpha = 1 - \exp(-kt)^n \quad (5)$$

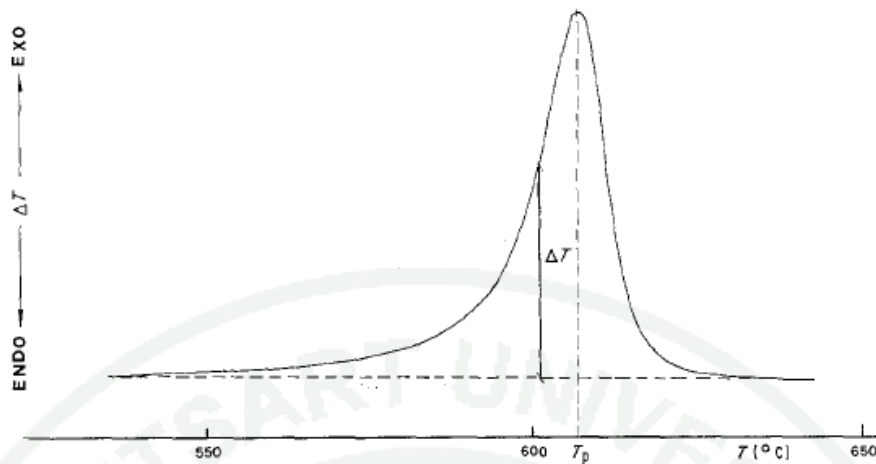


Figure 13 Crystallization peak of $\text{Li}_2\text{O}-2\text{SiO}_2$ glass detected by DTA.

Source: Marotta *et al.* (1981)

where n is a parameter corresponded to crystallization mechanism and crystal shape as well as k is the rate constant related to the absolute temperature (T) by Arrhenius equation.

$$k \propto N \exp\left(-\frac{E_c}{RT}\right) \quad (6)$$

The number of nuclei of glass crystallized at above the temperature of high nucleation rate cannot change during the crystallization process. The DTA curve in Figure 13, the ΔT deflection from the baseline is at each temperature (T) proportional to the reaction rate $d\alpha/dt$. When T equals to T_p , the ΔT deflection has a null temperature.

$$\frac{d\Delta T}{dT} = \frac{d}{dT}\left(\frac{d\alpha}{dt}\right) = 0 \quad (7)$$

$$kt = 1 \quad \text{when } T = T_p \quad (8)$$

Equation 8 is taken into Equation 6 and presumed that time of heating at each temperature is proportional to the reciprocal of the heating rate as presented by

$$\ln \beta - \ln N = -\frac{E_c}{R} \frac{1}{T_p} + \text{constant.} \quad (9)$$

For the DTA runs at the same heating rate of samples, β , N_B and N_S are constant. Therefore, the total number of nuclei per unit volume is the sum of a constant nuclei number (N_0) and the bulk nuclei formed during the previous heat treatment of nucleation (N_H) which depends on the temperature and time of the heat treatments.

$$N = N_0 + N_H \quad (10)$$

N are replaced in Equation 9.

Therefore,
$$\ln(N_0 + N_H) = c_1 \frac{1}{T_p} + c_2 \quad (11)$$

where c_1 and c_2 are constants.

Due to the low specific of the bulk sample, it is assumed that $N_0 \ll N_H$. The difference between the peak crystallization temperature of the sample (T_p^*) and those of nucleated sample (T_p) can be expressed in

$$T_p^* - T_p = c_3 \ln N_H + c_4 \quad (12)$$

where c_3 and c_4 are constants.

If the samples are held for the same time at different nucleation temperature, the data of $T_p^* - T_p$ are plotted as shown in Figure 14.

This plot shows the same shape and maximum at the same temperature of the curve in Figure 12. To determine optimum time of nucleation, if the samples are held for the same temperature at different times, the data of $T_p^* - T_p$ are plotted as shown in Figure 15.

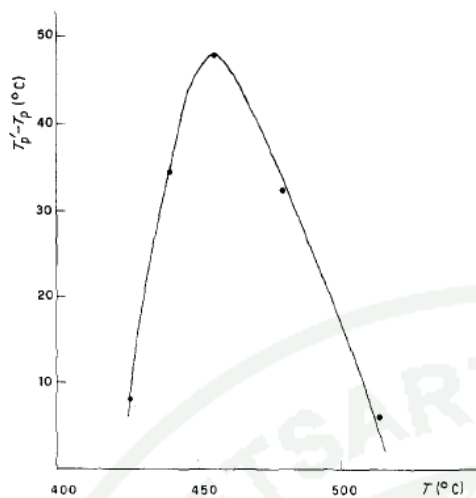


Figure 14 $T_p^* - T_p$ plotted as a function of temperature of heat treatment of $\text{Li}_2\text{O}-2\text{SiO}_2$ glass.

Source: Marotta *et al.* (1981)

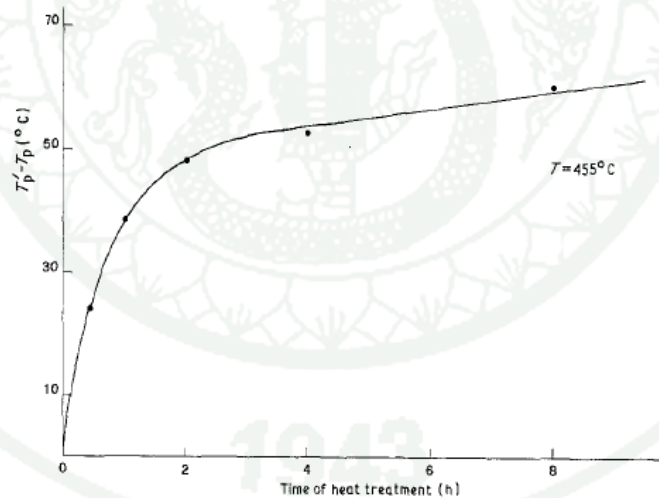


Figure 15 $T_p^* - T_p$ plotted as a function of time of heat treatment of $\text{Li}_2\text{O}-2\text{SiO}_2$ glass.

Source: Marotta *et al.* (1981)

3.3 Procedure of the preparation of glass-ceramics

The steps used in processing a glass-ceramic body are illustrated in Figure 16. The glass material is melted and formed at high temperature around 1250° to 1600°C, depending upon the glass compositions and then often cooled to annealing temperature. For nucleation step, nucleating agents are active to produce the initial nuclei. In order to grow up the crystals, the material is heated to crystallization temperature and held at the temperature.

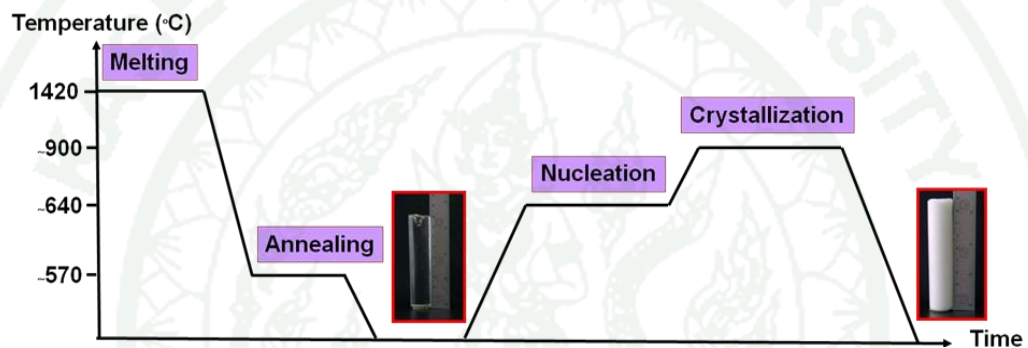


Figure 16 Schematic of heat-treated profile of glass-ceramic.

3.4 Applications of glass-ceramics

Utilization of glass-ceramics are present for, e.g., mechanical engineering as production pipes, valves and seals, electronic engineering as manufacturing high temperature insulator, capacitor as well as part of spaceship (McMillan, 1979). Moreover, they have been used to replace the bone and teeth which are damaged.

4. International Standard ISO 6872:2008(E) (ISO 6872:2008(E), 2008)

ISO 6872:2008(E) identifies the requirements and the test methods for dental ceramic materials for fixed all-ceramic and metal-ceramic restorations and prostheses.

4.1 Type and class identifications

Dental ceramic materials are designated in two types. Type I includes ceramic products which are provided as powders, pastes or aerosols. Type II includes all other forms of ceramic products. Moreover, each type of ceramic products is divided into classes according to their applications. Therefore, these ceramic materials produced in this study are identified as type II.

4.2 Tests of mechanical and chemical properties

Ceramic materials used for dental restorations need to consider their mechanical properties. Because they are used to replace in the mouth, they should be tested for chemical solubility test. Mechanical and chemical properties of the ceramic materials recommended in ISO 6872:2008(E) are present in Table 2.

Table 2 Classification of ceramics for dental restoration as ISO 6872:2008(E) with recommended mechanical and chemical properties.

Class	Clinical indications	Properties		
		Flexural strength (MPa)	Fracture toughness (MPa·m ^{1/2})	Chemical solubility (µg·cm ⁻²)
1	a) Aesthetic ceramic for coverage of a metal or a ceramic substructure*.			
	b) Aesthetic-ceramic: single-unit anterior prostheses, veneers, inlays, or onlays.	>50	>0.7	<100
2	a) Aesthetic-ceramic: adhesively cemented, single-unit, anterior or posterior prostheses.	>100	>1.0	<100
	b) Adhesively cemented, substructure ceramic* for single-unit anterior or posterior prostheses.	>100	>1.0	<2000
3	Aesthetic-ceramic: non-adhesively cemented, single-unit, anterior or posterior prostheses.	>300	>2.0	<100
4	a) Substructure ceramic* for non-adhesively cemented, single-unit, anterior or posterior prostheses.	>300	>3.0	<2000
	b) Substructure ceramic* for three-unit prostheses not involving molar restoration.			
5	Substructure ceramic* for three-unit prostheses involving molar restoration.	>500	>3.5	<2000
6	Substructure ceramic* for prostheses involving four or more units.	>800	>5.0	<100

***Remarks:**

For definitions of “substructure ceramic” for a dental restoration referred in Table 2, it is explained in ISO 6872:2008(E) as followings:-

3.1.16 substructure (core) dental ceramic: dental ceramic which provides a supporting substructure which one or more layers of dental ceramic or dental polymer material are applied, either partially or totally, to form a dental restoration or prostheses.

MATERIALS AND METHODS

Materials

1. Chemicals

- 1.1 Magnesium Fluoride (MgF_2) : Granules about 1.25 mm, Merck
- 1.2 Silicon Dioxide (SiO_2) : $\geq 99.865\%$, Fluka
- 1.3 Aluminum Oxide (Al_2O_3) : $\geq 99.695\%$, Fluka
- 1.4 Strontium Carbonate (SrCO_3) : $\geq 98.4\%$ Aldrich
- 1.5 Calcium Carbonate (CaCO_3) : 99.0%, BDH
- 1.6 Calcium Fluoride (CaF_2) : $\geq 97\%$, BDH
- 1.7 Magnesium Oxide (MgO) : $\geq 98\%$, Merck
- 1.8 Phosphorous Pentoxide (P_2O_5) : $>97\%$, Fluka
- 1.9 Acetic acid (CH_3COOH) : 99.8% analytical grade, Merck
- 1.10 Sodium hydroxide (NaOH) :
- 1.11 Hydrofluoric acid (HF) : 48%, BDH
- 1.12 Distilled water

2. Materials and Machines for Glass-Ceramic Productions

- 2.1 Polypropylene bottles
- 2.2 Analytical balance

: Denver Series TB-403 with a readability of 0.001 g, Germany

- 2.3 Glove box
- 2.4 Roller
- 2.5 Alumina crucibles
- 2.6 Platinum crucibles
- 2.7 Stainless steel tank
- 2.8 Sieve mesh: 10[#], 18[#], 170[#] and 325[#]
- 2.9 Carbon mould: inner diameter = 20 mm, height = 100 mm
- 2.10 Flame retardant coat
- 2.11 Heat resistant gloves
- 2.12 Heat and light resistant mask

- 2.13 Tongs
- 2.14 Goggles
- 2.15 Acid resisting gloves
- 2.16 Dust resisting mask
- 2.17 Electric furnaces: Nabertherm, Germany and Linn, England
- 2.18 Hot oven: ESPEC, series PH-101, Japan
- 2.19 Ultrasonic cleaner : Kerry, England
- 2.20 Low speed cutter : Imptech series PC10, South Africa
- 2.21 Polishing machine : Imptech series 101, South Africa
- 2.22 Abrasive paper No. 800,1000, 1200 and 2500
- 2.23 Diamond pastes 3 μm
- 2.24 Alumina powder 1 μm
- 2.25 Volume metric flask 100 mL
- 2.26 Measuring pipette 2 mL
- 2.27 Bubble
- 2.28 Dropper
- 2.29 Cellulose thimbles
- 2.30 Extractor

3. The Instruments for Analysis

- 3.1 Differential Thermal Analyser (DTA): Perkin Elmer Series DTA7,
Germany
- 3.2 X-ray Diffractometer (XRD): Philips series X'Pert, the Netherlands
- 3.3 Scanning Electron Microscope (SEM) and Energy Dispersive
Spectroscopy: Phillips Series XL30 & EDAX, the Netherlands
- 3.4 Micro Hardness Tester: Shimadzu series HMV-2000, Japan
- 3.5 Universal Testing Machine (UTM): Hounsfield Series 50KN,
England
- 3.6 Dilatometer: Netzsch Series DIL 402 PC, Germany
- 3.7 Computerized Numerical Controller (CNC): DECKEL Series FP4A,
Germany
- 3.8 Optical microscope and image analyzer: Nikon series ECLIPSE ME
600, Japan

3.9 Vernier caliper: Mitutoyo, Japan

Methods**1. Experimental Preparation**

1.1 Glass preparation

The glass compositions consisted of SiO₂, Al₂O₃, SrCO₃, MgO, MgF₂, CaCO₃, CaF₂, and P₂O₅ were weighed and collected in a clean plastic bottle. The compositions of fluorapatite forming in each glass-ceramic were given in Table 3. In order to homogenize the compositions, the bottle was rolled for 2 hours and then all chemicals were poured into an alumina crucible which was covered with an alumina lid to avoid volatility of components such as silicon tetrafluorine (SiF₄) (McMillan, 1979).

Table 3 Varied fluorapatite composition of the glass (g).

Glass-ceramics	CaF ₂	CaCO ₃	P ₂ O ₅
GCF3.0	0.52	5.97	2.82
GCF3.5	0.60	6.87	3.25
GCF4.0	0.67	7.76	3.67
GCF4.5	0.75	8.62	4.07
GCF5.0	0.82	9.46	4.47

They were melted in the furnace at 1420°C for an hour with a heating rate of 10 °C/min. The melted glass was quenched in water at room temperature to obtain the glass frit. The frit was dried, ground and sieved to distinguish size for subsequent experiments. Aperture sizes of sieve used in this experiment were 2 mm (10[#] mesh), 1 mm (18[#] mesh), 90 μm (170[#] mesh) and 45 μm (325[#] mesh).

1.2 Preparation for thermal behaviors analysis

The glass transition, peak crystallization and melting temperatures of each glass were analyzed by differential thermal analysis (DTA). The sub 45 μm frit powder was weighed 55 mg into a platinum crucible. α -alumina was used as a reference in this experiment. The powder was heated to 1200 $^{\circ}\text{C}$ with a heating rate of 10 $^{\circ}\text{C}/\text{min}$. When it was fully heated in the machine, DTA curve of each glass was shown the glass transition (T_g), peak crystallization (T_p) and melting (T_m) temperatures. If the curve appears several peak crystallizations or melting temperatures, they were identified as T_{p1} , T_{p2} and T_{p3} or T_{m1} , T_{m2} and T_{p3} , respectively.



Figure 17 Differential thermal analyzer.

For determination of glass transition, the main parameters used to characterize the glass transition are shown in Figure 17. It need to know the temperature range from $T_{g,i}$ (initial T_g) to $T_{g,f}$ (finish T_g). Characterization of these temperatures is difficult to give clear instructions for their measurement. The situation is improved by consideration extrapolated onset-temperature ($T_{g,e}$) and half-step temperature ($T_{g,1/2}$) related to C_p change. The use of the latter meaningful as this temperature is better the second characteristic quantity of the glass transition, C_p change. (Höhne *et al.*, 2003)

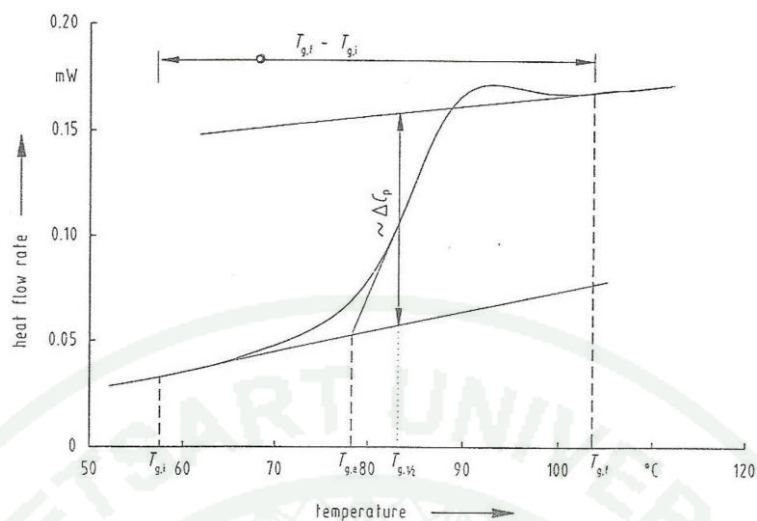


Figure 18 Definition of the most frequently used conventional quantities for characterization of the glass transition.

Source: Höhne *et al.* (2003)

1.3 Fabrication of glass rod

The frits were re-melted at the previous condition in a furnace while another furnace was heated to warm a carbon mould at annealing temperature which was determined by DTA. Then the melted glass was poured into the mould that inclined about 45 degree in order to get rid of chase the bubbles. The carbon mould with glass inside was annealed to release internal stress for 1.30 hours and cooled down to room temperature in the furnace. Finally, a clear transparent glass rod was taken out from the carbon mould.

1.4 Preparation for optimum nucleation temperature of glass-ceramics

According to the research of Marotta *et al.* in 1981, optimum nucleation temperature of glass-ceramic was determined by using DTA. Each of sub 45 μm glass was heated up to temperature of T_g and soaked at this temperature for an hour after that it was heated to 1000°C and cooled down in the furnace. The diagram showed a new T_p which was called T_p^* . In this research, the new diagram appeared 2 T_p^* , the

peaks were identified T_{p1}^* and T_{p2}^* , respectively. In order to repeat the previous procedures, the soaking temperatures were changed from T_g to T_g-30 , T_g-15 , T_g+15 and T_g+30 , respectively. Then the graph in figure 19 was plotted between $T_p^* - T_p$ and those different five temperatures, drew two lines from plotted data and then the intersection of two lines were found. A vertical line was drawn from the intersection to meet the X-axis and the optimum nucleation temperature of the glass-ceramic was determined.

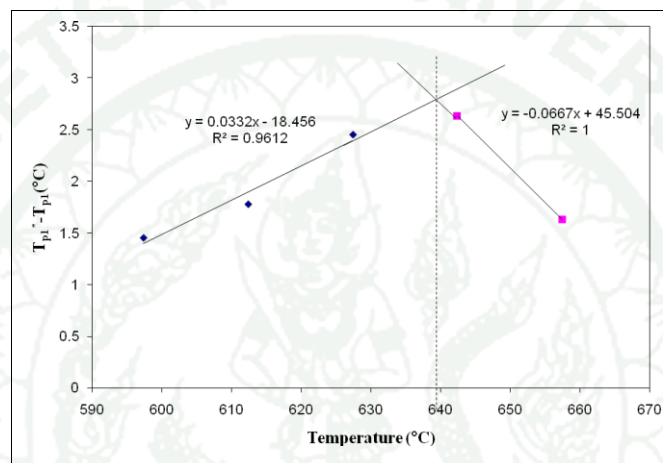


Figure 19 Determination of the optimum nucleation temperature of glass-ceramics.

1.5 Preparation for optimum nucleation time of glass-ceramics

The optimum nucleation time had been examined the same procedure as the optimum nucleation temperature. The sample was heated to the optimum nucleation temperature, held at this temperature for half an hour and heated to 1000°C . The diagram showed T_p^* . The characteristic of the curve was the same as that of the analysis in 1.4. The experiment was repeated but the soaking times were varied as 1, 2, 4 and 10 hours, respectively. The graph was plotted between $T_p^* - T_p$ and those different times. Consequently, two lines were drawn and the intersection of two lines is the optimum nucleation time.

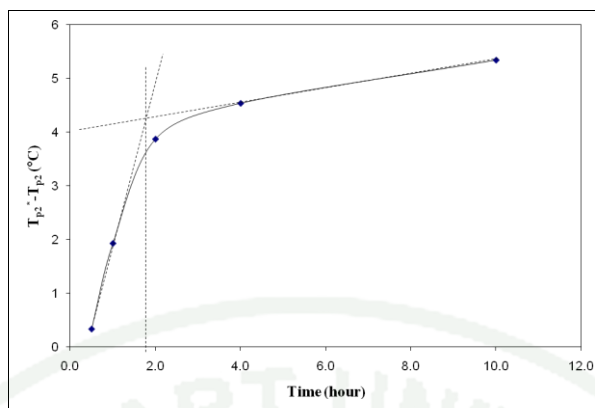


Figure 20 Determination of the optimum nucleation time of glass-ceramics.

1.6 Heat treatment

Because each glass had to be transformed into a glass-ceramic, the glass rod was heated from the room temperature to the optimum nucleation temperature and held for the optimum nucleation time. Then it was heated to the crystallization temperature which is higher than its T_p for 20°C, soaked at the same time as the optimum nucleation time and cooled down to room temperature in the furnace.

2. Properties testing

2.1 Biaxial fractural strength

The glass-ceramic rod was cut in shape of disks with a thickness of 2.5 mm by a high precision diamond cutter. The glass-ceramic of each batch was tested for 10 specimens. Both sides of disks were ground with 800, 1000, 1200 and 2500 grit abrasive paper and polished with 3 micron diamond paste and 1 micron alumina powder, respectively. The finished disk showed absolutely scratch free under an optical microscope.



Figure 21 Universal testing machine.

For the biaxial flexural strength of the glass-ceramics, it could be examined by a universal testing machine (UTM) at a constant displacement rate of 0.1 mm/min. A 1000 N load cell was used. The thickness and diameter of the specimen were measured in order to calculate the strength. The specimen was placed on supporting circle being three balls and covered with a plastic sheet to ensure that the load was evenly distributed over the all loading surface.

A calculation of the strength of biaxial flexural strength is given in equation 13 as followings:

$$\sigma = -0.2387P \frac{(X - Y)}{d^2} \quad (13)$$

Where

σ is the maximum center tensile stress (MPa)

P is the load at fracture (N)

$$X = (1 + \nu) \ln \left(\frac{r_2}{r_3} \right)^2 + \left[\frac{(1 - \nu)}{2} \right] \left(\frac{r_2}{r_3} \right)^2 \quad (14)$$

$$Y = (1 + \nu) \left(1 + \ln \left(\frac{r_1}{r_2} \right)^2 \right) + (1 - \nu) \left(\frac{r_1}{r_3} \right)^2 \quad (15)$$

In which

ν is Poisson's ratio. If the value for the ceramic concerned is not known, use

Poisson's ratio = 0.25

r_1 is the radius of support circle (mm)

r_2 is the radius of loaded area (mm)

r_3 is the radius of specimen (mm)

d is the specimen thickness at fracture origin (mm)

2.2 Hardness

The parts of the specimen broken from the flexural strength testing were used for a Vickers hardness testing. The testing was used a load of 0.5 kg and a loading time of 15 s.



Figure 22 Vickers microhardness tester.

The Vickers hardness was calculated by the Vickers equation:

$$H_v = 1.8544 \frac{P}{d^2} \quad (16)$$

where

P is the applied load (kg)

d is the mean length of diagonals of the indentation (mm).

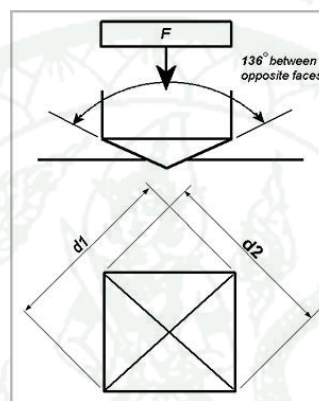


Figure 23 Schematic indentation of Vickers hardness.

Source: McColm (1990)

2.3 Fracture toughness

A calculation of fracture toughness can be obtained by using the full Charles and Evans equation (McColm, 1990) as in equation 17.

$$K_{IC} = 0.016H_v a^{1/2} \left(\frac{c}{a} \right)^{-3/2} \quad (17)$$

Where

H_v is the Vickers hardness (MPa)

a is the half diagonal of the indentation (m)

c is the half distance between the opposite crack tips (m)

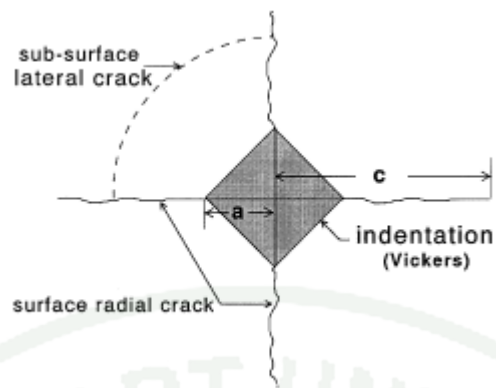


Figure 24 Schematic representation of Vickers indent fracture system, showing characteristic c and a dimensions of crack.

Source : Scherrer *et al.* (1998).

2.4 Microstructure

The glass-ceramics were observe bulk and surface by hitting the glass-ceramics which have size more than 2 mm and cleaned them with an ultrasonic cleaner to remove the residue. The cleaned glass-ceramics were separated into two parts. One part was coated gold with the sputtering technique and the other part was immersed in 10 vol% hydrofluoric acid solution for 25 s then cleaned and also coated gold.



Figure 25 Scanning electron microscope.

2.5 Crystalline phase

The crystalline phases in the glass frits and glass–ceramics obtained were determined by X-ray powder diffraction (XRD) analysis and were interpreted on the basis of IDCC (International Centre of Diffraction Data). In this experiment, diffractometer with Cu K_α radiation was used to measure the diffraction angles 2θ ranged from 5 to 80 with step size of 0.05 and a count time per step of 0.5 s



Figure 26 X-rays diffractometer.

2.6 Coefficient of thermal expansion

The coefficient of thermal expansion can be examined by a dilatometer. The glass-ceramic rods were cut that have length more than 30 mm and width more than 10 mm. Perform an expansion measurement of the test specimen at 10°C/min between 25°C and 500°C. For each of the specimens was determined the linear expansion coefficient between 25°C and 400°C by referring to plotted curves.

$$\alpha = \frac{1}{L_0} \frac{\Delta L}{\Delta T} \quad (18)$$

Where

L_0 = the overall length of material in the direction being measure

ΔL = the change in length of material in the direction being measure

ΔT = the change in temperature over which ΔL is measured

2.7 Machinability

The prepared glass-ceramics, thickness 2.0 mm, were drilled by Computerized Numerical Controller (CNC) using a 3.0 mm hard alloy with speed of 630 rpm and feed rate of 19 mm/min.

2.8 Chemical solubility

According to International Standard ISO 6872:2008(E), specimens were washed with distilled water, dried at 150°C for four hours and weighed. They were measured lengths, widths and thicknesses to calculate the total surface area in centimeters. Subsequently, they were placed in the interred glass-bottomed thimble and extracted with 4% (V/V) acetic acid solution by refluxing for 16 hours. Then the specimens in the thimble were washed with distilled water, dried at 150°C for four hours and reweighed. Chemical solubility was examined by calculating the mass loss in micrograms per square the surface area. The others solutions were used for testing, e.g., have 0.1M sodium hydroxide (NaOH) and distilled water.

RESULTS AND DISCUSSION

The experiments were set in the laboratory and were categorized into 3 parts for example, 1) thermal properties 2) microstructures and crystalline phases and 3) mechanical properties such as biaxial flexural strength, Vickers hardness, fracture toughness, machinability, coefficient of thermal expansion and chemical solubility.

1. Thermal Properties

1.1 Glass transition, peak crystallization and melting temperature

The effect of the variation of chemicals for fluorapatite, e.g., CaCO_3 , CaF_2 and P_2O_5 on the thermal behaviors of the glasses in the SiO_2 - Al_2O_3 - MgO - MgF_2 - SrCO_3 - CaCO_3 - CaF_2 and P_2O_5 system is indicated by DTA resulted in Figure 27. Each of the DTA curves shows a glass-transition temperature, two exothermic and several endothermic peaks. On account of more than one peak of both exothermic and endothermic peaks, the former are named T_{p1} and T_{p2} , respectively, and the latter called T_{m1} , T_{m2} , T_{m3} and T_{m4} , respectively. Exothermic peak identifies the constructed bond temperature to form crystals. On the other hand, endothermic peak indicates the degrade bond temperature of crystals. T_g of the glasses appeared a temperature range of 618-627 °C. The first and the second peak crystallization temperatures appeared a temperature range of 757-783 and 864-889 °C, respectively. Several melting temperatures appeared in a range of 1043-1186°C.

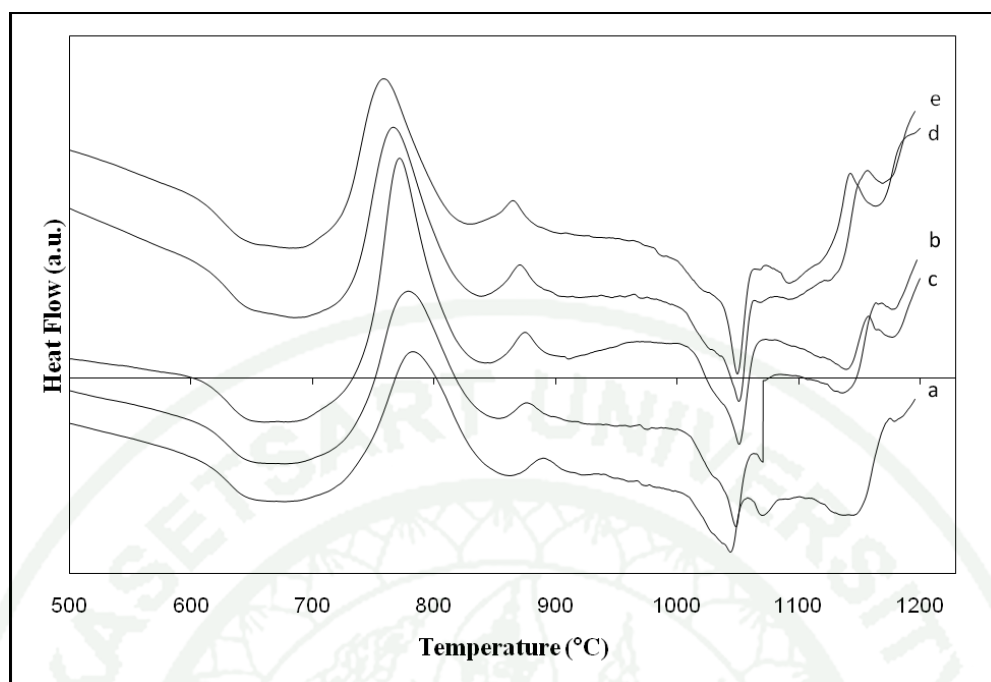


Figure 27 DTA curves of the glasses: (a) GCF3.0, (b) GCF3.5, (c) GCF4.0, (d) GCF4.5, (e) GCF5.0.

The values of thermal behaviors of all glasses were given in Table 4. The T_g , T_{p1} and T_{p2} decreased with the increasing fluorapatite content from 3.0 to 5.0 mol%, in agreement with the previous study (Rafferty *et al.*, 2000). It was believed that the increasing chemicals, especially CaF_2 , for fluorapatite affect to the reduction of those temperatures. Because the fluorine ion, a radius of 1.36 \AA , is very close in size to the oxygen ion, a radius of 1.40 \AA , so that a fluorine ion can replace a oxygen ion in the glass network without causing a disturbance in the arrangement of other ions. The fluorine ion is monovalent, however, the overall replacement must be of two fluorine ions for each oxygen ion to ensure electroneutrality. Generally, incorporation of the fluoride ion in silicate glasses results in the substitution of strong Si-O-Si linkages by weak Si-F linkages; consequently, the glass network structures are weakened. This effect is reflected in decreased viscosity of glasses (McMillan, 1979).

Table 4 Thermal behaviors of all the glasses (°C).

Glass-ceramics	T _g	T _{p1}	T _{p2}	T _{m1}	T _{m2}	T _{m3}	T _{m4}
GCF3.0	627	783	889	1043	1070	1148	1186
GCF3.5	627	778	886	1048	1070	1140	1181
GCF4.0	625	777	881	1051	1085	1147	1179
GCF4.5	622	765	870	1050	1096	1170	1177
GCF5.0	618	757	864	1049	1091	1164	1175

The crystallization peak characteristics of T_{p1} and T_{p2} are broad, it may be presumed that there are formations of various crystal phases at the temperatures due to several melting points shown in the DTA curves.

1.2 Optimum nucleation temperature and time

The important parameters of the nucleation and crystallization steps to transform a glass into a glass-ceramic are suitable temperatures and times for the heat treatment process as well as the effective nucleating agents. The resultant data on Appendix Table A1-A10 were used for optimum nucleation temperature determination of all glasses.

The whole of data are plotted as graphs in order to analyze optimum nucleation temperature as given in Appendix Figure A76-A85 and concluded in Table 5. It is found that the optimum nucleation temperature shows a tendency of increase of both T_{p1} and T_{p2} with the increase of fluorapatite content because induction of CaO, CaF₂ and P₂O₅ contents enhance to high crystal phase formations in the glass-ceramics.

Table 5 Optimum nucleation temperatures of all glass-ceramics (°C).

Glass-ceramics	T_{p1}	T_{p2}
GCF3.0	616	634
GCF3.5	629	634
GCF4.0	646	653
GCF4.5	639	655
GCF5.0	640	626

The data of optimum nucleation time are presented in Appendix Table A11-A20 and Appendix Figure A86-A95. Consequently, most of the optimum nucleation time is 2 hours. Optimum nucleation times at the different peak temperature are concluded in Table 6.

Table 6 Optimum nucleation times of all glass-ceramics (hour).

Glass-ceramic	T_{p1}	T_{p2}
GCF3.0	2	2
GCF3.5	2	2
GCF4.0	3	2
GCF4.5	2	2
GCF5.0	2	2

1.3 Heat treatment

The resultant glass-ceramics are successfully heat-treated because of no cracks. In Figure 28, it shows representatives of glasses before and after heat treatment. When the glasses are heat-treated, they become glass-ceramics which possess more opacity. In addition, the heat-treated glass-ceramics at T_{p1} appear more translucent than those at T_{p2} . This result is able to identify that the crystallized glass-ceramics at T_{p2} had more degree of crystallization than those at T_{p1} , confirmed by

characterization of microstructures and crystalline phases by SEM and XRD, respectively.

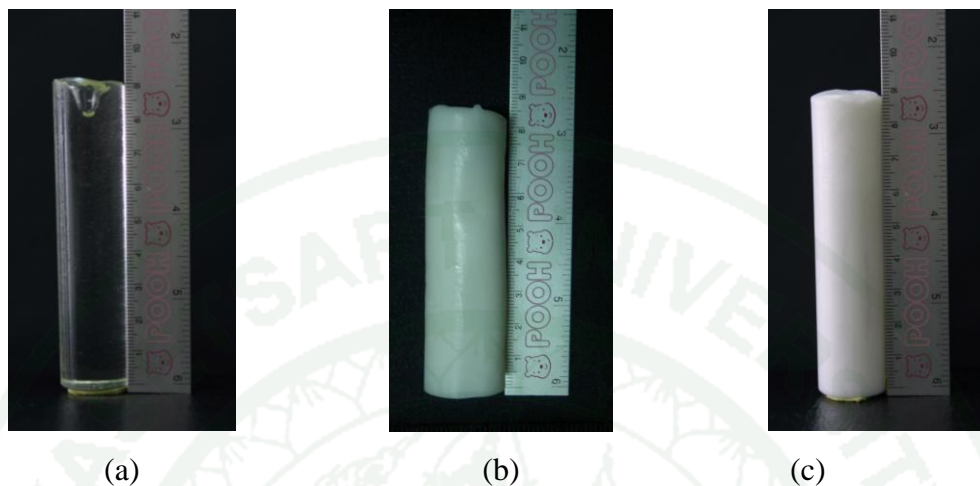


Figure 28 Representatives of (a) a glass rod (b) a glass-ceramic heat-treated at T_{p1} and (c) a glass-ceramic heat-treated at T_{p2} of GCF4.0.

2. Characteristics of Crystalline Phases and Microstructures

2.1 Crystalline phases

The all glasses and glass-ceramics were characterized crystalline phases by XRD. The XRD patterns of as-received glasses appeared hump peaks indicated that they were only amorphous structures. Thus, there were not crystalline phases in the glasses. On account of the glasses consisting of nucleating agents such as MgF_2 , CaF_2 and P_2O_5 , they presented crystalline phases when they were heat-treated as results in Figure 29 and 30.

For the crystallized glass-ceramics at T_{p1} , they were found calcium-mica ($Ca_{0.5}Mg_3AlSi_3O_{10}F_2$, 25-0155), fluorapatite ($Ca_{10}(PO_4)_6F_2$, 83-0537) as the major crystalline structures. In addition, calcium aluminum silicate ($Al_3Ca_{0.5}Si_3O_{11}$, 46-0744), forsterite (Mg_2SiO_4 , 71-1083), magnesium silicate ($MgsiO_3$, 80-0573), anorthite ($CaAl_2Si_2O_8$, 03-0559), strontium oxide (SrO , 48-1477), silicon oxide

(SiO₂, 82-1556) and stishovite (SiO₂, 82-1646) were the minor crystalline structures of those.

While the components of fluorapatite were increasing, the intensity of identified fluorapatite and anorthite peaks increased also. However, it seemed some peaks such as calcium-mica, mica, forsterite to reduce the intensity until GCF4.0. When the fluorapatite contents were greater than GCF4.0, e.g. 4.5 and 5.0, those peaks were shown a little change in a rise in intensities because fluorapatite and calcium-mica phases resulted from the varied chemicals e.g. CaF₂ and P₂O₅. McMillan and Hench explained that CaF₂ and P₂O₅ played the role as nucleating agents of fluorapatite crystals. Moreover, CaCO₃ and CaF₂ are components to form calcium-mica crystals (McMillan, 1979, Hench and Wilson, 1993).

Crystalline phases of the heat-treated glass-ceramics of at T_{p2} as illustrated in Figure 30 possess as same as those at T_{p1} but higher intensities than those of at T_{p1}. This difference was described again in the next place. When the varied components increased, the peaks arise clearly such as fluorapatite, calcium-mica, mica, forsterite and anorthite. However, some peaks could not be interpreted which were named unknown.

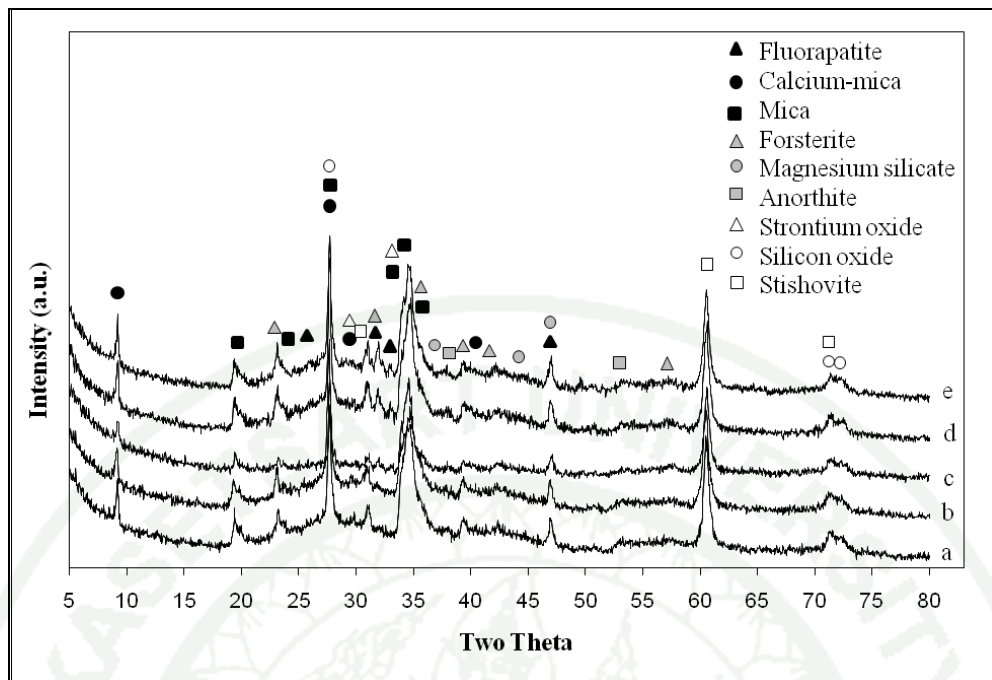


Figure 29 XRD patterns of heat-treated glass-ceramics at T_{p1} of GCF: (a) 3.0, (b) 3.5, (c) 4.0, (d) 4.5, (e) 5.0.

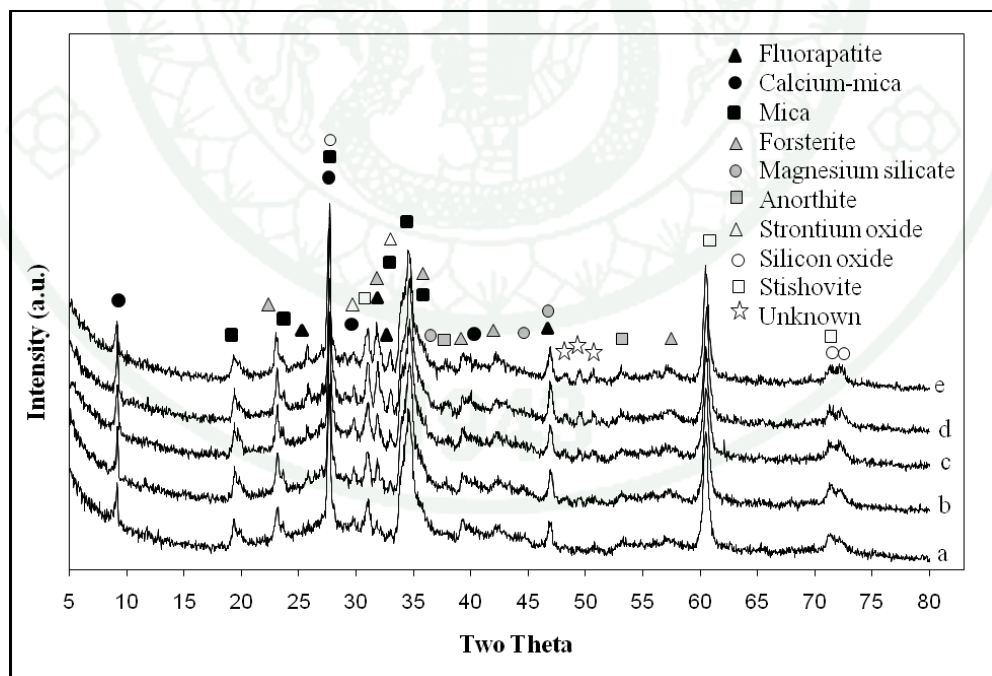


Figure 30 XRD patterns of heat-treated glass-ceramics at T_{p2} of GCF: (a) 3.0, (b) 3.5, (c) 4.0, (d) 4.5, (f) 5.0.

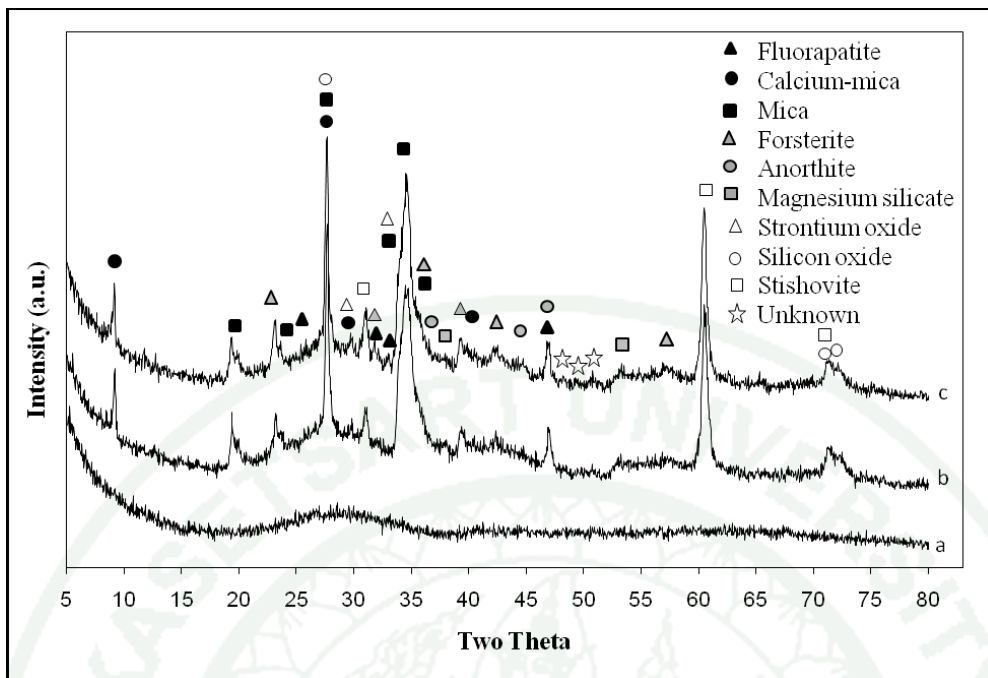


Figure 31 XRD patterns of GCF3.0: (a) as-received glass, (b) heat-treated glass-ceramic at T_{p1} , (c) heat-treated glass-ceramic at T_{p2} .

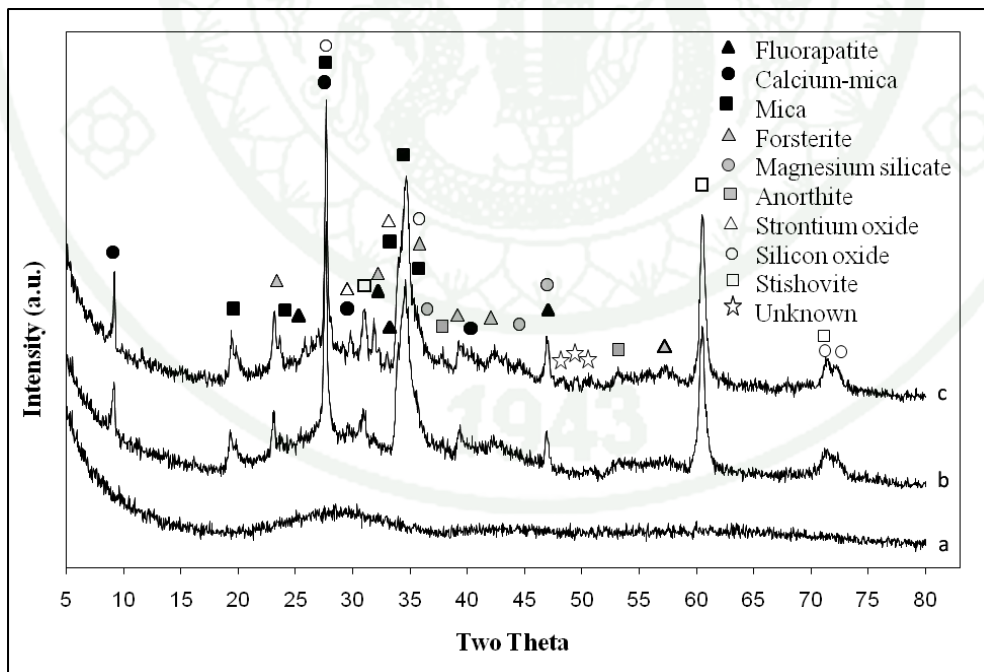


Figure 32 XRD patterns of GCF3.5: (a) as-received glass, (b) heat-treated glass-ceramic at T_{p1} , (c) heat-treated glass-ceramic at T_{p2} .

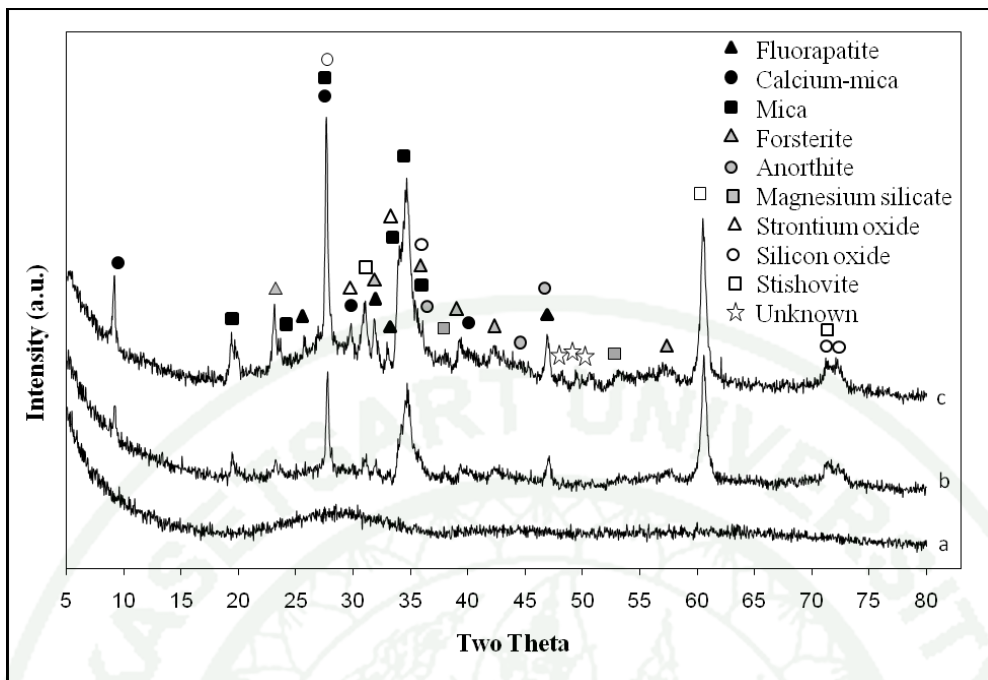


Figure 33 XRD patterns of GCF4.0: (a) as-received glass, (b) heat-treated glass-ceramic at T_{p1} , (c) heat-treated glass-ceramic at T_{p2} .

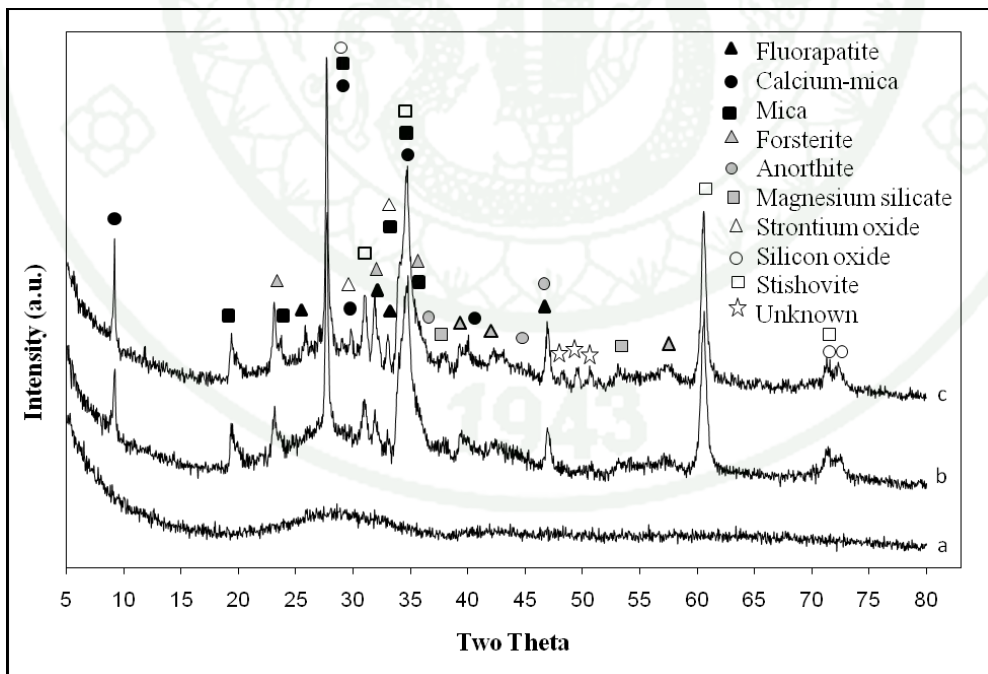


Figure 34 XRD patterns of GCF4.5: (a) as-received glass, (b) heat-treated glass-ceramic at T_{p1} , (c) heat-treated glass-ceramic at T_{p2} .

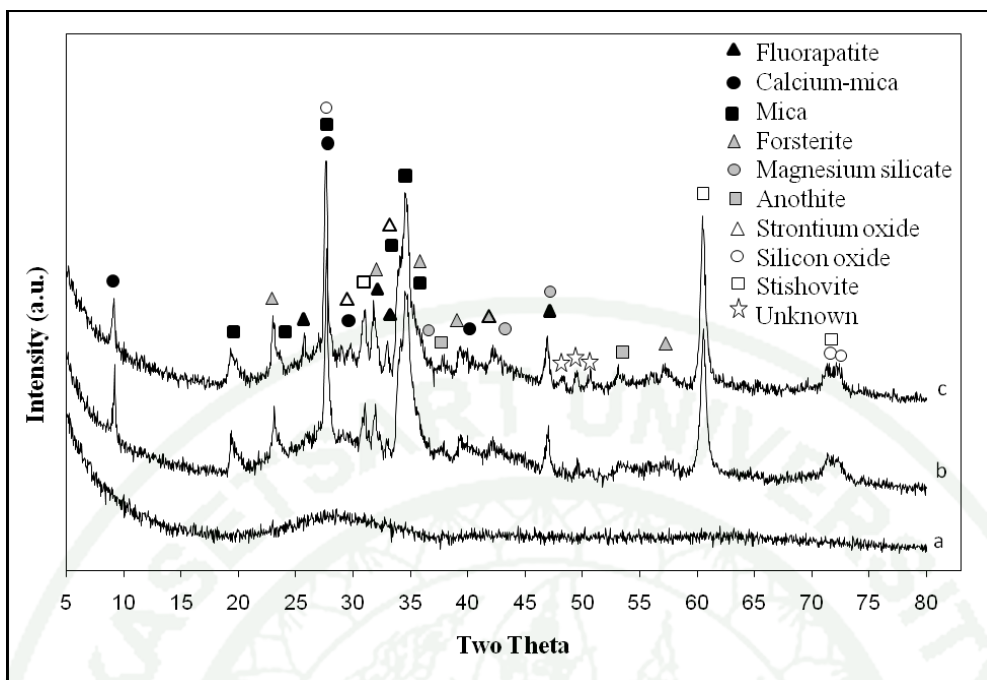


Figure 35 XRD patterns of GCF5.0: (a) as-received glass, (b) heat-treated glass-ceramic at T_{p1} , (c) heat-treated glass-ceramic at T_{p2} .

If it was considered in terms of differences of the intensity of the crystalline phases of the same composition at the different heat-treated temperature the XRD patterns were illustrated in Figure 31-35. Each of the temperatures for the heat treatment of glass-ceramics consisted of many phases which correspond to assumption in the DTA results. The intensities of peaks of at T_{p2} were found rather stronger than those of at T_{p1} because the crystalline phases in the glass-ceramics crystallized at T_{p2} were incorporated into those at T_{p1} . Furthermore, the numbers of peaks of a T_{p2} were observed more obviously than those of T_{p1} , especially at the 2θ positions of at 47.94, 49.46 and 50.66. Therefore, the heat-treated glass-ceramics at T_{p2} possessed the higher degree of crystallinity than those at T_{p1} corresponding to the physical characterization.

2.2 Microstructures

The microstructures of glass-ceramics were investigated by SEM. The bulk microstructures of all samples are given in Figure 36-45. They were found feather-like structures in no etching and plate-like structures in with etching by 10% HF. This morphology is a characteristic of calcium-mica crystals formed highly interlocking (Xiang *et al.*, 2007). The increased chemicals for the fluorapatite formation affected the volume and size of crystalline phases. For this research, the more chemical compositions, the larger both the volume and size of crystals. In addition, the heat treatment temperature influenced also the microstructure of glass-ceramics. It was observed that the glass-ceramics heat-treated at higher temperature showed larger crystal size and denser interlocking than those at the lower temperature.

For the microstructures on the surface, there were needle-like and angular crystals, known as fluorapatite and likely calcium-mica, sparsely clustered on glass-ceramics in Figures 46-50. It was explained that CaCO_3 played the role of a glass former in calcium-mica formation whereas CaF_2 and P_2O_5 play the role of nucleating agents accelerating and inducing the formation of fluorapatite and calcium-mica phases [5,6]. Hence, GCF3.0 possessed more less amounts of crystals and higher aspect ratios than those of other glass-ceramics. The temperature difference of heat treatment affects also the microstructures of bulk.

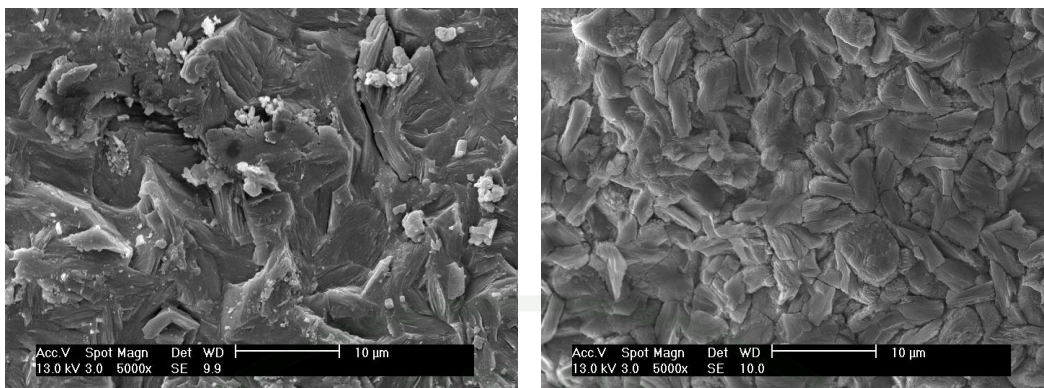


Figure 36 Bulk microstructures of GCF3.0 heat-treated at T_{p1} (a) no etching and (b) etching with HF, 5,000X.

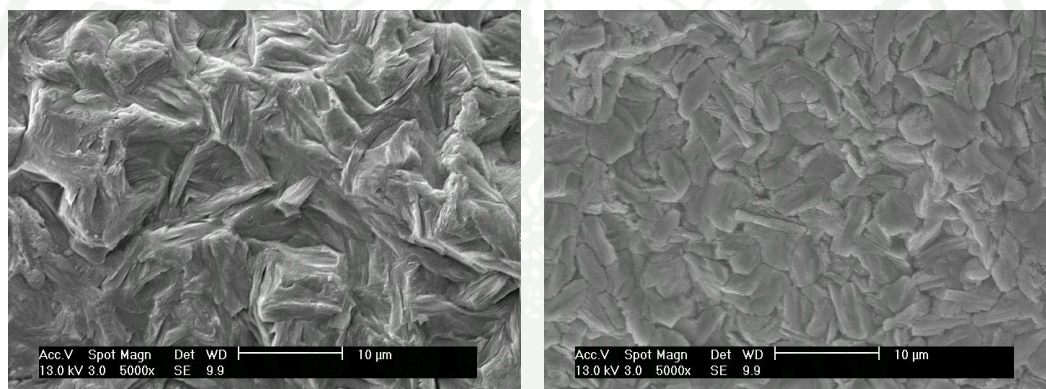


Figure 37 Bulk microstructures of GCF3.0 heat-treated at T_{p2} (a) no etching and (b) etching with HF, 5,000X.

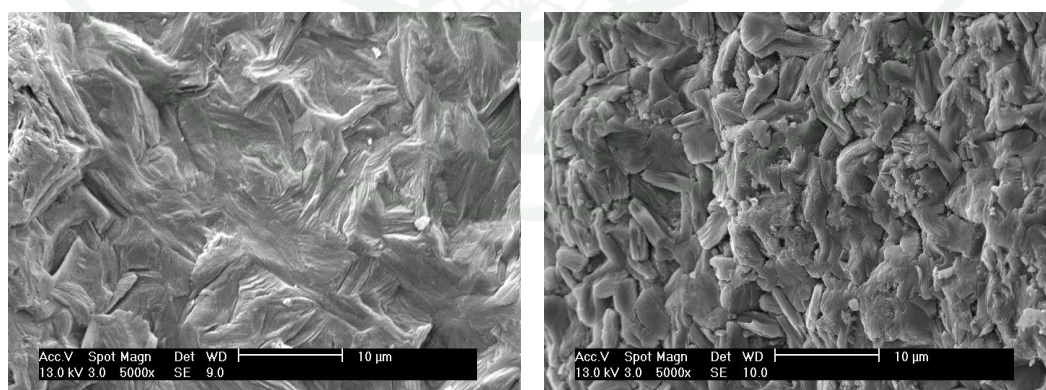


Figure 38 Bulk microstructures of GCF3.5 heat-treated at T_{p1} (a) no etching and (b) etching with HF, 5,000X.

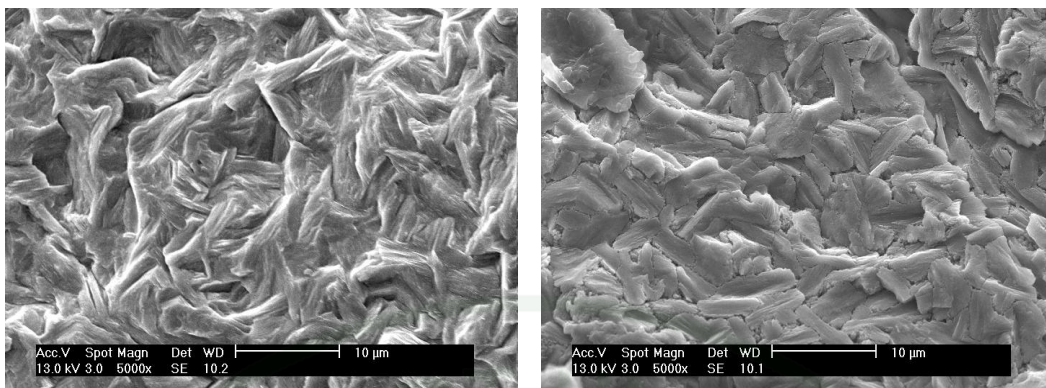


Figure 39 Bulk microstructures of GCF3.5 heat-treated at T_{p2} (a) no etching and (b) etching with HF, 5,000X.

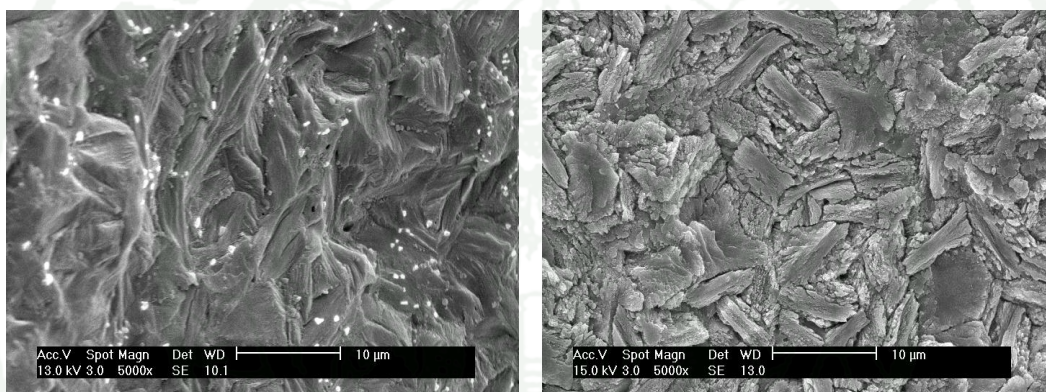


Figure 40 Bulk microstructures of GCF4.0 heat-treated at T_{p1} (a) no etching and (b) etching with HF, 5,000X.

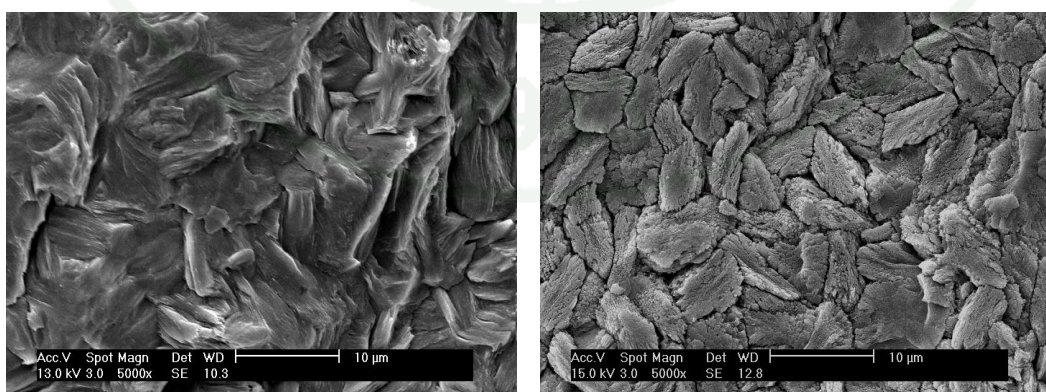


Figure 41 Bulk microstructures of GCF4.0 heat-treated at T_{p2} (a) no etching and (b) etching with HF, 5,000X.

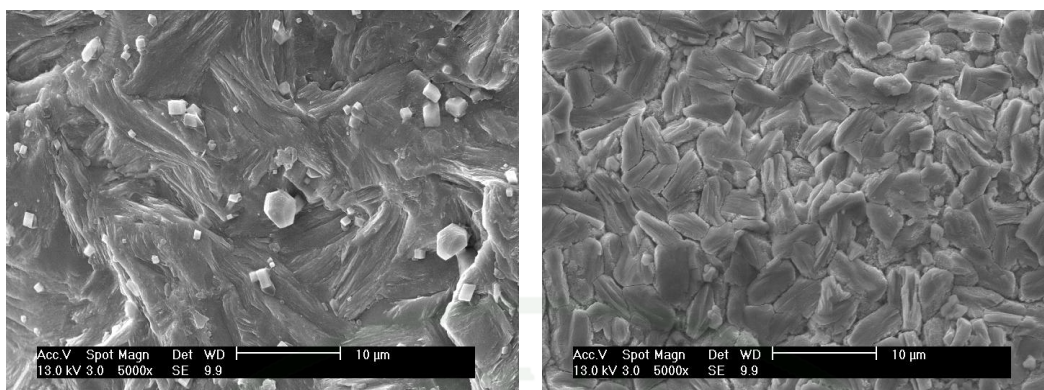


Figure 42 Bulk microstructures of GCF4.5 heat-treated at T_{p1} (a) no etching and (b) etching with HF, 5,000X.

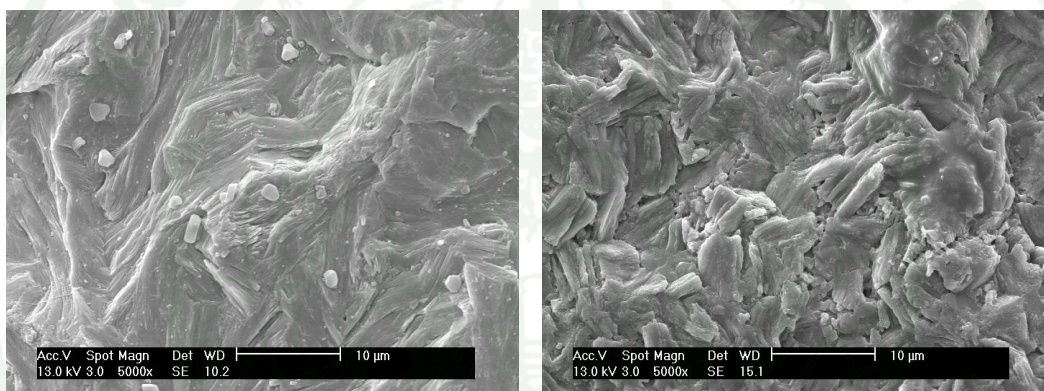


Figure 43 Bulk microstructures of GCF4.5 heat-treated at T_{p2} (a) no etching and (b) etching with HF, 5,000X.

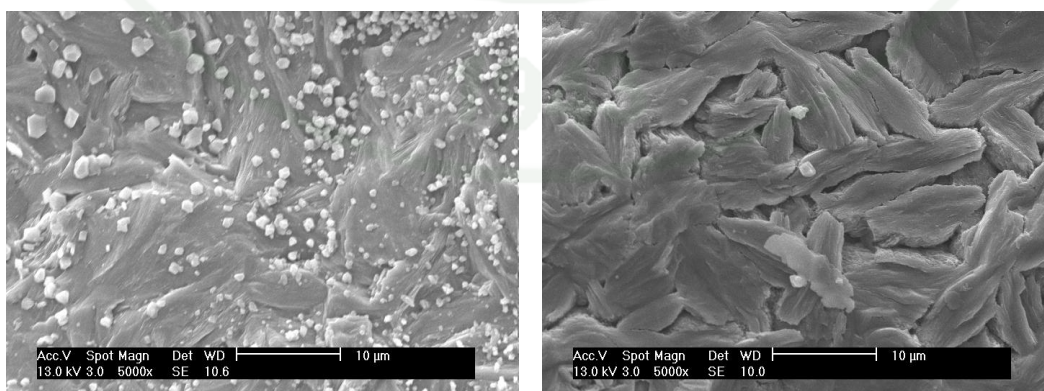


Figure 44 Bulk microstructures of GCF5.0 heat-treated at T_{p1} (a) no etching and (b) etching with HF, 5,000X.

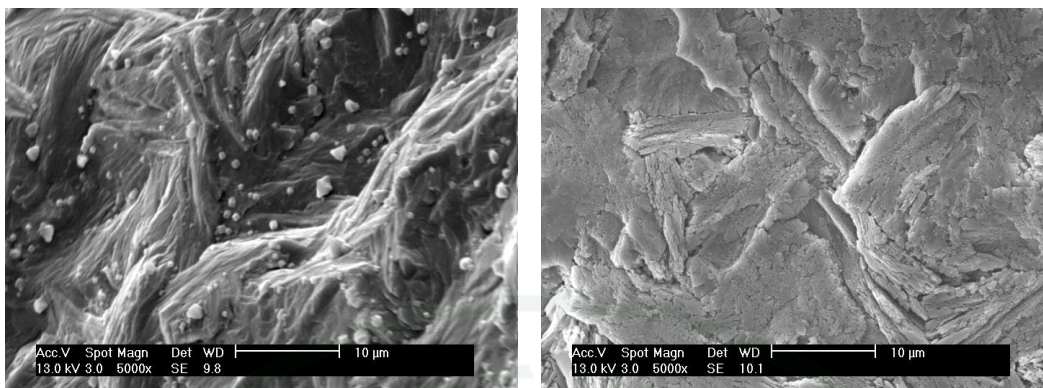


Figure 45 Bulk microstructures of GCF5.0 heat-treated at T_{p2} (a) no etching and (b) etching with HF, 5,000X.

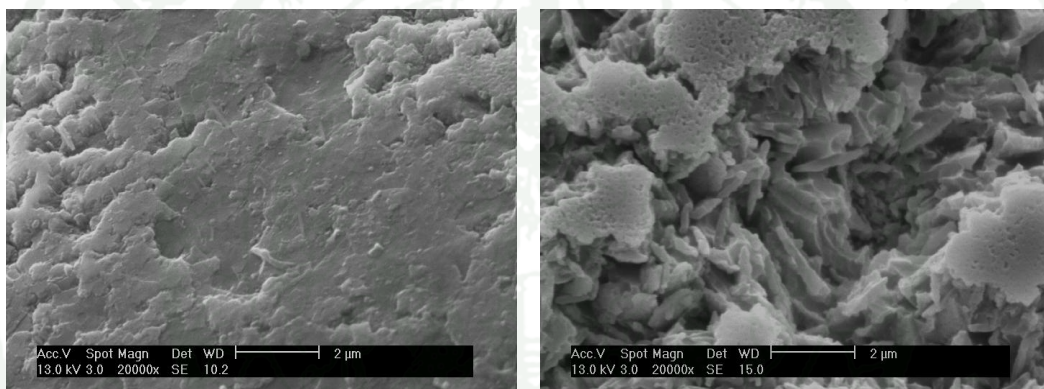


Figure 46 Surface microstructures of etched with HF GCF3.0 heat-treated at (a) T_{p1} and (b) T_{p2} 20,000X.

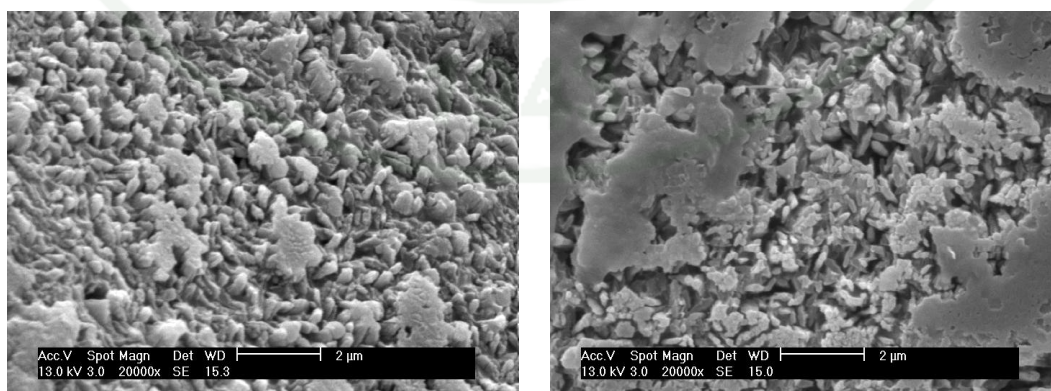


Figure 47 Surface microstructures of etched with HF GCF3.5 heat-treated at (a) T_{p1} and (b) T_{p2} , 20,000X.

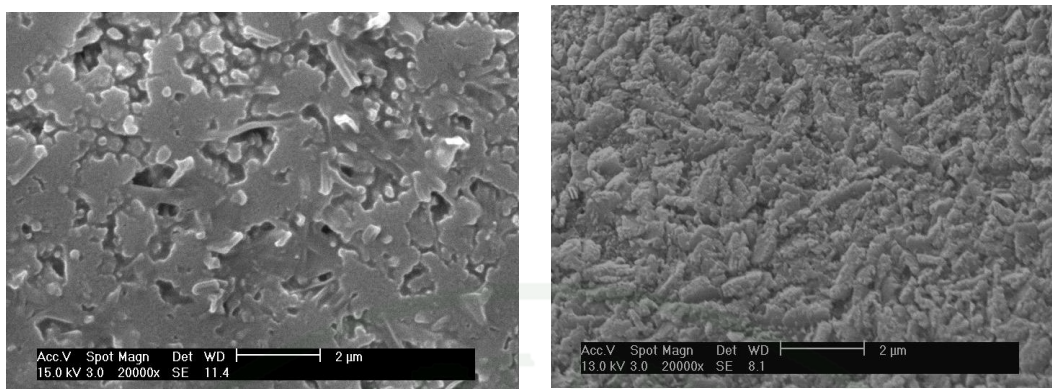


Figure 48 Surfaced micro structures of etched with HF GCF4.0 heat-treated at (a) T_{p1} and (b) T_{p2} , 20,000X.

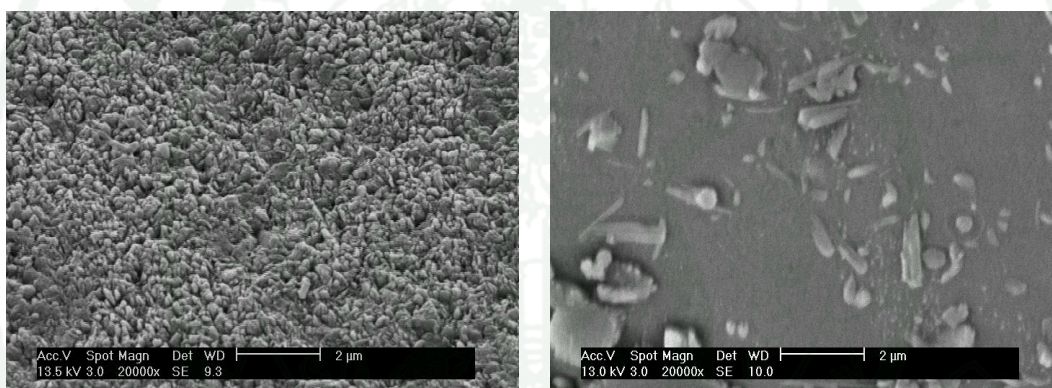


Figure 49 Surface microstructures of etched with HF GCF4.5 heat-treated at (a) T_{p1} and (b) T_p , 20,000X

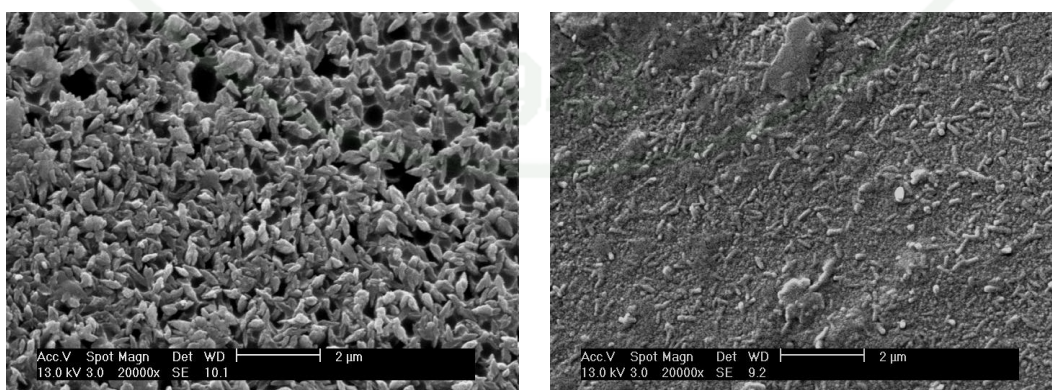


Figure 50 Surface microstructures of etched with HF GCF5.0 heat-treated at (a) T_{p1} and (b) T_{p2} , 20,000X.

3. Characterized Properties

3.1 Mechanical properties

In general, it is known that a finer particle size results in higher strength (Grossman, 1978). In this research, the higher content of fluorapatite influenced initially increasing of mechanical properties such as the biaxial flexural strength, Vickers hardness and fracture toughness but they were gradually declined as shown in Figure 51-53, respectively. For the bulk microstructures observation, it was found that the difference of fluorapatite content affected the increased crystalline size. Structures of that phase consist of layer which forms of silica and alumina, producing triple layer unit structures and giving a negative charge. This charge is balanced by addition of calcium cations atom that links the layer with double bond. Between the two layers, these calcium ions hold the triple layers together with ionic bonding forces. Although the interlayer bonds provided by the balancing cations are stronger than those by van der Waals forces, they are still weaker than the bonding with the units. Hence, the calcium-mica possesses the easy cleavage (Gallagher and Brown, 2003). Therefore, the biaxial flexural strength, hardness and fracture toughness values of glass-ceramics have a tendency to decrease.

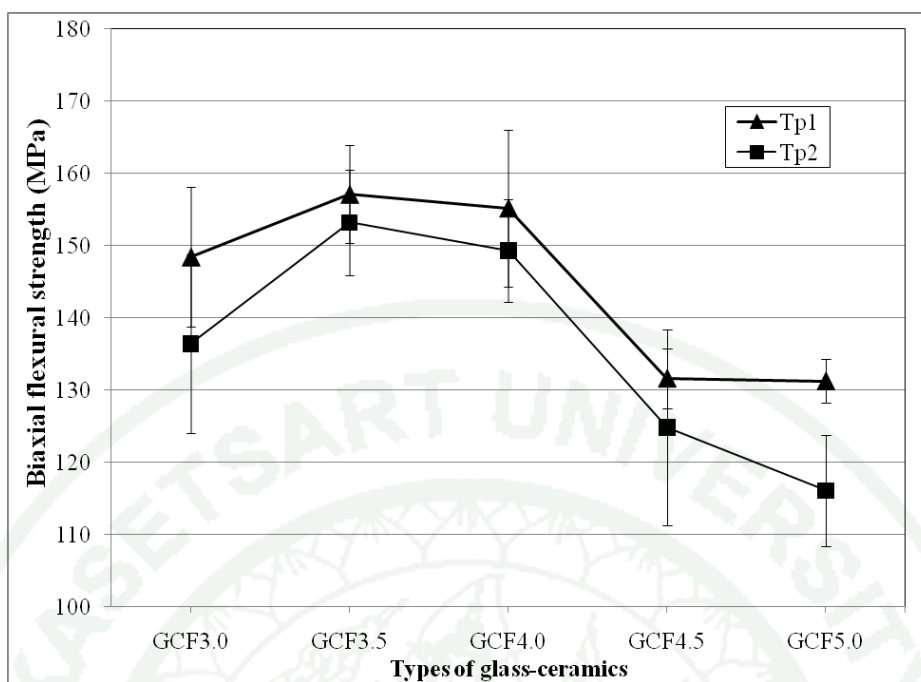


Figure 51 Biaxial flexural strength of all glass-ceramics heat-treated at T_{p1} and T_{p2} .

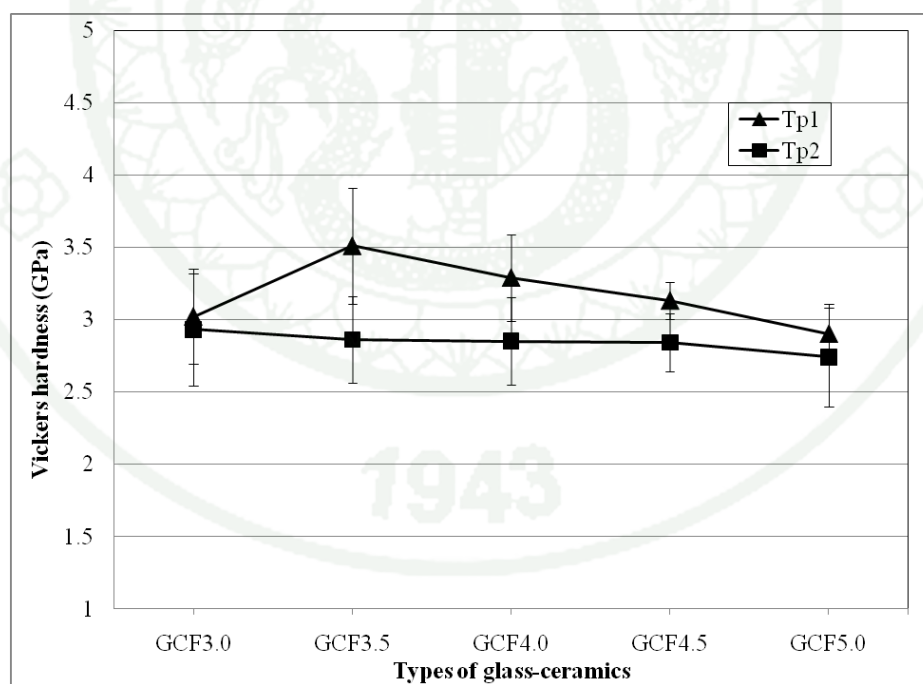


Figure 52 Vickers hardness of all glass-ceramics heat-treated at T_{p1} and T_{p2} .

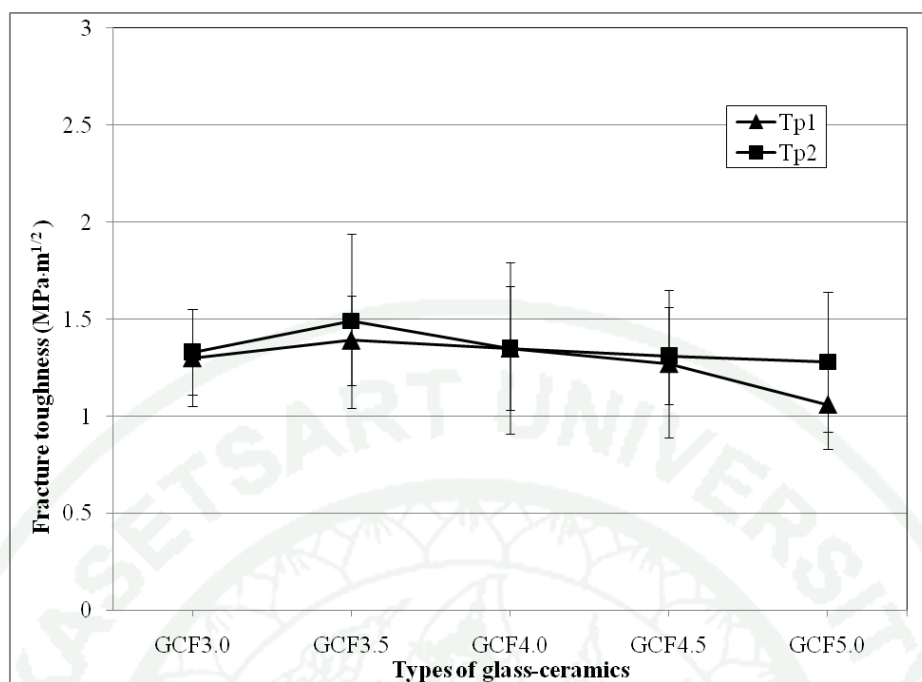


Figure 53 Fracture toughness of all glass-ceramics heat-treated at T_{p1} and T_{p2} .

In addition, the increasing of crystallization temperatures influenced the reducing of all three properties due to the rise of several crystalline phases, especially the calcium-mica.

Table 7 Mechanical properties of all-ceramic dental restorations.

Core materials	Flexural strength (MPa)	Hardness (GPa)	Fracture toughness (MPa·m ^{1/2})
Enamel	65-75	-	1
Dentine	16-20	-	2.5
Dicor	152	3.5	2.5
Empress 2	400	5.3	3.3
In-Ceram Alumina	500	11.5	3.9
Procera Zirconia Y-TZP	1121	-	10

Source: Ironside and Swain (1998); Ban (2008)

According to ISO 6872:2008(E) classifying ceramics for clinical indications, the entire data of the strength and the fracture toughness of mica-based glass-ceramics were accepted as dental ceramic type II class 2 as a substructure ceramic for single-unit anterior or posterior prostheses, e.g., inlays, onlays, crowns and veneers. In addition to the mechanical properties of glass-ceramics were near to all-ceramic materials for dental restoration, especially Dicor glass-ceramic.

3.2 Machinability

The machinability of mica glass-ceramics depends on the volume content of mica crystals and the degree of crystal interlocking. The higher the aspect ratio, the lower the volume fraction of mica phase (Grossman, 1978). In addition, the aspect ratio has to be high enough to cause a high degree of interlocking. It is required containing as little as 1/3 by volume of crystal to attain machinability (Brodkin *et al.*, 2003). For the drilling test, all prepared glass-ceramics based on calcium-mica crystals could be machined thorough into the specimens shown in Figure 54. The aspect ratio of mica crystal increases with the increase of crystallization temperature, resulting in an interconnected microstructures (Yu *et al.*, 2006).

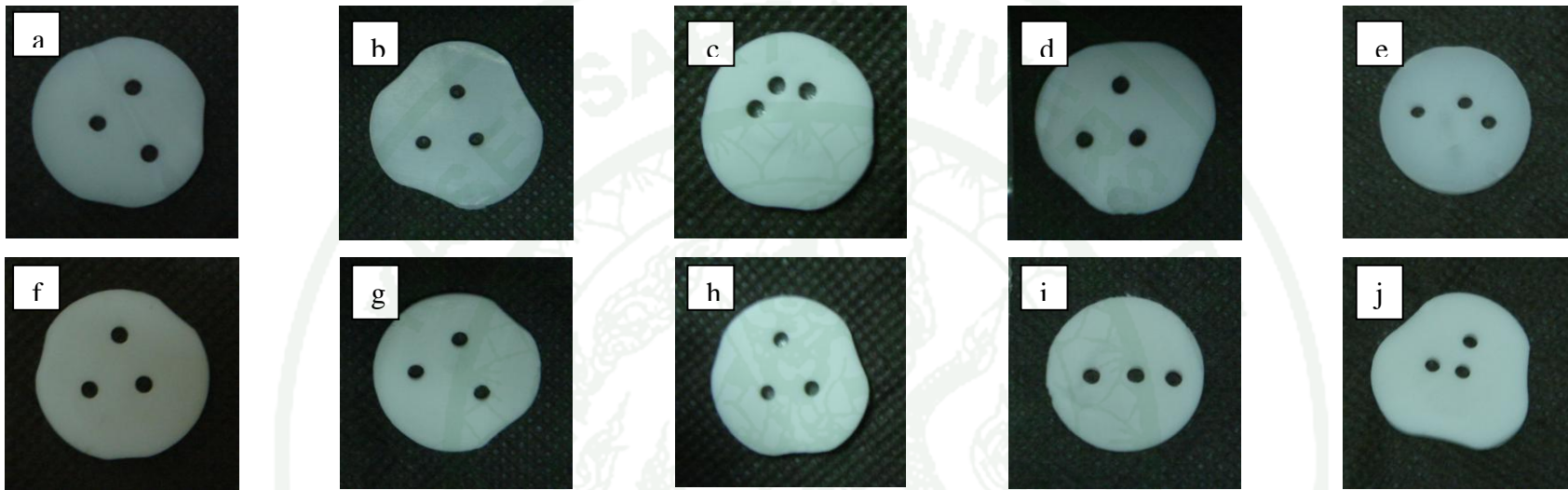


Figure 54 Drilling test for the heat-treated glass-ceramics after heat-treated at T_{p1} (above line) and at T_{p2} (below line):
 (a) and (f) of GCF3.0, (b) and (g) of GCF3.5, (c) and (h) of GCF4.0, (d) and (i) of GCF4.5, and (e) and (j) of GCF5.0.

3.3 Coefficient of thermal expansion

The coefficient of thermal expansion (CTE) is totally important for applications such as using combination with other materials. For glass-ceramic materials, the thermal expansion depends on their type and content of crystalline phases (Strnad, 1986).

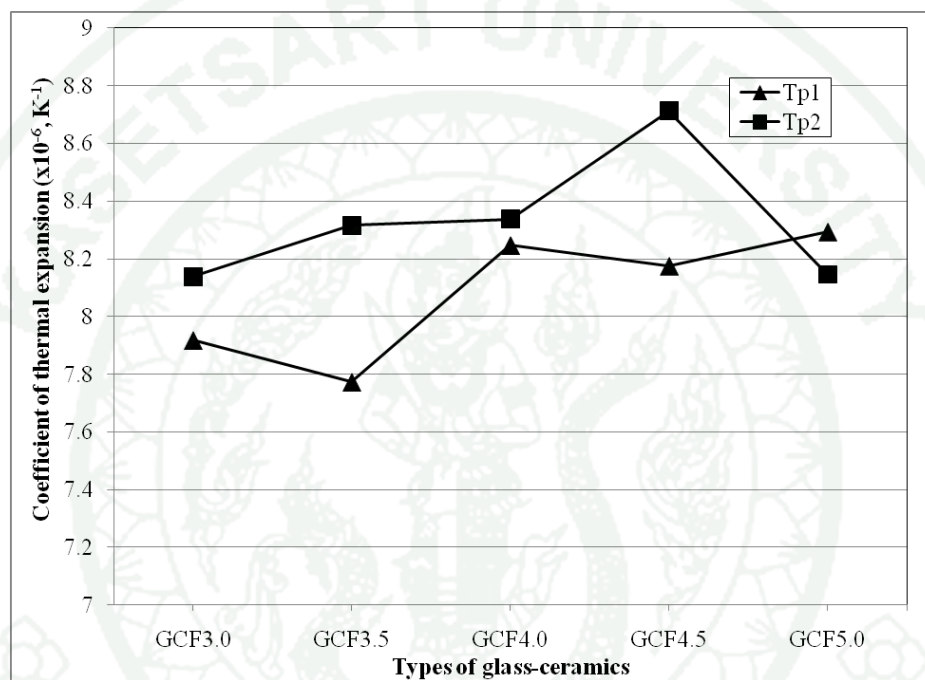


Figure 55 Coefficient of thermal expansion of all glass-ceramics.

From XRD results, the degree of crystallinity of the glass-ceramics is induced when the chemical compositions of fluorapatite and crystallization temperature of heat treatment increase. The consequent results presented in Figure 55 are found that an increase in amount of fluorapatite compositions enhances a rise of CTE values. In addition, the higher temperatures of heat treatment affect also CTE.

Table 8 Coefficient of thermal expansion of restorative materials ($\times 10^{-6}$, K^{-1}).

Material	Coefficient of thermal expansion
Dicor	7.2
In-Ceram alumina	7.4
Empress 2	10.6
Procera Zirconia Y-TZP	10.4

Source: Ban (2008)

3.4 Chemical solubility

Generally, the chemical solubility of glass-ceramic materials is affected by the composition of the crystalline phases and by the composition and the number of residual glass phases as well as its morphology. Alkali metal ions are much more stable in the crystalline phase than in the residual glass phase. Therefore, the residual glass phases in glass-ceramic materials should not contain high concentrations of alkali oxides so that they have good chemical resistance (Strnad, 1986). In addition, chemical stability of glass-ceramics is able to be improved by alkali earth oxides such as MgO and CaO due to the increased volume of crystalline phases (McMillan, 1979).

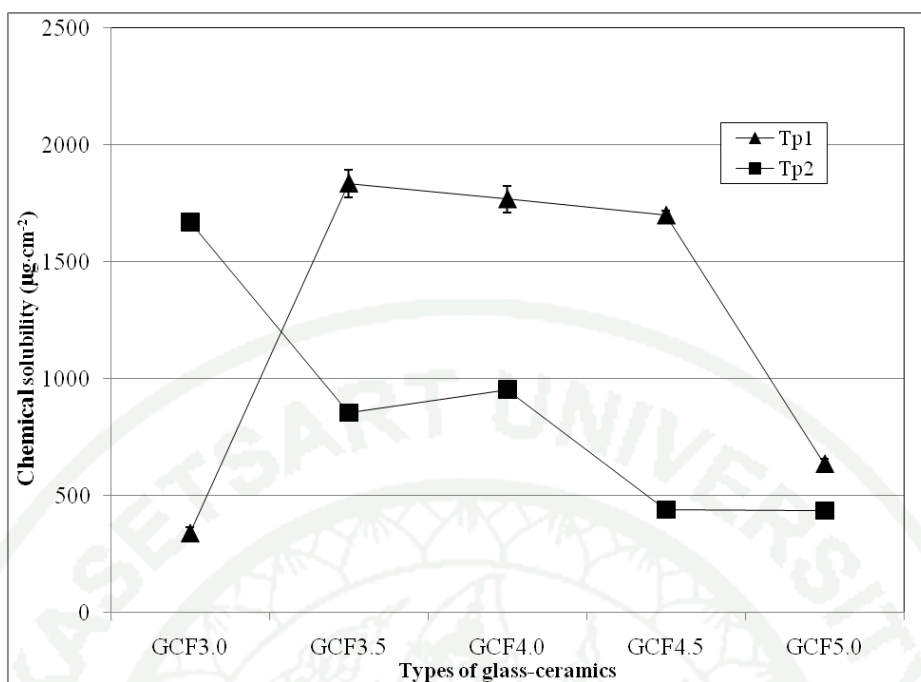


Figure 56 Chemical solubility of all glass-ceramics in 4%(v/v) acetic acid.

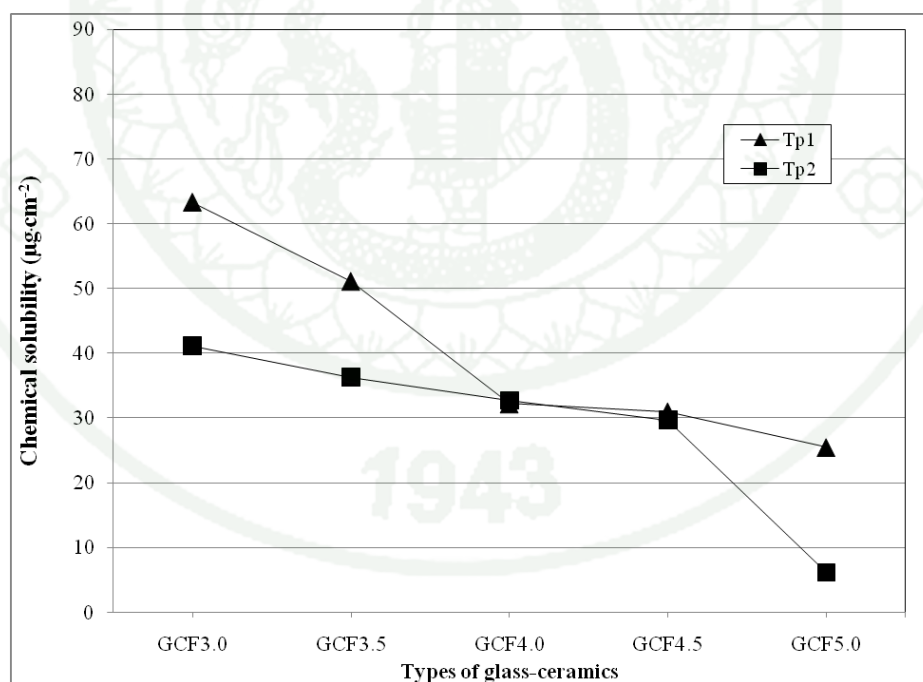


Figure 57 Chemical solubility of all glass-ceramics in distilled water.

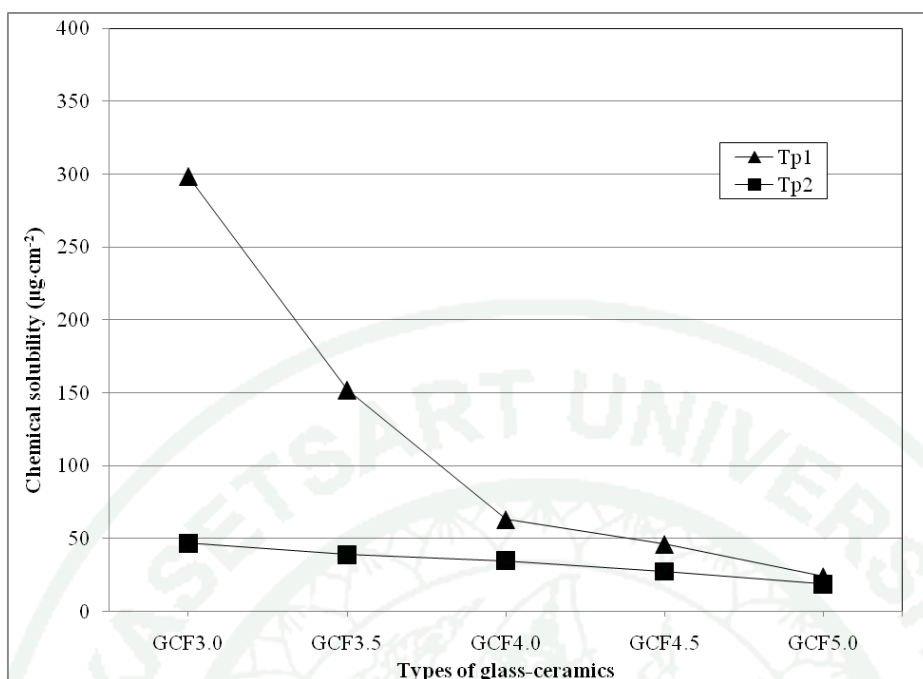


Figure 58 Chemical solubility of all glass-ceramics in 0.1 M sodium hydroxide.

In Figures 56-58, it is found that the glass-ceramics are capable of resisting in the distilled water, based and acidic environment, respectively. Moreover, the chemical solubility depends upon the fluorapatite contents and heat treatment temperatures. CaO resulted from thermal decomposition of CaCO_3 is one of the components of formation of the fluorapatite content in glass-ceramics, therefore, the more added components of CaCO_3 , the higher chemical durability of glass-ceramics. These results were related to the research of Taruta (Taruta *et al.*, 2001). At the same compositions, the higher temperatures of heat-treatment enhances the lower chemical solubility since they contain a larger amount of the degree of crystallinity as comparing with the lower temperatures of those.

Normally, the chemical solubility of the core ceramic materials must be less than $2000 \mu\text{g}\cdot\text{cm}^{-2}$ and that of the body ceramic materials contacting directly with the oral environment should be less than $100 \mu\text{g}\cdot\text{cm}^{-2}$ (ISO 6872, 2008) as show in Table 2. Therefore, all glass-ceramics in this research are acceptable according to ISO 6872:2008(E) as core ceramics considering in terms of chemical solubility.

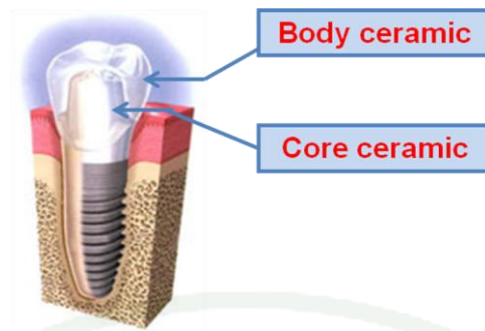
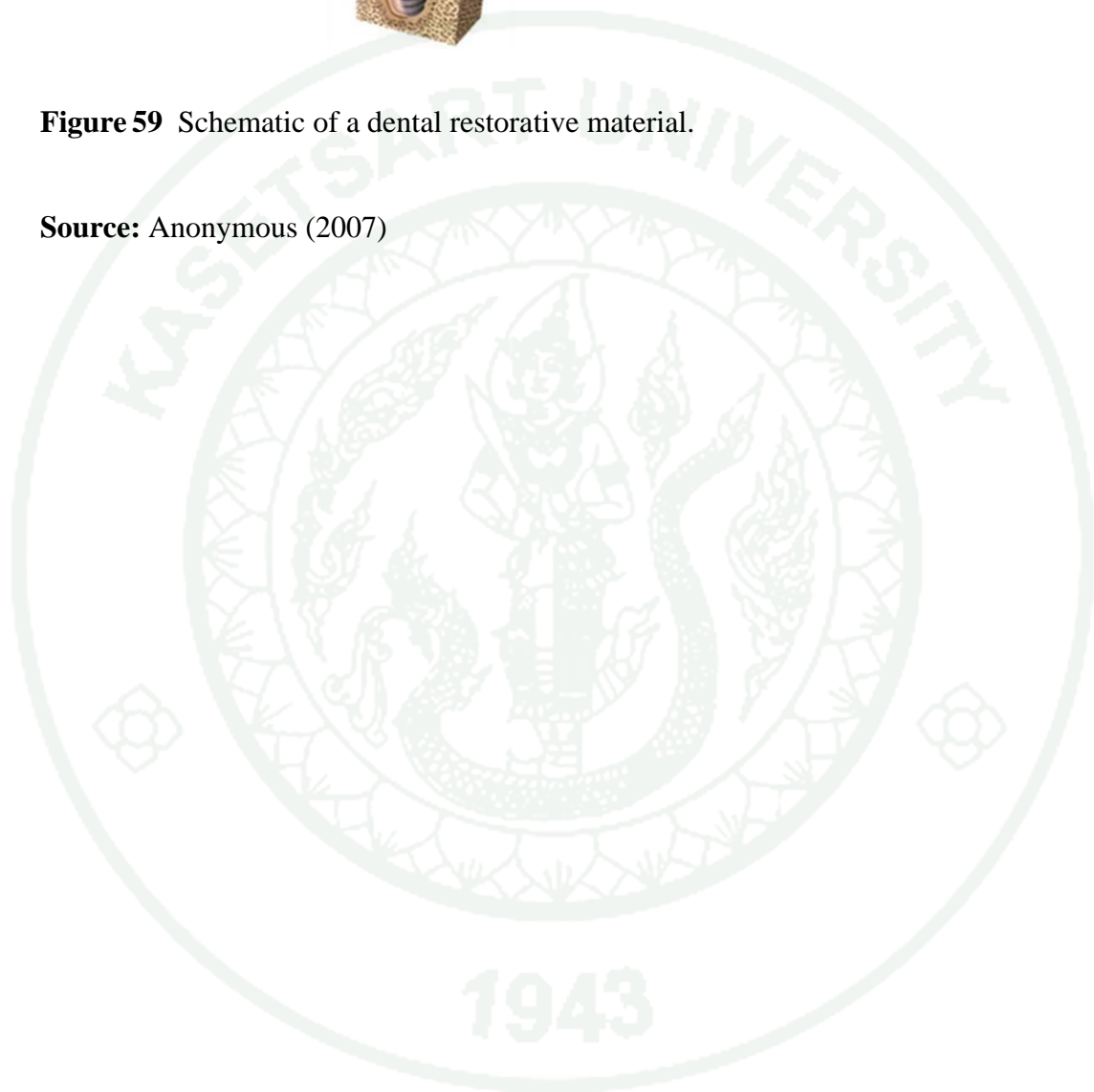


Figure 59 Schematic of a dental restorative material.

Source: Anonymous (2007)



CONCLUSIONS AND RECOMMENDATIONS

Conclusions

The main crystalline phases of the prepared glass-ceramics possessed fluorapatite and calcium mica, which were confirmed with XRD and SEM results. The mechanical and chemical properties of all glass-ceramics in this experiment were acceptable by ISO 6872:2008(E) as dental ceramic type II class 2 as a substructure ceramic for single-unit anterior or posterior prostheses. From the results of mechanical properties and chemical solubility, all glass-ceramics could be used for dental restorations as core materials, especially GCF3.5 heat-treated at T_{p1} . However, it needs to be developed further in order for similarity to natural human teeth.

Recommendation

Because all glass-ceramics could be machined by drilling without difficulties, it is possible to fabricate further with CAD/CAM techniques.

LITERATURE CITED

- Anonymous. 2005. **Inlays, Onlays from Aurora Colorado Dentiat-Main Street Dental.** General Treatment. Available Source: <http://www.southlandsdentistry.com/dental-information/general-treatment/inlays-onlays>, September 15, 2009.
- Anonymous. 2007. **Experienced Service of Dental Implant in Thailand by Bangkok Dental Image.** Bangkok Dental Image. Available Source: http://www.bangkokdentalimage.com/English/Thailand_dental_implant.html, December 28, 2009.
- Anonymous. 2008. **CA Esthetics-Cad/Cam technology.** California Esthetics. Available Source: <http://www.california-esthetics.com/Cad-Cam-Technology.html>, November 8, 2009.
- Ban, S. 2008. Reliability and Properties of Core Materials for All-Ceramic Dental Restorations. **Jpn. Dent. Sci. Rev.** 44: 3-21.
- Barth, A.P., Kropf, C. and T. Poth. 2007. **Oral and Dental Care Product.** U.S. Patent 20070154411 A1.
- Bogdanov, B.I., Pashev, P.S., Hristov, J.H. and I.G. Markovska. 2008. Bioactive Fluorapatite-Containing Glass-Ceramics. **Ceram. Int.** 35: 1651-1655.
- Brodkin, D., Panzera, C. and P. Panzera. 2003. **Machinable glass-ceramics.** U.S. Patent 6645285B2.
- Conrad, H.J., Seong, W.J. and I.J. Pesun. 2007. Current Ceramic Materials and Systems with Clinical Recommendations: A Systematic Review. **J. Prosthet. Dent.** 98: 389404.

- Denry, I.L. 1996. Recent Advances in Ceramics for Dentistry. **Crit.Rev. Oral. Bio.Med.** 7: 134-143.
- Fathi, H., Johnson, A., Noort, R.V., Ward, J.M. and L.M. Brook. 2005. The Effect of Calcium Fluoride (CaF₂) on the Chemical Solubility of an Apatite-Mullite Glass-Ceramic Material. **Dent. Mater.** 21: 551-556.
- Fathi, H., Johnson, A., Noort, R.V., Ward, J.M. and L.M. Brook. 2005. The Influence of Calcium Fluoride (CaF₂) on Biaxial Flexural Strength of Apatite-Mullite Glass-Ceramic Material. **Dent. Mater.** 21: 846-851.
- Feng, Y.Z., Wang, Y.C., Tan, Y.N., Liu, Y., Xian, Q.J. and X.X. Seng. 2007. Bioactivity of Mica/Apatite Glass Ceramics. **Trans. Nonferrous. Met. Soc. China** 17: 828-831.
- Liu, Y., Xiang, Q., Sheng, X. and X. Dan. 2008. Nucleation and Growth of Needle-Like Fluorapatite Crystals in Bioactive Glass-Ceramics. **J. Non-Cry. Sol.** 354: 938-944.
- Liu, Y., Xiang, Q., Sheng, X., Dan. X. and Q. Xiang. 2006. Preparation of Mica/Apatite Glass-Ceramics Biomaterials. **Mat. Sci. Eng.** 26: 1390-1394.
- Gallagher, P.K. and M.E. Brown. 2003. **Handbook of Thermal Analysis and Calorimetry: Application to Inorganic and Miscellaneous Materials.** Elsevier, Amsterdam.
- Grossman, D.G. and J.L.M Johnson. 1987. **Glass-Ceramic Compositions for Dental Constructs.** U.S. Patent 4,652,312.
- Habelitz, S., Carl, G., Rüssel, C., Thiel, S., Gerth, U., Schnapp, J.D., Jordanov, A. and H. Knake. 1997. Mechanical Properties of Oriented Mica Glass Ceramic. **J. Non-Cry. Sol.** 220: 291-298.

- Happer, C.A. 2001. **Handbook of Ceramics, Glasses, and Diamonds**. McGraw-Hill, New York.
- Hench, L.L. and J. Wilson. 1993. **An Introduction to Bioceramics**. World Scientific Publishing, Singapore.
- Höhne, G.W.H, Hemminger, W.F. and H.-J. Flammersheim. 2003. **Differential Scanning Calorimetry**. Springer-Verlag Berlin Heidelberg, New York.
- Höland, W. and G. Beall. 2006. **Glass-Ceramic Technology**. American Ceramic Society, United States of America.
- Höland, W., Rheinberger, V., Apel, E., Hoen, C.V., Höland, M., Dommann, A., Obrecht, M., Mauth, C. and U. Graf-Hausner. 2006. Clinical Applications of Glass-Ceramics in Dentistry. **J. Mater. Sci.** 17: 1037-1042.
- Höland, W., Rheinberger, V., Apel, E., Ritzberger, C., Rothbrust, F., Kappert, H., Krumeich, F. and R. Nesper. 2008. Future Perspectives of Biomaterials for Dental Restoration. **J. Eur. Ceram. Soc.** 29: 1291-1297.
- Ironside, J.G. and M.V. Swain. 1998. **Ceramics in Dental Restorations – A Review and Critical Issues**. The A to Z of materials. Available source: <http://www.azom.com/Details.asp?ArticleID=1682>
- Kingery, W.D., Bowen, H.K. and D.R. Uhlmann. 1991. **Introduction to Ceramics**. 2nd ed. John Wiley & Sons, Inc., Singapore.
- Pilathadka S., Vahalová D. and T. Vosáhló. 2007. The Zirconia: a New Dental Ceramic Material. An Overview. **Prague Medical Report**. 108: 5–12.
- Pinasco, M.R., Natali, A., Loria, P., Bolla, M. and F.J. Hagege. 2007. Dental Materials and Implants, pp. 601-654. In Rolando Barbucci, ed. **Integrated Biomaterials Science**. Kluwer Academic/Plenum, New York.

Powers, J.M. and R.L. Sakaguchi. 2006. **Craig's Restorative Dental Materials**. 12th ed. Elsevier Inc, United States of America.

McColm, I.J. 1990. **Ceramic Hardness**. Plenum Press, New York.

McMillan, P.W. 1979. **Glass-Ceramics**. Academic Press, London.

Moiescu, C., Höche, T., Carl, G., Keding, R., Rüssel, C. and W.D. Heerdegen. 2001. Influence of the Ca/P Ratio on the Morphology of Fluorapatite Crystals in SiO₂-Al₂O₃-CaO-P₂O₅-K₂O-F⁻ Glass-Ceramics. **J. Non-Cry. Sol.** 289: 123-134.

Mojumdar, S.C., Kozánková, J., Chocholousek, J., Majling, J. and D. Fábryová. 2004. Fluoroapatite-Material for Medicine Growth, Morphology and Thermoanalytical Properties. **J. Therm. Anal. Cal.** 78: 73-82.

Rafferty, A., Clifford, A. and R. Hill. 2000. Influence to Fluorine Content in Apatite-Mullite Glass-Ceramics. **J. Am. Ceram. Soc.** 83: 2833-2838.

Scherrer, S.S., Denry, I.L. and H.A. Wiskott. 1998. Comparison of Three Fracture Toughness Testing Techniques Using a Dental Glass and a Dental Ceramic. **Dent. Mater.** 14:246-255.

Smyth, S.C. 2007. **High-Tech Dentistry**. CEREC-How it's done. Available Source: <http://www.drcerec.co.uk/Flash%20Presentations/CEREC%20-%20How%20it's%20done.htm>, July 25, 2009.

Strnad, Z. 1986. **Glass-Ceramic Materials**. Elsevier, New York.

Whitters, C.J., Strang, R., Brown, D., Clarke, R.L., Curtis, R.V., Hatton, P.V., Ireland, A.J., Lloyd, C.H., McCabe, J.F., Nicholson, J.W., Scrimgeour, S.N., Setcos, J.C., Sherriff, M., Noort, R.V., Watts, D.C. and D. Wood. 1999. Dental Materials: 1997 Literature Review. **J. Dent.** 27: 401-435.

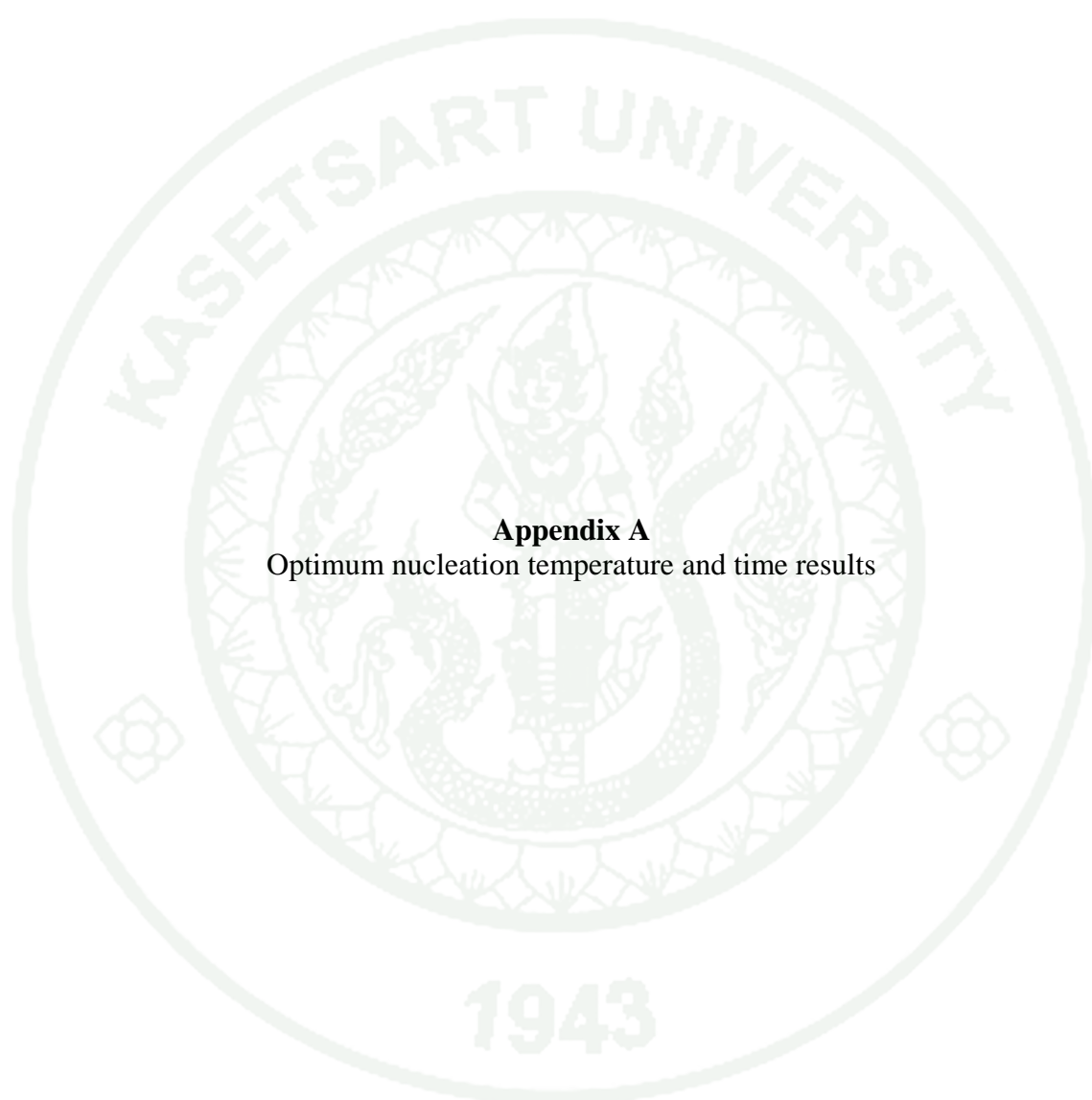
Xiang, Q., Liu, Y., Sheng, X. and X. Dan. 2007. Preparation of Mica-Based Glass-Ceramics with Needle-Like Fluorapatite. **Dent. Mater.** 23: 251-258.

Yu, L., Xiao, H. and Y. Cheng. 2006. Influence of Magnesia on the Structure and Properties of MgO-Al₂O₃-SiO₂-F- Glass-Ceramics. **Ceram. Int.** 34: 63-68.

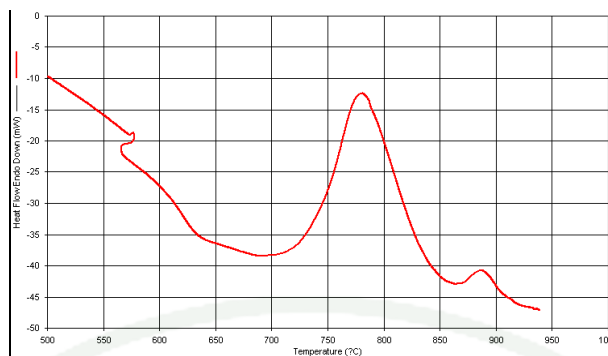
Zachariasen, W.H. 1932. The Atomic Arrangement in Glass. **J. Am. Chem. Soc.** 54: 3841-3851.



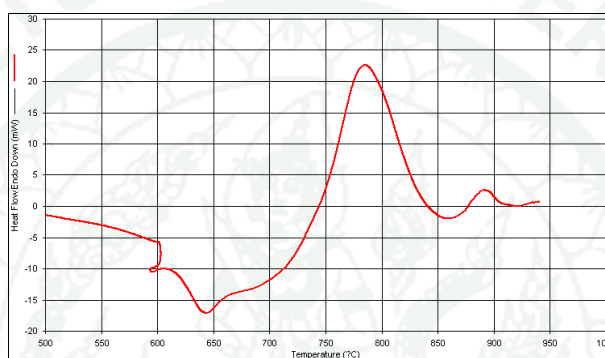
APPENDICES



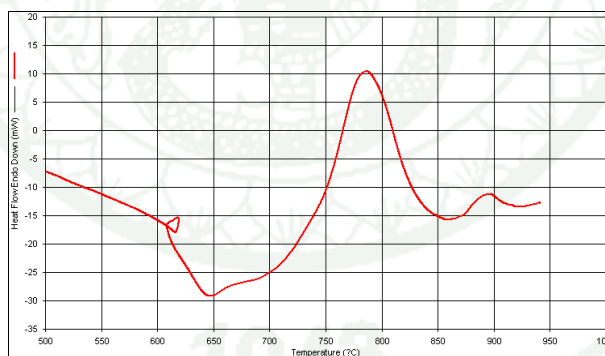
Appendix A
Optimum nucleation temperature and time results



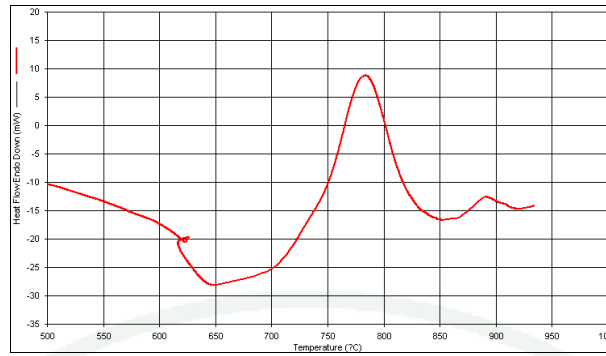
Appendix Figure A1 Crystallized GCF3.0 hold at $T_g - 30$ °C for 1.0 hour.



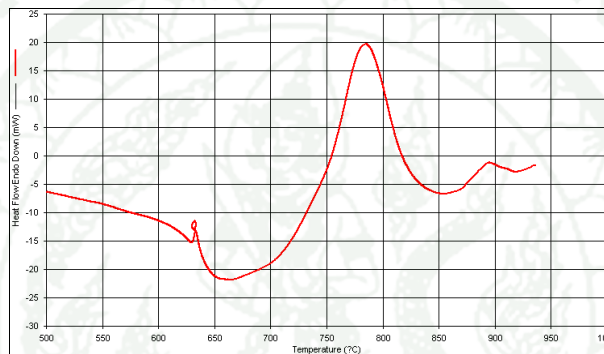
Appendix Figure A2 Crystallized GCF3.0 hold at $T_g - 15$ °C for 1.0 hour.



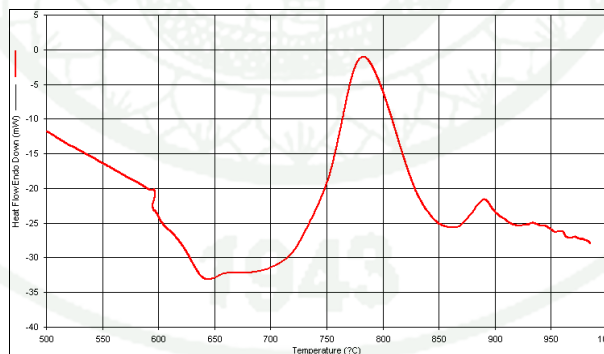
Appendix Figure A3 Crystallized GCF3.0 hold at T_g °C for 1.0 hour.



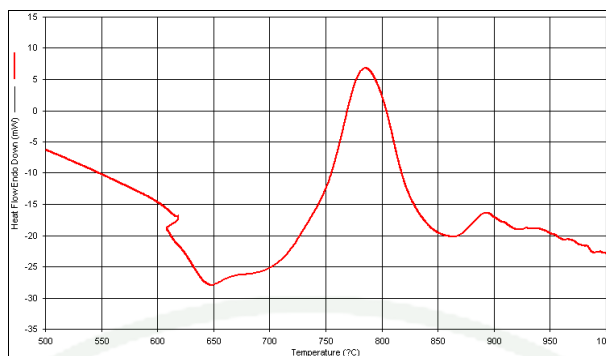
Appendix Figure A4 Crystallized GCF3.0 hold at T_g+15 °C for 1.0 hour.



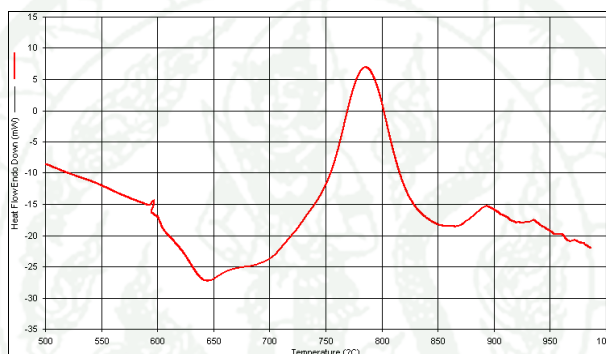
Appendix Figure A5 Crystallized GCF3.0 hold at T_g+30 °C 1.0 for hour.



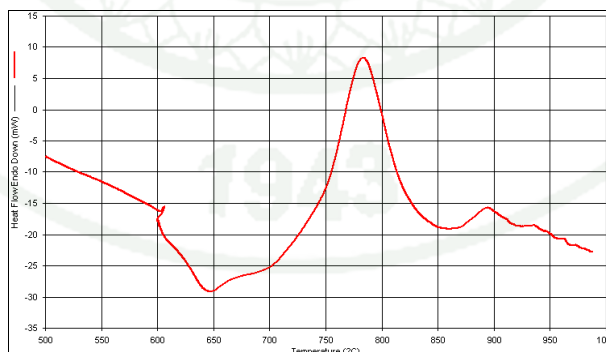
Appendix Figure A6 Crystallized GCF3.0 hold at optimum nucleation of T_{p1} for 0.5 hours.



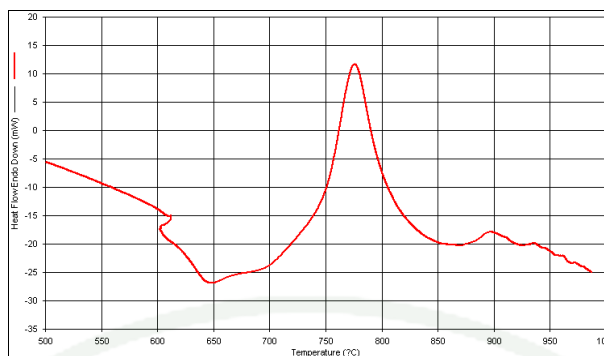
Appendix Figure A7 Crystallized GCF3.0 hold at optimum nucleation of T_{p1} for 1.0 hours.



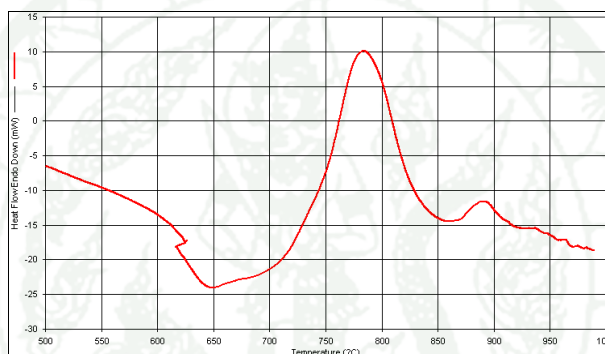
Appendix Figure A8 Crystallized GCF3.0 hold at optimum nucleation of T_{p1} for 2.0 hours.



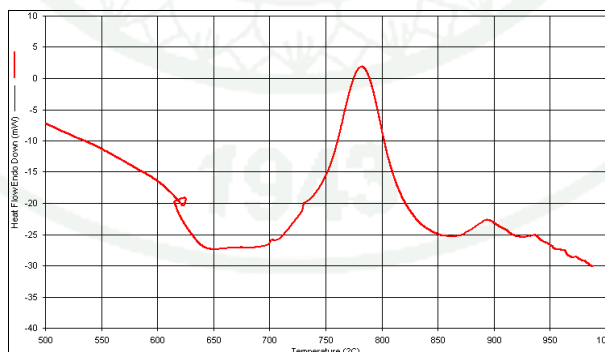
Appendix Figure A9 Crystallized GCF3.0 hold at optimum nucleation of T_{p1} for 4.0 hours.



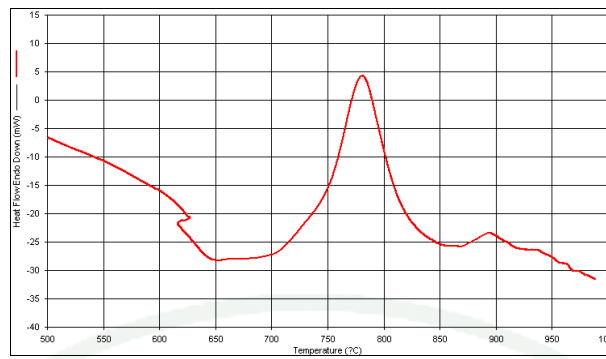
Appendix Figure A10 Crystallized GCF3.0 hold at optimum nucleation of T_{p1} for 10 hours.



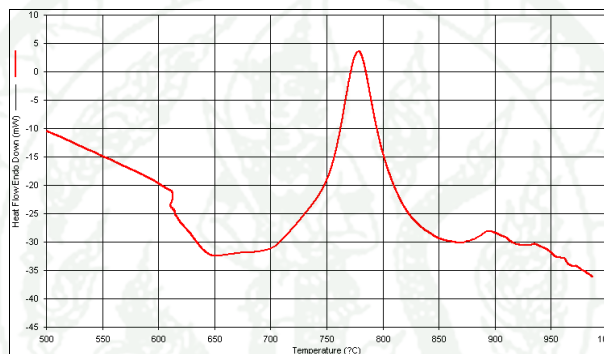
Appendix Figure A11 Crystallized GCF3.0 hold at optimum nucleation of T_{p2} for 0.5 hours.



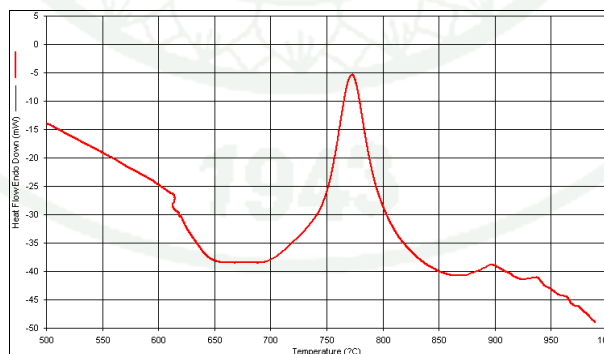
Appendix Figure A12 Crystallized GCF3.0 hold at optimum nucleation of T_{p2} for 1.0 hours.



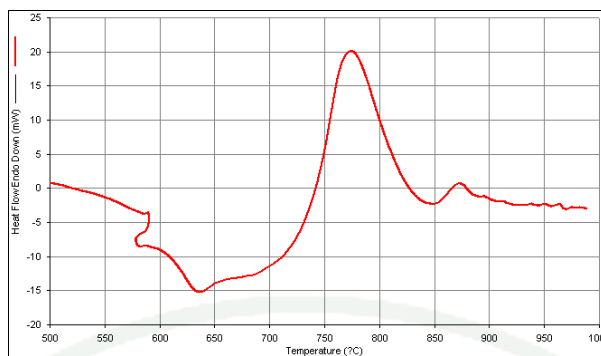
Appendix Figure A13 Crystallized GCF3.0 hold at optimum nucleation of T_{p2} for 2.0 hours.



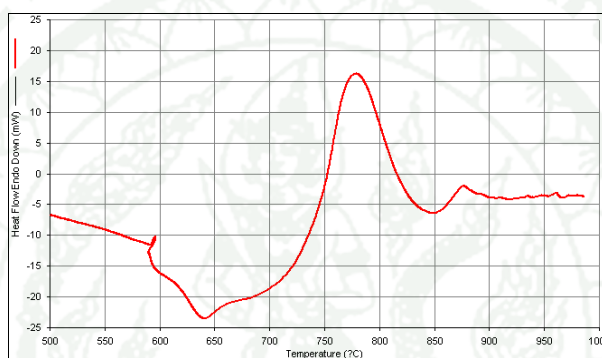
Appendix Figure A14 Crystallized GCF3.0 hold at optimum nucleation of T_{p2} for 4.0 hours.



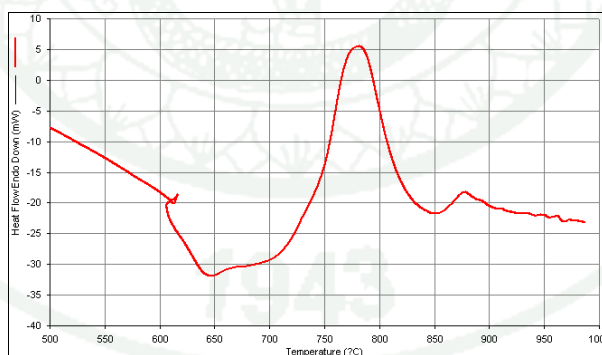
Appendix Figure A15 Crystallized GCF3.0 hold at optimum nucleation of T_{p2} for 10 hours.



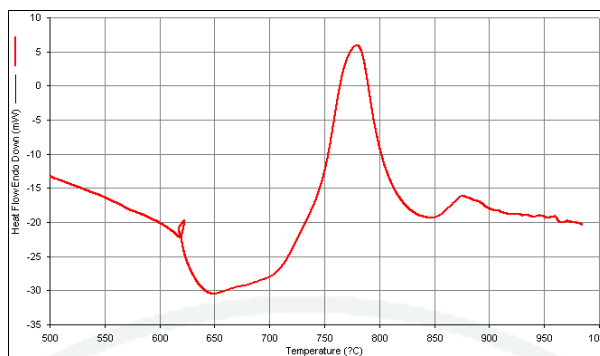
Appendix Figure A16 Crystallized GCF3.5 hold at $T_g - 30^\circ\text{C}$ for 1.0 hour.



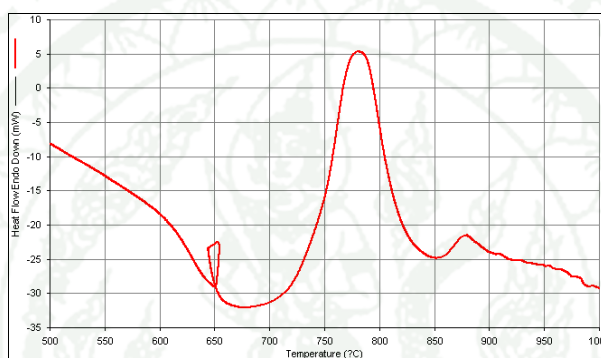
Appendix Figure A17 Crystallized GCF3.5 hold at $T_g - 15^\circ\text{C}$ for 1.0 hour.



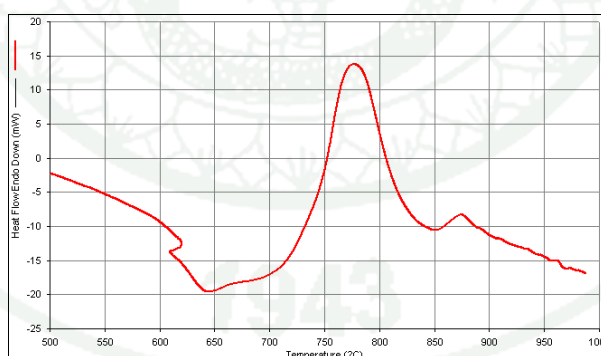
Appendix Figure A18 Crystallized GCF3.5 hold at T_g for 1.0 hour.



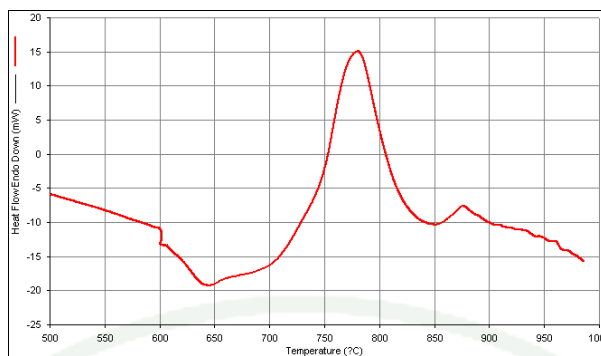
Appendix Figure A19 Crystallized GCF3.5 hold at $T_g + 15^\circ\text{C}$ for 1.0 hour.



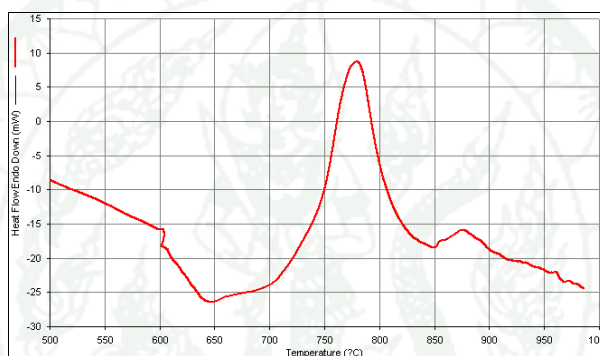
Appendix Figure A20 Crystallized GCF3.5 hold at $T_g + 30^\circ\text{C}$ for 1.0 hour.



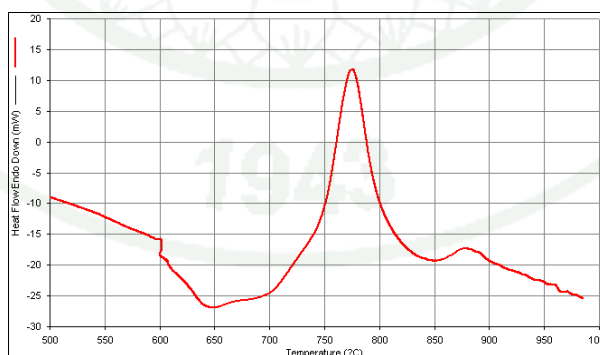
Appendix Figure A21 Crystallized GCF3.5 hold at optimum nucleation of T_{p1} for 0.5 hours.



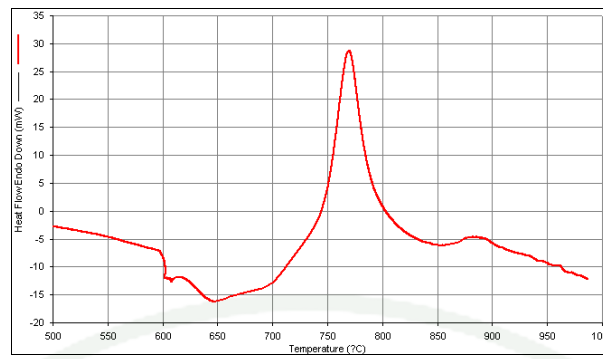
Appendix Figure A22 Crystallized GCF3.5 hold at optimum nucleation of T_{p1} for 1.0 hours.



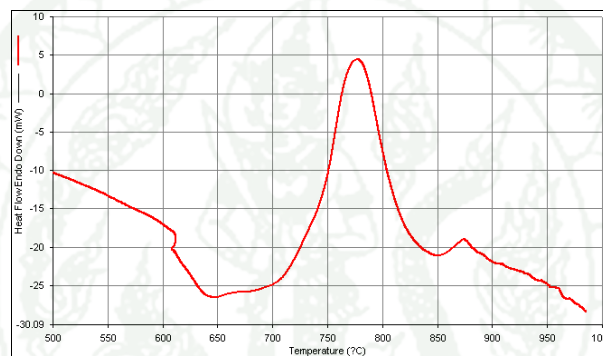
Appendix Figure A23 Crystallized GCF3.5 hold at optimum nucleation of T_{p1} for 2.0 hours.



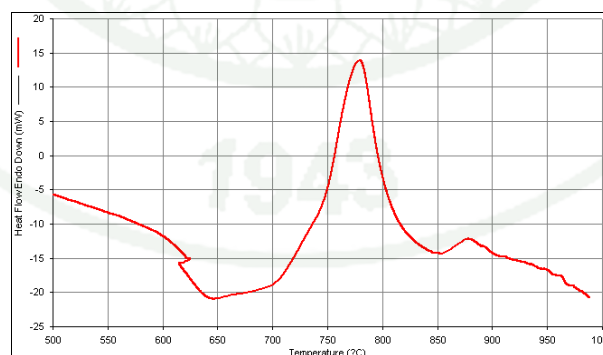
Appendix Figure A24 Crystallized GCF3.5 hold at optimum nucleation of T_{p1} for 4.0 hours.



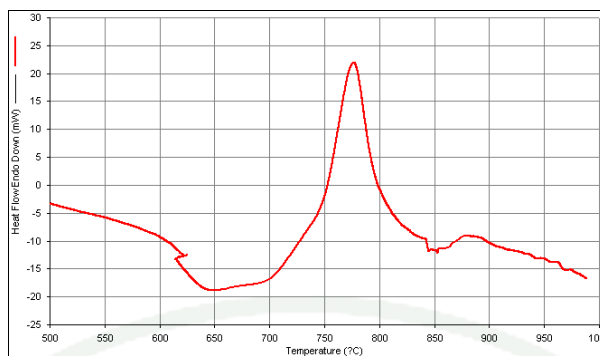
Appendix Figure A25 Crystallized GCF3.5 hold at optimum nucleation of T_{p1} for 10 hours.



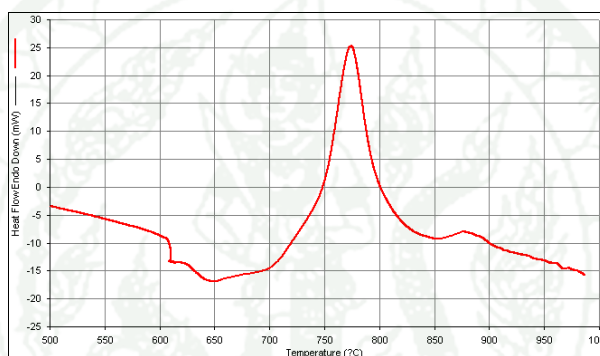
Appendix Figure A26 Crystallized GCF3.5 hold at optimum nucleation of T_{p2} for 0.5 hours.



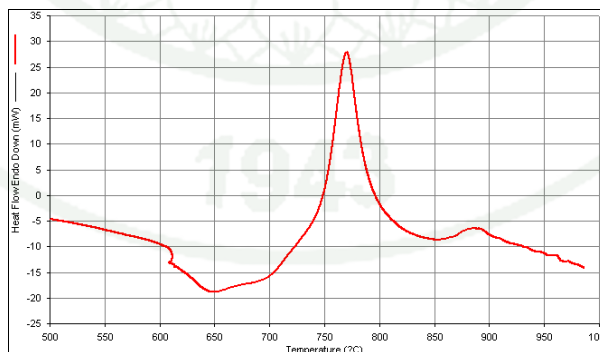
Appendix Figure A27 Crystallized GCF3.5 hold at optimum nucleation of T_{p2} for 1.0 hours.



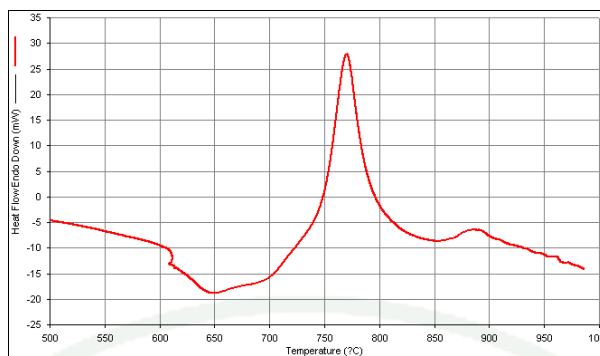
Appendix Figure A28 Crystallized GCF3.5 hold at optimum nucleation of T_{p2} for 2.0 hours.



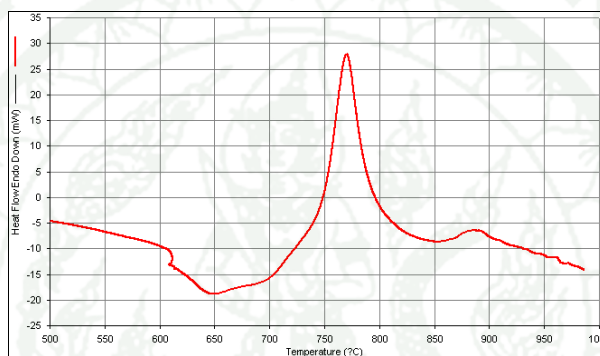
Appendix Figure A29 Crystallized GCF3.5 hold at optimum nucleation of T_{p2} for 4.0 hours.



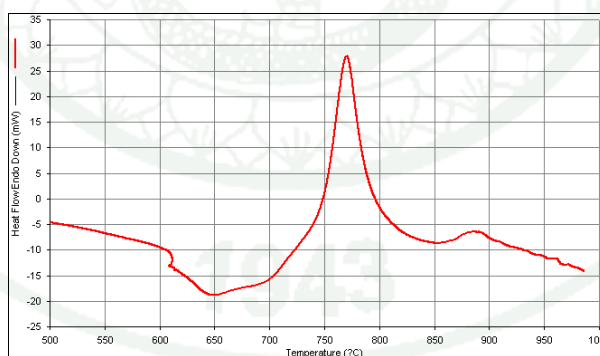
Appendix Figure A30 Crystallized GCF3.5 hold at optimum nucleation of T_{p2} for 10 hours.



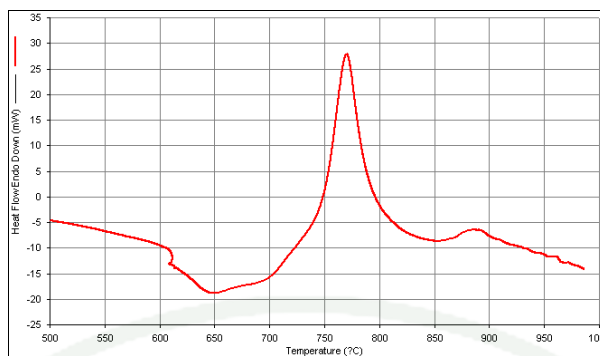
Appendix Figure A31 Crystallized GCF4.0 hold at $T_g - 30^\circ\text{C}$ for 1.0 hour.



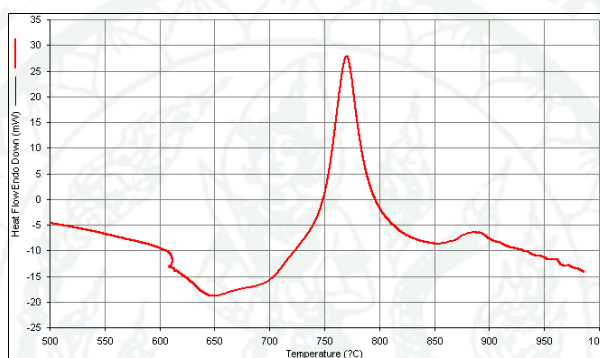
Appendix Figure A32 Crystallized GCF4.0 hold at $T_g - 15^\circ\text{C}$ for 1.0 hour.



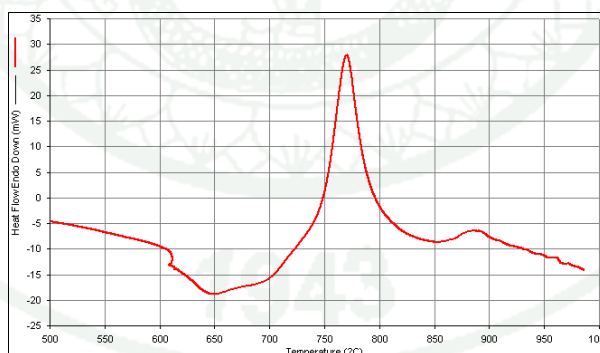
Appendix Figure A33 Crystallized GCF4.0 hold at T_g for 1.0 hour.



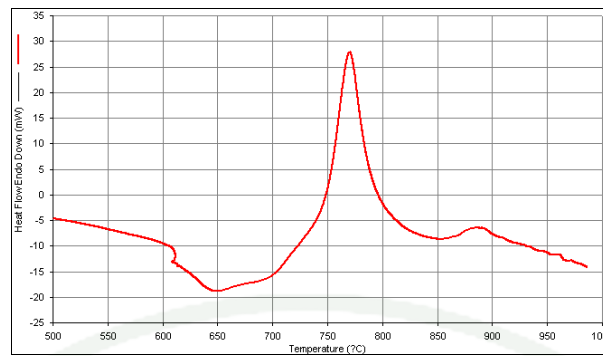
Appendix Figure A34 Crystallized GCF4.0 hold at $T_g + 15^\circ\text{C}$ for 1.0 hour.



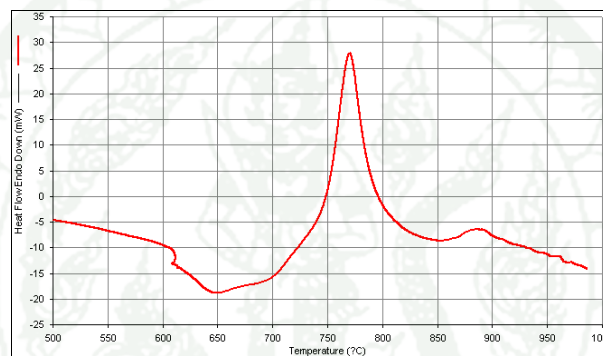
Appendix Figure A35 Crystallized GCF4.0 hold at $T_g + 30^\circ\text{C}$ for 1.0 hour.



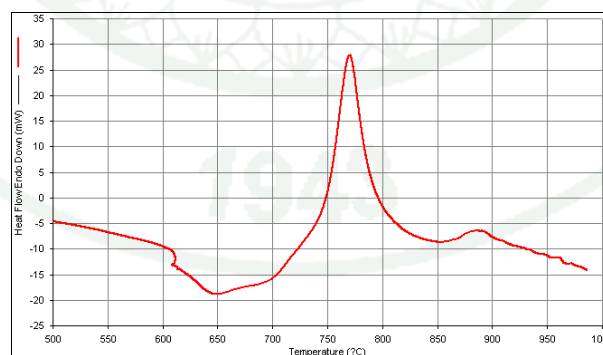
Appendix Figure A36 Crystallized GCF4.0 hold at optimum nucleation of T_{p1} for 0.5 hours.



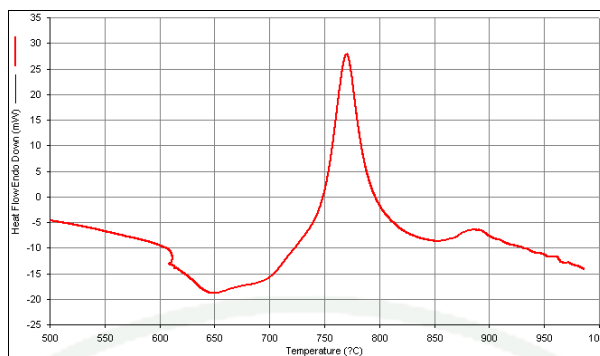
Appendix Figure A37 Crystallized GCF4.0 hold at optimum nucleation of T_{p1} for 1.0 hours.



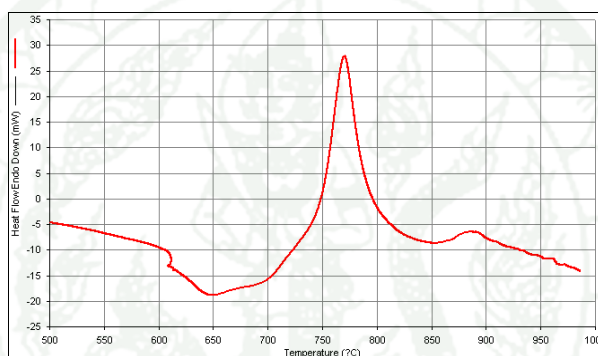
Appendix Figure A38 Crystallized GCF4.0 hold at optimum nucleation of T_{p1} for 2.0 hours.



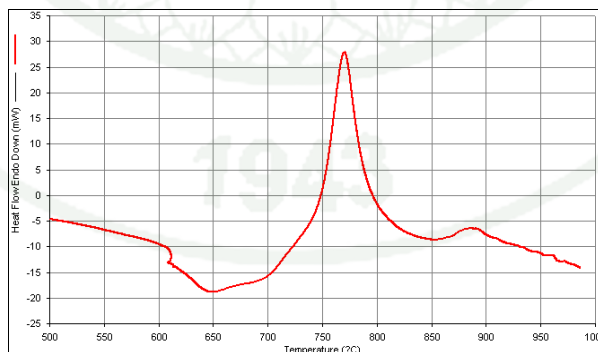
Appendix Figure A39 Crystallized GCF4.0 hold at optimum nucleation of T_{p1} for 4.0 hours.



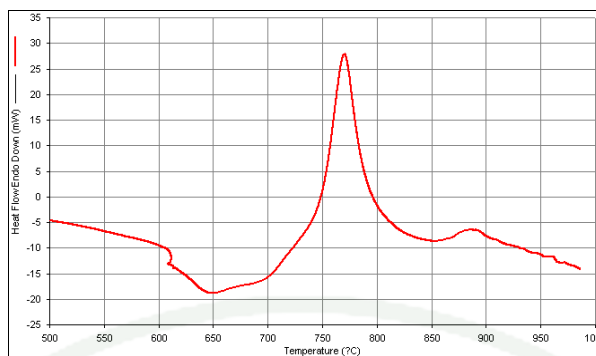
Appendix Figure A40 Crystallized GCF4.0 hold at optimum nucleation of T_{p1} for 10 hours.



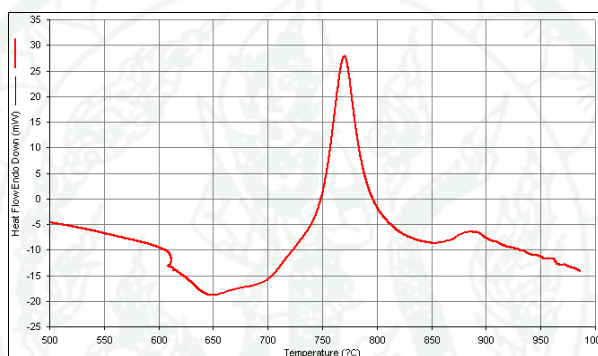
Appendix Figure A41 Crystallized GCF4.0 hold at optimum nucleation of T_{p2} for 0.5 hours.



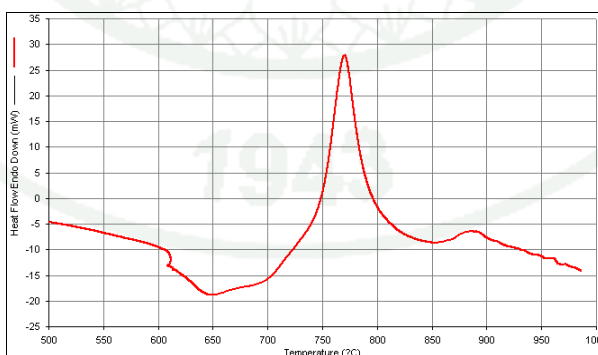
Appendix Figure A42 Crystallized GCF4.0 hold at optimum nucleation of T_{p2} for 1.0 hours.



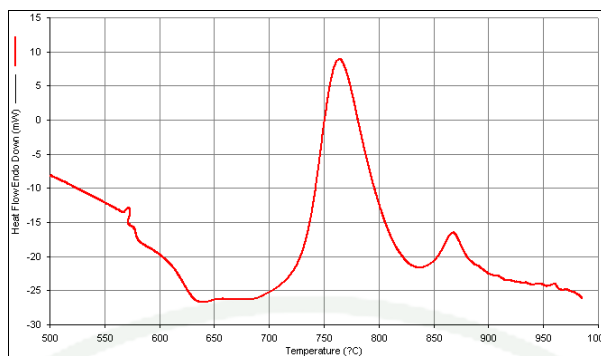
Appendix Figure A43 Crystallized GCF4.0 hold at optimum nucleation of T_{p2} for 2.0 hours.



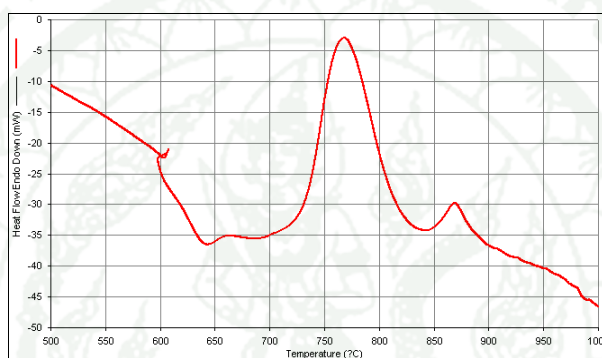
Appendix Figure A44 Crystallized GCF4.0 hold at optimum nucleation of T_{p2} for 4.0 hours.



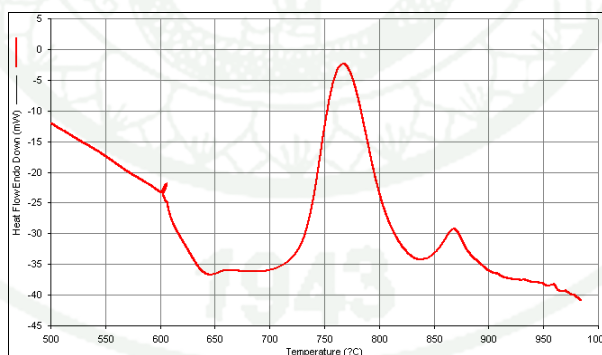
Appendix Figure A45 Crystallized GCF4.0 hold at optimum nucleation of T_{p2} for 10 hours.



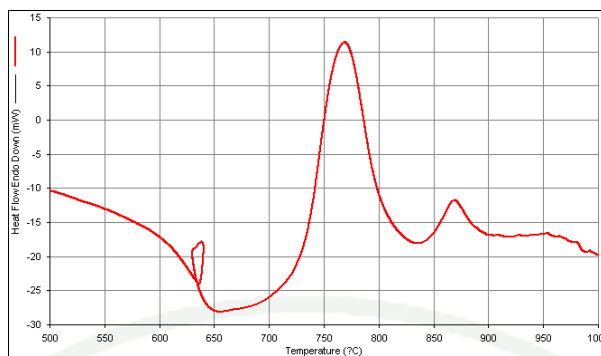
Appendix Figure A46 Crystallized GCF4.5 hold at $T_g - 30^\circ\text{C}$ for 1.0 hour.



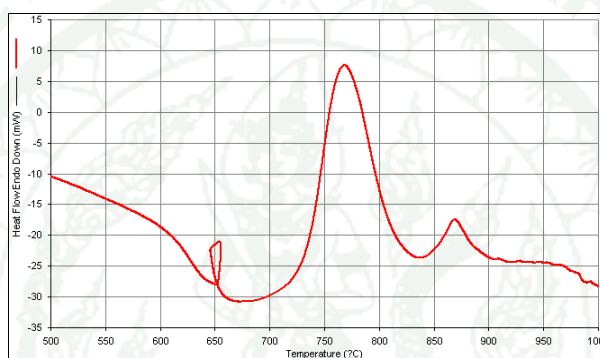
Appendix Figure A47 Crystallized GCF4.5 hold at $T_g - 15^\circ\text{C}$ for 1.0 hour.



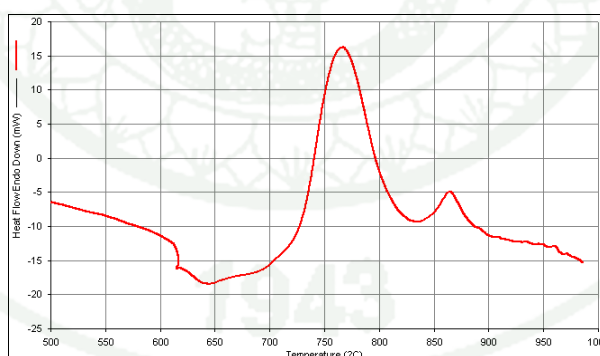
Appendix Figure A48 Crystallized GCF4.5 hold at T_g for 1.0 hour.



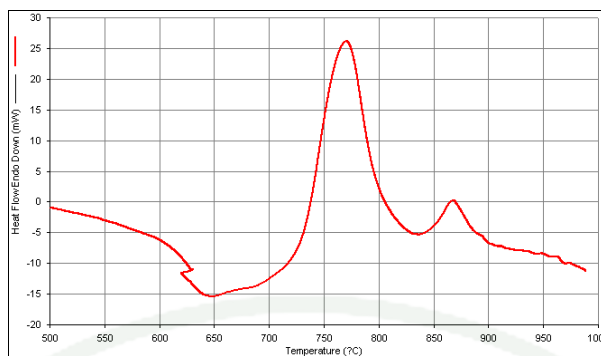
Appendix Figure A49 Crystallized GCF4.5 hold at $T_g+15^\circ\text{C}$ for 1.0 hour.



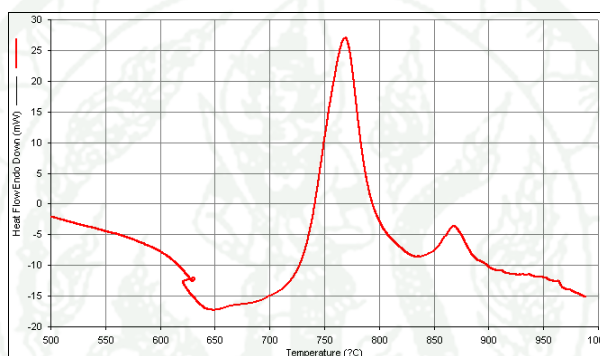
Appendix Figure A50 Crystallized GCF4.5 hold at $T_g+30^\circ\text{C}$ for 1.0 hour.



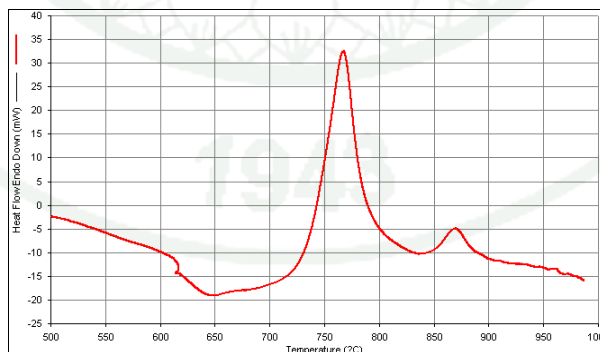
Appendix Figure A51 Crystallized GCF4.5 hold at optimum nucleation of T_{p1} for 0.5 hours.



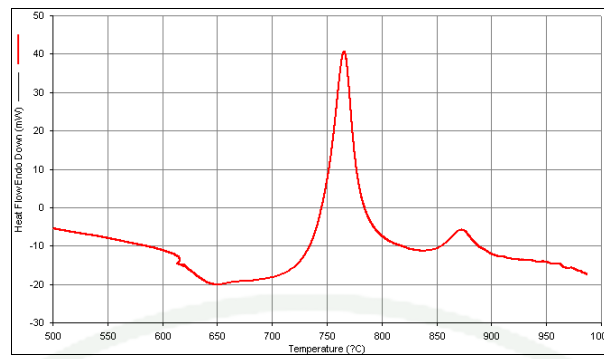
Appendix Figure A52 Crystallized GCF4.5 hold at optimum nucleation of T_{p1} for 1.0 hours.



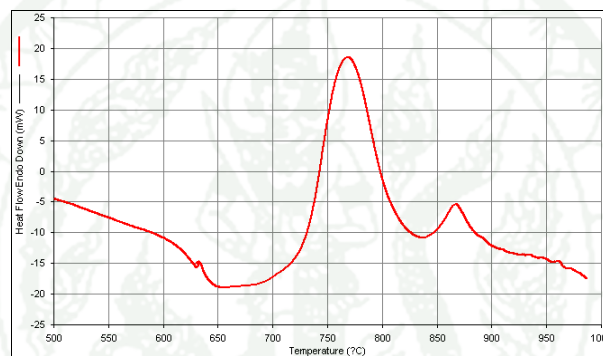
Appendix Figure A53 Crystallized GCF4.5 hold at optimum nucleation of T_{p1} for 2.0 hours.



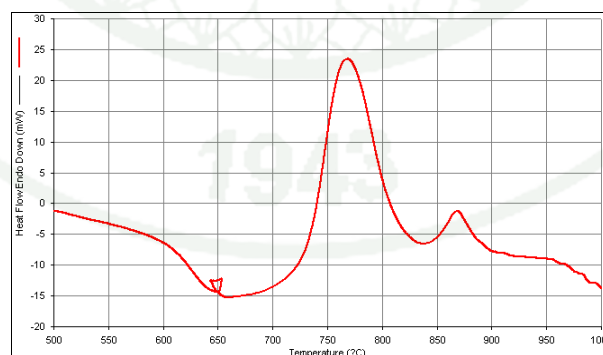
Appendix Figure A54 Crystallized GCF4.5 hold at optimum nucleation of T_{p1} for 4.0 hours.



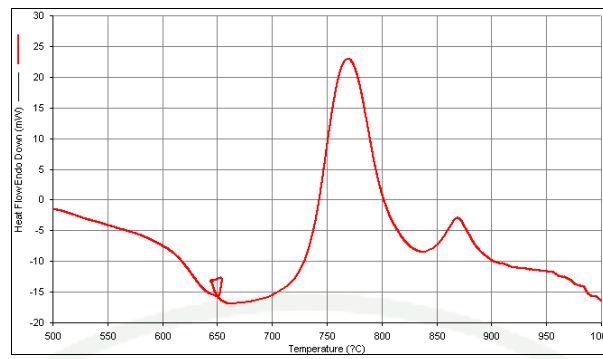
Appendix Figure A55 Crystallized GCF4.5 hold at optimum nucleation of T_{p1} for 10 hours.



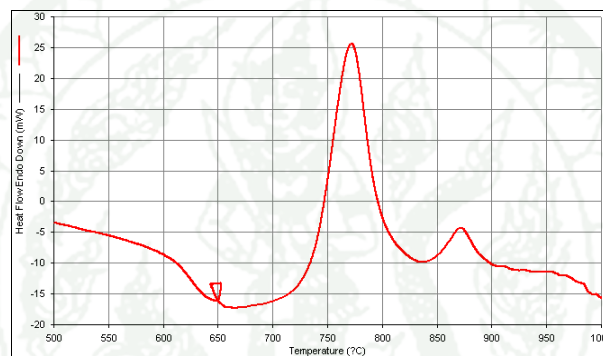
Appendix Figure A56 Crystallized GCF4.5 hold at optimum nucleation of T_{p2} for 0.5 hours.



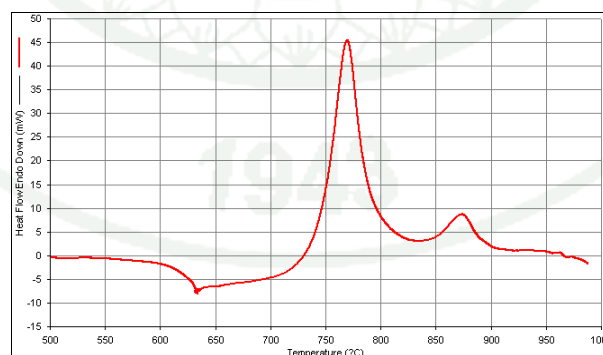
Appendix Figure A57 Crystallized GCF4.5 hold at optimum nucleation of T_{p2} for 1.0 hours.



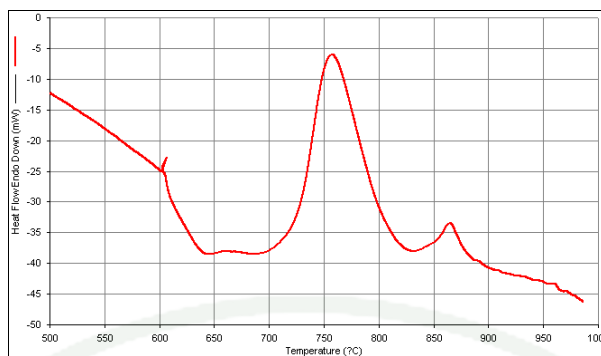
Appendix Figure A58 Crystallized GCF4.5 hold at optimum nucleation of T_{p2} for 2.0 hours.



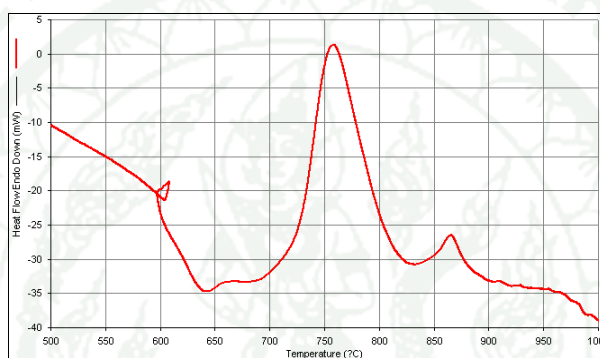
Appendix Figure A59 Crystallized GCF4.5 hold at optimum nucleation of T_{p2} for 4.0 hours.



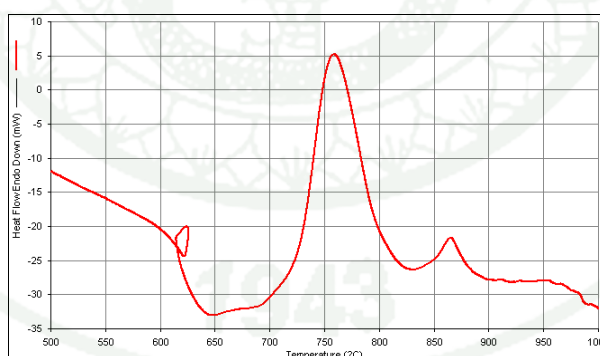
Appendix Figure A60 Crystallized GCF4.5 hold at optimum nucleation of T_{p2} for 10 hours.



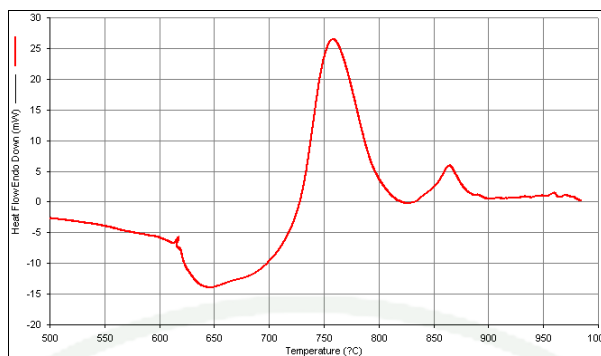
Appendix Figure A61 Crystallized GCF5.0 hold at $T_g - 30^\circ\text{C}$ for 1.0 hour.



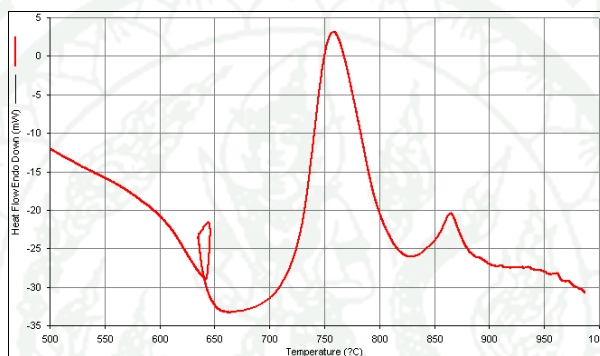
Appendix Figure A62 Crystallized GCF5.0 hold at $T_g - 15^\circ\text{C}$ for 1.0 hour.



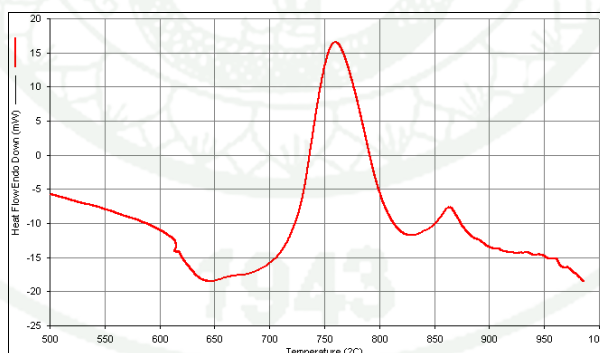
Appendix Figure A63 Crystallized GCF5.0 hold at T_g for 1.0 hour.



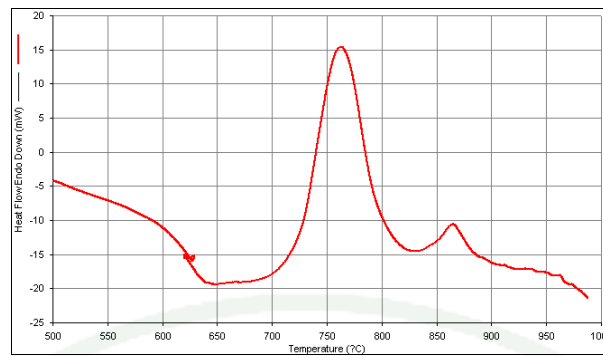
Appendix Figure A64 Crystallized GCF5.0 hold at $T_g + 15^\circ\text{C}$ for 1.0 hour.



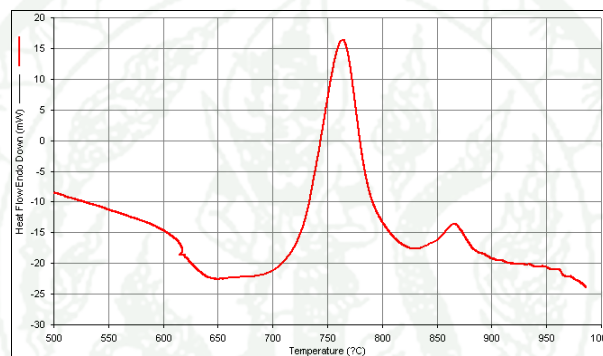
Appendix Figure A65 Crystallized GCF5.0 hold at $T_g + 30^\circ\text{C}$ for 1.0 hour.



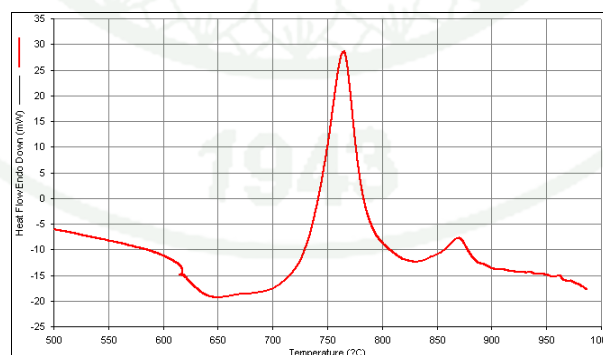
Appendix Figure A66 Crystallized GCF5.0 hold at optimum nucleation of T_{p1} for 0.5 hours.



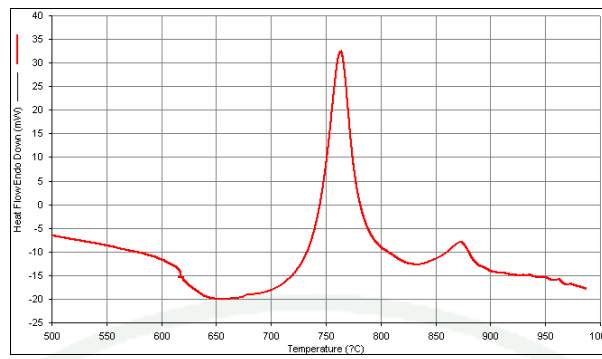
Appendix Figure A67 Crystallized GCF5.0 hold at optimum nucleation of T_{p1} for 1.0 hours.



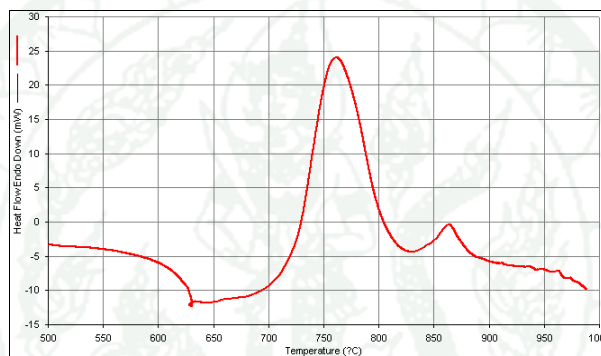
Appendix Figure A68 Crystallized GCF5.0 hold at optimum nucleation of T_{p1} for 2.0 hours.



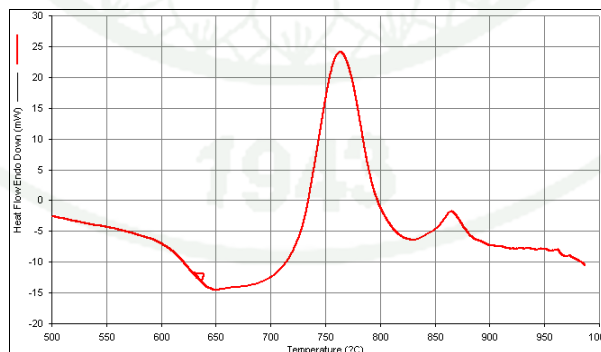
Appendix Figure A69 Crystallized GCF5.0 hold at optimum nucleation of T_{p1} for 4.0 hours.



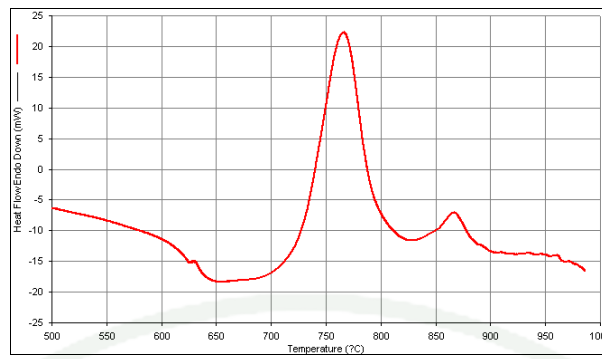
Appendix Figure A70 Crystallized GCF5.0 hold at optimum nucleation of T_{p1} for 10 hours.



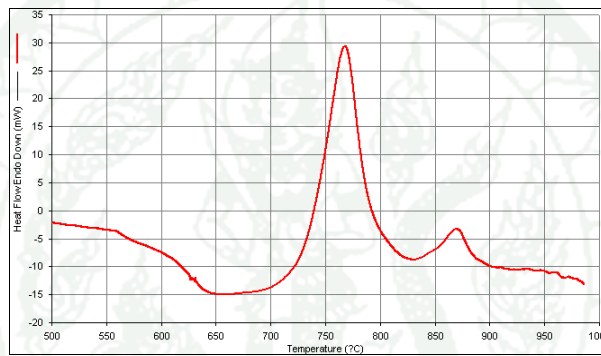
Appendix Figure A71 Crystallized GCF5.0 hold at optimum nucleation of T_{p2} for 0.5 hours.



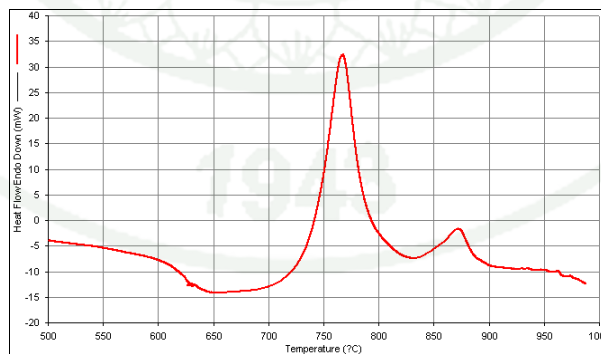
Appendix Figure A72 Crystallized GCF5.0 hold at optimum nucleation of T_{p2} for 1.0 hours.



Appendix Figure A73 Crystallized GCF5.0 hold at optimum nucleation of T_{p2} for 2.0 hours.



Appendix Figure A74 Crystallized GCF5.0 hold at optimum nucleation of T_{p2} for 4.0 hours.



Appendix Figure A75 Crystallized GCF5.0 hold at optimum nucleation of T_{p2} for 10 hours.

Appendix Table A1 Data of optimum nucleation temperature determination of heated GCF3.0 at T_{p1} .

Temperature with hold on 1 hour (°C)	T_{p1}	T_{p1}^*	$T_{p1}^* - T_{p1}$
Tg-30	782.944	784.39	1.446
Tg-15	782.944	785.366	2.422
Tg	782.944	786.341	3.397
Tg+15	782.944	782.764	-0.18
Tg+30	782.944	780.976	-1.968

Appendix Table A2 Data of optimum nucleation temperature determination of heated GCF3.0 at T_{p2} .

Temperature with hold on 1 hour (°C)	T_{p2}	T_{p2}^*	$T_{p2}^* - T_{p2}$
Tg-30	899.479	890.732	-8.747
Tg-15	899.479	891.707	-7.772
Tg	899.479	892.683	-6.796
Tg+15	899.479	892.764	-6.715
Tg+30	899.479	891.87	-7.609

Appendix Table A3 Data of optimum nucleation temperature determination of heated GCF3.5 at T_{p1} .

Temperature with hold on 1 hour (°C)	T_{p1}	T_{p1}^*	$T_{p1}^* - T_{p1}$
Tg-30	777.583	771.963	-5.62
Tg-15	777.583	777.103	-0.48
Tg	777.583	781.288	3.705
Tg+15	777.583	780.488	2.905
Tg+30	777.583	779.512	1.929

Appendix Table A4 Data of optimum nucleation temperature determination of heated GCF3.5 at T_{p2} .

Temperature with hold on 1 hour (°C)	T_{p2}	T_{p2}^*	$T_{p2}^* - T_{p2}$
Tg-30	876.024	873.171	-2.853
Tg-15	876.024	874.146	-1.878
Tg	876.024	877.073	1.049
Tg+15	876.024	877.873	1.849
Tg+30	876.024	876.098	0.074

Appendix Table A5 Data of optimum nucleation temperature determination of heated GCF4.0 at T_{p1} .

Temperature with hold on 1 hour (°C)	T_{p1}	T_{p1}^*	$T_{p1}^* - T_{p1}$
Tg-30	776.890	774.869	-2.023
Tg-15	776.890	775.952	-0.94
Tg	776.890	776.664	-0.228
Tg+15	776.890	778.174	1.282
Tg+30	776.890	776.323	-0.569

Appendix Table A6 Data of optimum nucleation temperature determination of heated GCF4.0 at T_{p2} .

Temperature with hold on 1 hour (°C)	T_{p2}	T_{p2}^*	$T_{p2}^* - T_{p2}$
Tg-30	776.890	879.251	-2.163
Tg-15	776.890	879.532	-1.882
Tg	776.890	879.977	-1.437
Tg+15	776.890	882.159	0.745
Tg+30	776.890	879.783	-1.631

Appendix Table A7 Data of optimum nucleation temperature determination of heated GCF4.5 at T_{p1} .

Temperature with hold on 1 hour (°C)	T_{p1}	T_{p1}^*	$T_{p1}^* - T_{p1}$
Tg-30	765.489	763.446	-2.043
Tg-15	765.489	765.854	0.365
Tg	765.489	766.770	1.281
Tg+15	765.489	767.750	2.261
Tg+30	765.489	767.166	1.677

Appendix Table A8 Data of optimum nucleation temperature determination of heated GCF4.5 at T_{p2} .

Temperature with hold on 1 hour (°C)	T_{p2}	T_{p2}^*	$T_{p2}^* - T_{p2}$
Tg-30	870.894	867.210	-3.684
Tg-15	870.894	867.539	-3.355
Tg	870.894	867.982	-2.912
Tg+15	870.894	868.726	-2.168
Tg+30	870.894	868.454	-2.44

Appendix Table A9 Data of optimum nucleation temperature determination of heated GCF5.0 at T_{p1} .

Temperature with hold on 1 hour (°C)	T_{p1}	T_{p1}^*	$T_{p1}^* - T_{p1}$
Tg-30	755.521	756.976	1.455
Tg-15	755.521	757.301	1.780
Tg	755.521	757.973	2.452
Tg+15	755.521	758.155	2.634
Tg+30	755.521	757.154	1.633

Appendix Table A10 Data of optimum nucleation temperature determination of heated GCF5.0 at T_{p2} .

Temperature with hold on 1 hour (°C)	T_{p2}	T_{p2}^*	$T_{p2}^* - T_{p2}$
Tg-30	864.390	864.030	-0.36
Tg-15	864.390	864.677	0.287
Tg	864.390	865.256	0.866
Tg+15	864.390	864.740	0.35
Tg30	864.390	864.300	-0.09

Appendix Table A11 Data of optimum nucleation time determination of heated GCF3.0 at T_{p1} .

Time (hour)	T_{p1}	T_{p1}^*	$T_{p1}^* - T_{p1}$
0.5	755.521	759.633	4.112
1.0	755.521	761.987	6.466
2.0	755.521	763.451	7.93
4.0	755.521	764.688	9.167
10.0	755.521	763.902	8.381

Appendix Table A12 Data of optimum nucleation time determination of heated GCF3.0 at T_{p2} .

Time (hour)	T_{p2}	T_{p2}^*	$T_{p2}^* - T_{p2}$
0.5	863.916	863.328	-0.588
1.0	863.916	865.267	1.351
2.0	863.916	866.932	3.016
4.0	863.916	868.932	5.016
10.0	863.916	871.845	7.929

Appendix Table A13 Data of optimum nucleation time determination of heated GCF3.5 at T_{p1} .

Time (hour)	T_{p1}	T_{p1}^*	$T_{p1}^* - T_{p1}$
0.5	778.537	779.512	0.975
1.0	778.537	779.921	1.384
2.0	778.537	780.488	1.951
4.0	778.537	774.634	-3.903
10.0	778.537	768.932	-9.605

Appendix Table A14 Data of optimum nucleation time determination of heated GCF3.5 at T_{p2} .

Time (hour)	T_{p2}	T_{p2}^*	$T_{p2}^* - T_{p2}$
0.5	874.797	875.122	0.325
1.0	874.797	876.722	1.925
2.0	874.797	878.668	3.871
4.0	874.797	879.336	4.539
10.0	874.797	880.142	5.345

Appendix Table A15 Data of optimum nucleation time determination of heated GCF4.0 at T_{p1} .

Time (hour)	T_{p1}	T_{p1}^*	$T_{p1}^* - T_{p1}$
0.5	776.892	776.759	-0.133
1.0	776.892	776.854	-0.038
2.0	776.892	779.203	2.311
4.0	776.892	783.052	6.16
10.0	776.892	781.458	4.566

Appendix Table A16 Data of optimum nucleation time determination of heated GCF4.0 at T_{p2} .

Time (hour)	T_{p2}	T_{p2}^*	$T_{p2}^* - T_{p2}$
0.5	881.414	869.144	-12.27
1.0	881.414	873.463	-7.951
2.0	881.414	875.475	-5.939
4.0	881.414	876.667	-4.747
10.0	881.414	878.455	-2.959

Appendix Table A17 Data of optimum nucleation time determination of heated GCF4.5 at T_{p1} .

Time (hour)	T_{p1}	T_{p1}^*	$T_{p1}^* - T_{p1}$
0.5	765.489	763.902	-1.587
1.0	765.489	767.367	1.878
2.0	765.489	768.78	3.291
4.0	765.489	769.756	4.267
10.0	765.489	766.854	1.365

Appendix Table A18 Data of optimum nucleation time determination of heated GCF4.5 at T_{p2} .

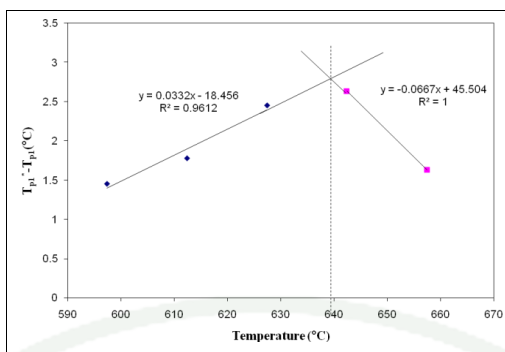
Time (hour)	T_{p2}	T_{p2}^*	$T_{p2}^* - T_{p2}$
0.5	869.593	866.896	-2.697
1.0	869.593	868.650	-0.943
2.0	869.593	870.339	0.746
4.0	869.593	872.247	2.654
10.0	869.593	873.712	4.119

Appendix Table A19 Data of optimum nucleation time determination of heated GCF5.0 at T_{p1} .

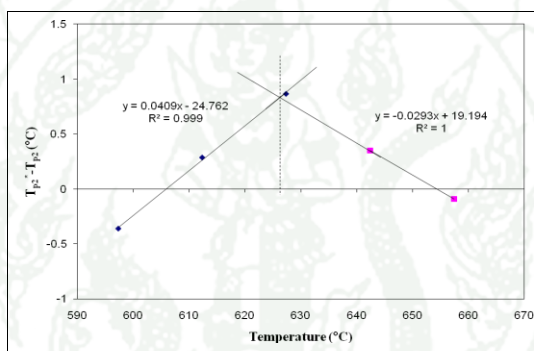
Time (hour)	T_{p1}	T_{p1}^*	$T_{p1}^* - T_{p1}$
0.5	781.463	784.390	2.927
1.0	781.463	785.366	3.903
2.0	781.463	786.341	4.878
4.0	781.463	785.336	3.873
10.0	781.463	775.610	-5.853

Appendix Table A20 Data of optimum nucleation time determination of heated GCF5.0 at T_{p2} .

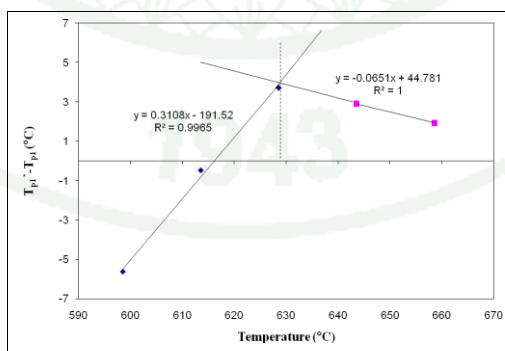
Time (hour)	T_{p2}	T_{p2}^*	$T_{p2}^* - T_{p2}$
0.5	889.479	891.792	2.313
1.0	889.479	892.683	3.204
2.0	889.479	893.659	4.180
4.0	889.479	895.108	5.629
10.0	889.479	897.064	7.585



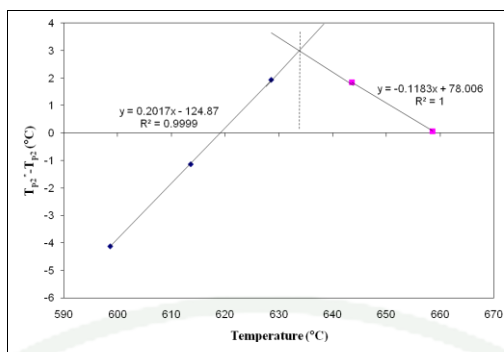
Appendix Figure A76 Analysis optimum nucleation temperature heated GCF3.0 of T_{p1} .



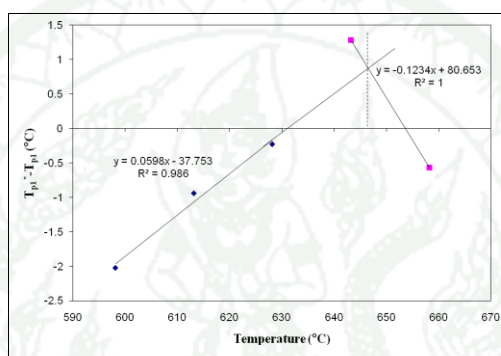
Appendix Figure A77 Analysis optimum nucleation temperature heated GCF3.0 of T_{p2} .



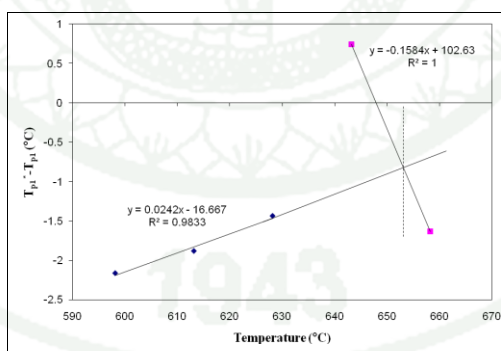
Appendix Figure A78 Analysis optimum nucleation temperature heated GCF3.5 of T_{p1} .



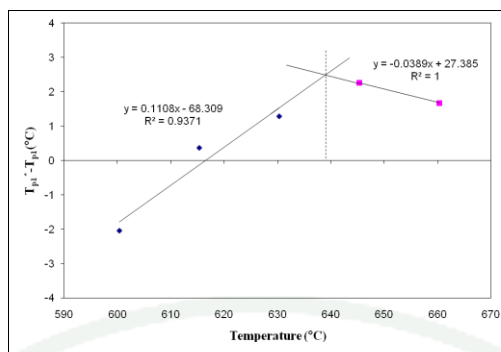
Appendix Figure A79 Analysis optimum nucleation temperature heated GCF3.5 of T_{p2} .



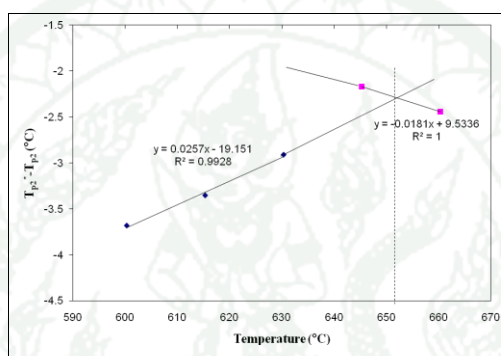
Appendix Figure A80 Analysis optimum nucleation temperature heated GCF4.0 of T_{p1} .



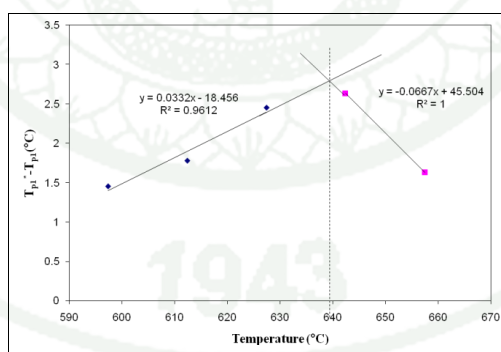
Appendix Figure A81 Analysis optimum nucleation temperature heated GCF4.0 of T_{p2} .



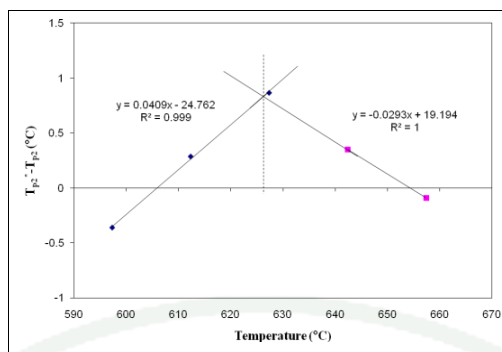
Appendix Figure A82 Analysis optimum nucleation temperature heated GCF4.5 of T_{p1} .



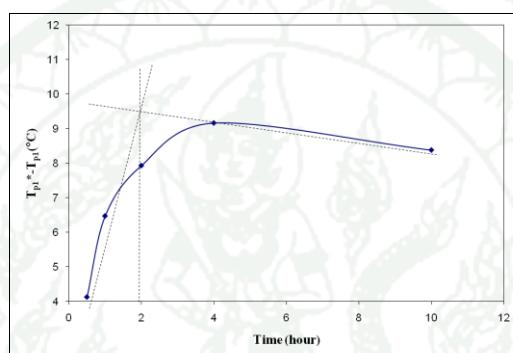
Appendix Figure A83 Analysis optimum nucleation temperature heated GCF4.5 of T_{p2} .



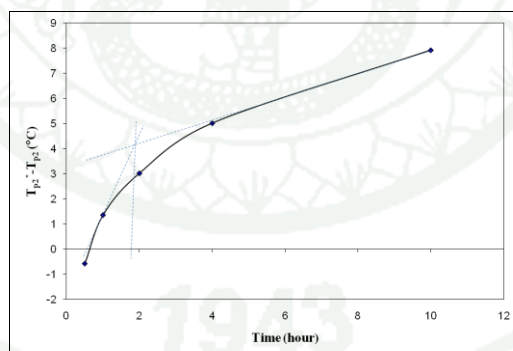
Appendix Figure A84 Analysis optimum nucleation temperature heated GCF5.0 of T_{p1} .



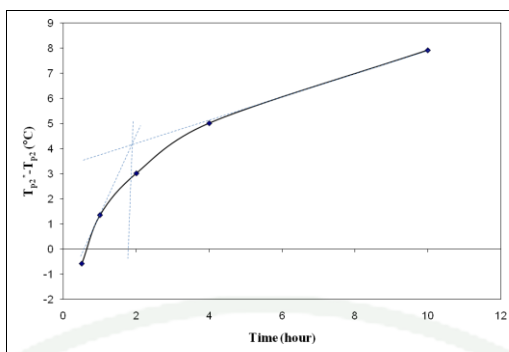
Appendix Figure A85 Analysis optimum nucleation temperature heated GCF5.0 of T_{p2} .



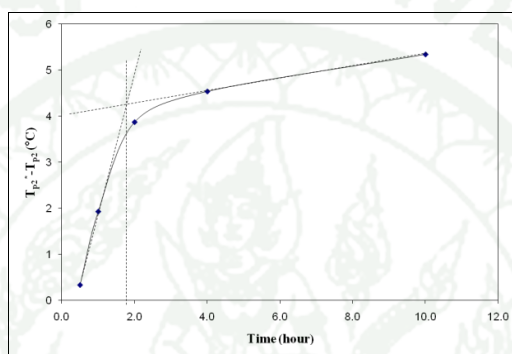
Appendix Figure A86 Analysis optimum nucleation time heated GCF3.0 of T_{p1} .



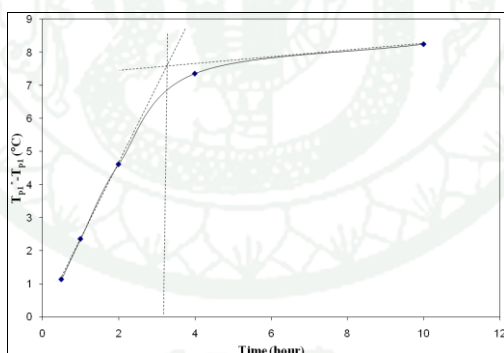
Appendix Figure A87 Analysis optimum nucleation time heated GCF3.0 of T_{p2} .



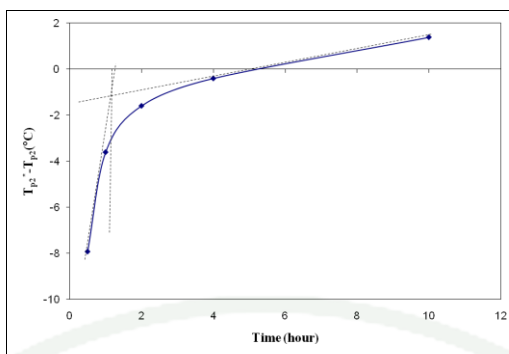
Appendix Figure A88 Analysis optimum nucleation time heated GCF3.5 of T_{p1} .



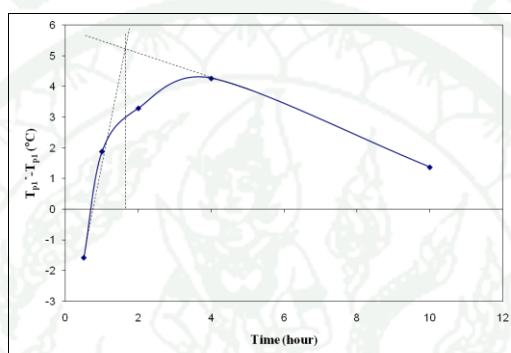
Appendix Figure A89 Analysis optimum nucleation time heated GCF3.5 of T_{p2} .



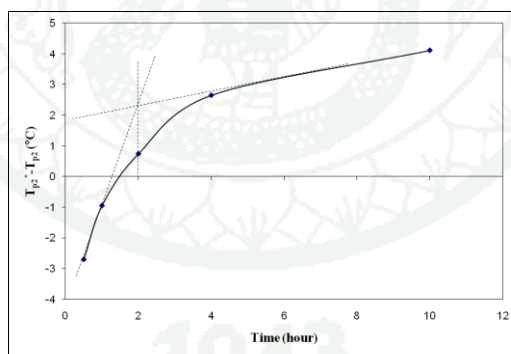
Appendix Figure A90 Analysis optimum nucleation time heated GCF4.0 of T_{p1} .



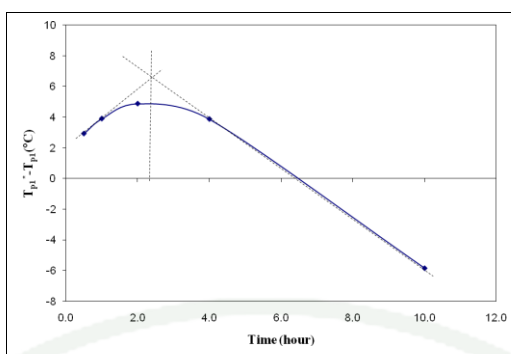
Appendix Figure A91 Analysis optimum nucleation time heated GCF4.0 of T_{p2} .



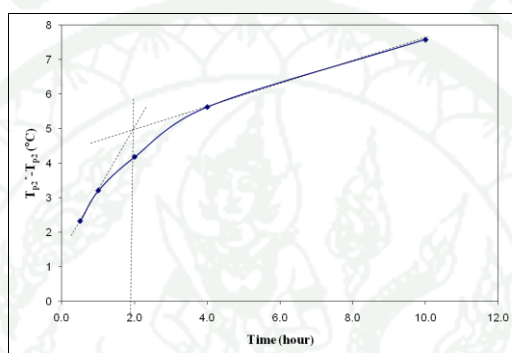
Appendix Figure A92 Analysis optimum nucleation time heated GCF4.5 of T_{p1} .



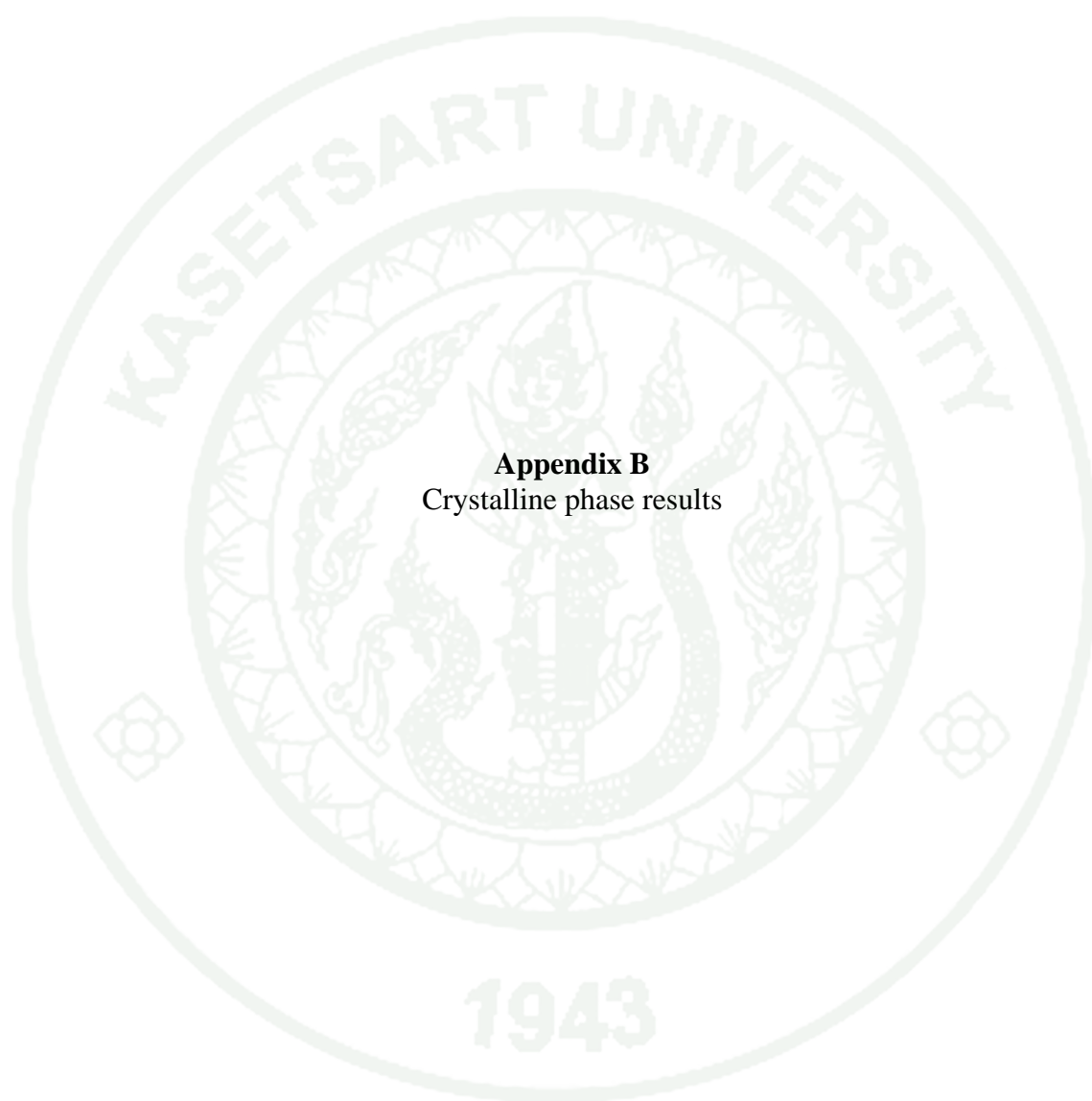
Appendix Figure A93 Analysis optimum nucleation time heated GCF4.5 of T_{p2} .



Appendix Figure A94 Analysis optimum nucleation time heated GCF5.0 of T_{p1} .



Appendix Figure A95 Analysis optimum nucleation time heated GCF5.0 of T_{p2} .



Appendix B
Crystalline phase results

Appendix Table B1 ICDD Powder Diffraction file No.03-0559.

Angle (2θ)	Intensity
28.774	100
36.648	50
43.470	30
46.281	30

Appendix Table B2 ICDD Powder Diffraction file No.25-0155.

Angle (2θ)	Intensity
9.110	100
27.594	70
29.160	15
40.041	10
40.416	10

Appendix Table B3 ICDD Powder Diffraction file No.46-0744.

Angle (2 θ)	Intensity
20.020	13
22.029	13
23.797	72
24.440	13
26.560	26
27.756	100
30.318	10
34.967	20
35.685	13
38.148	5
40.889	6
51.545	7

Appendix Table B4 ICDD Powder Diffraction file No.48-1477.

Angle (2 θ)	Intensity
29.970	89
34.740	100
62.280	18
73.330	7

Appendix Table B5 ICDD Powder Diffraction file No.71-1083.

Angle (2 θ)	Intensity
22.569	79
31.921	71
35.268	80
36.093	100
39.208	39
42.099	21
46.991	3
55.480	10
57.375	18

Appendix Table B6 ICDD Powder Diffraction file No. 80-0573.

Angle (2 θ)	Intensity
36.405	25
36.926	100
43.653	22
53.056	30
53.371	52
67.481	34

Appendix Table B7 ICDD Powder Diffraction file No. 82-1556.

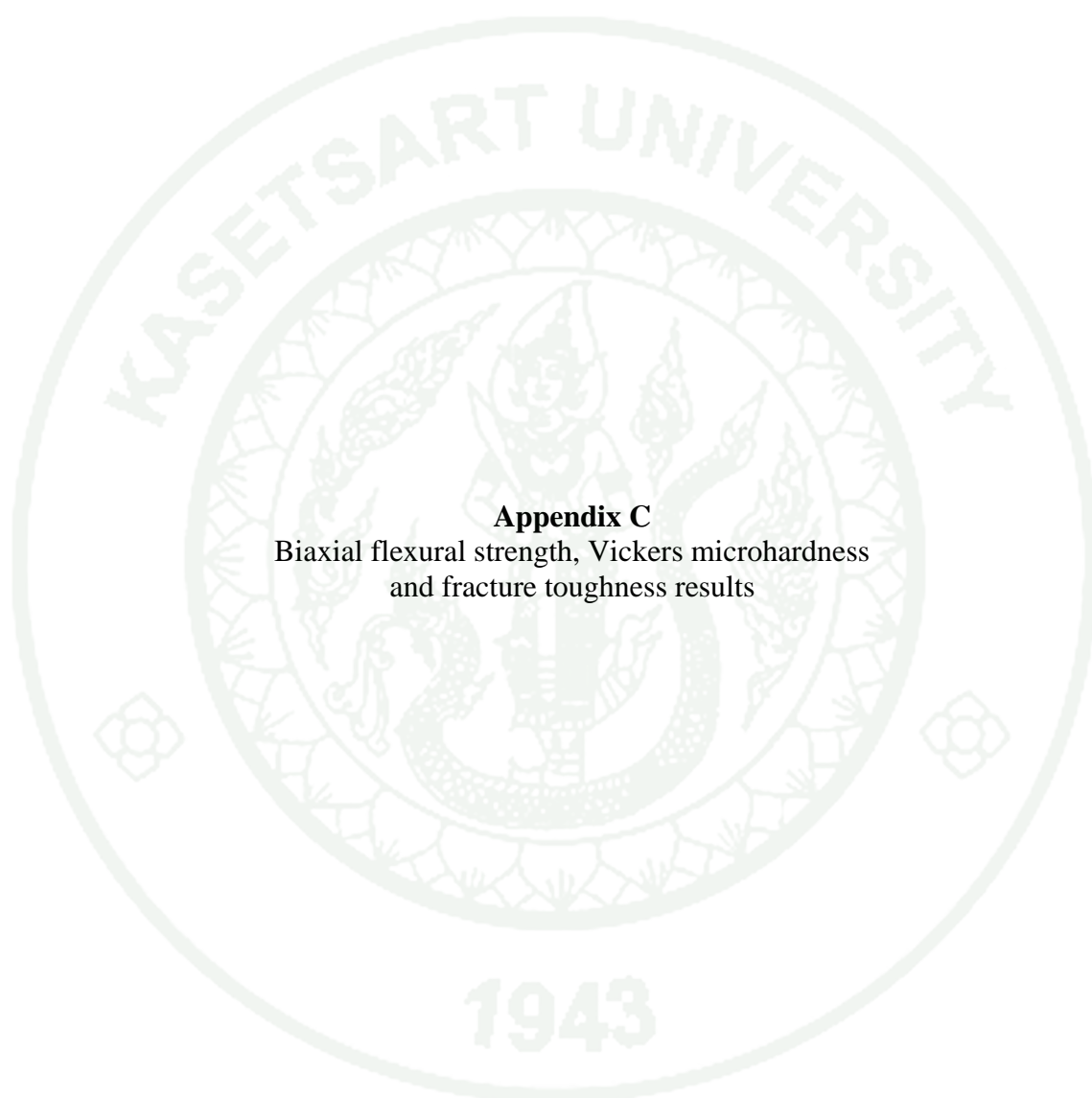
Angle (2θ)	Intensity
22.656	100
29.066	15
33.108	19
36.397	19
49.693	6
63.417	6

Appendix Table B8 ICDD Powder Diffraction file No. 82-1646.

Angle (2θ)	Intensity
30.617	100
39.982	25
45.850	36
49.346	12
60.828	45
63.744	14
69.891	7
77.958	17
78.206	15

Appendix Table B9 ICDD Powder Diffraction file No. 83-0557.

Angle (2θ)	Intensity
25.859	40
31.912	100
32.239	49
33.084	67
49.564	36



Appendix C
Biaxial flexural strength, Vickers microhardness
and fracture toughness results

Appendix Table C1 The biaxial flexural strength of glass-ceramics.

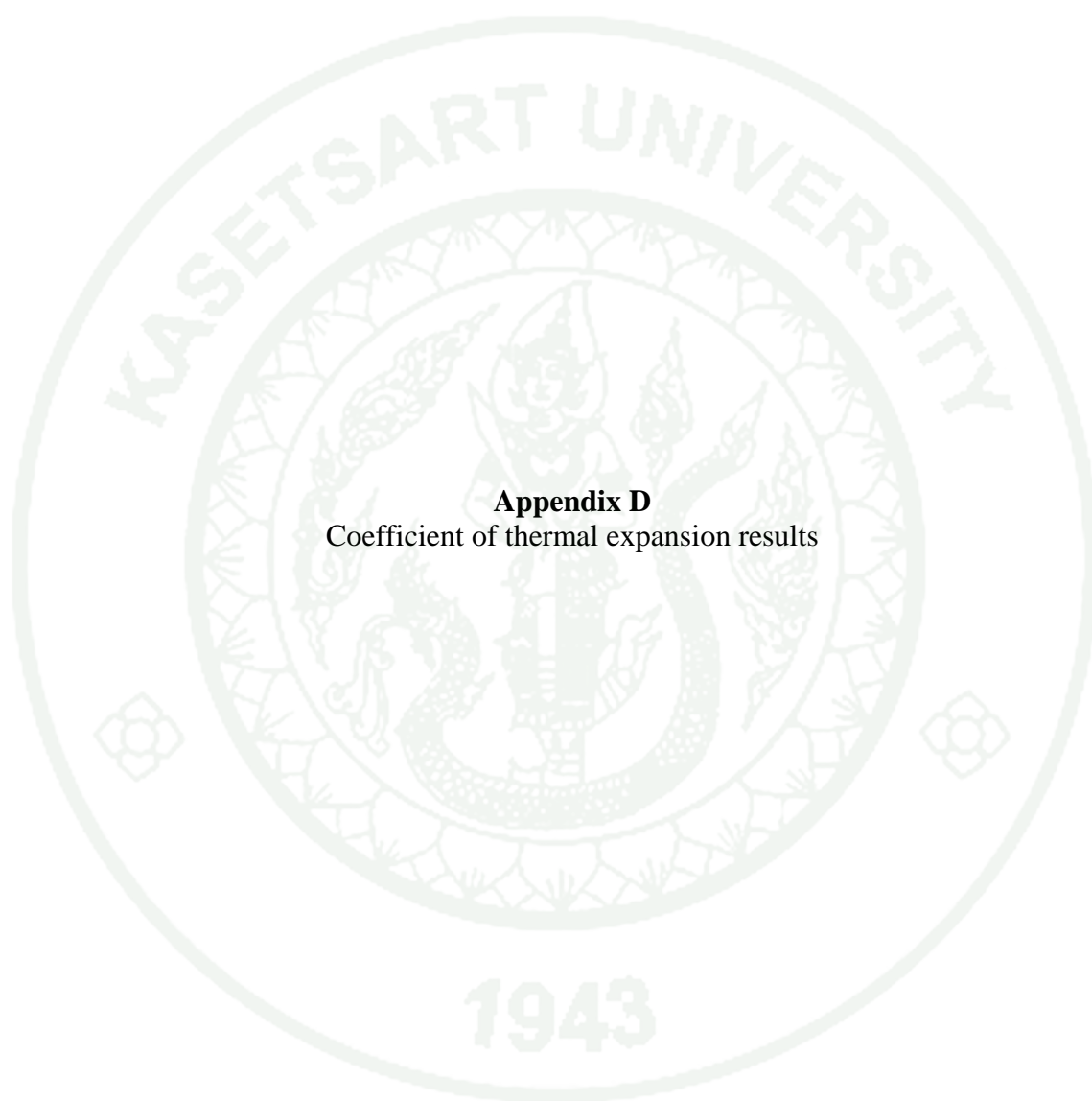
Sample No.	Maximum center tensile stress (MPa)									
	GCF3.0		GCF3.5		GCF4.0		GCF4.5		GCF5.0	
	T _{p1}	T _{p2}	T _{p1}	T _{p2}	T _{p1}	T _{p2}	T _{p1}	T _{p2}	T _{p1}	T _{p2}
1	160.44	128.88	155.83	148.53	162.69	150.98	129.18	125.48	133.47	111.67
2	144.54	153.36	163.60	155.19	157.90	149.29	128.76	100.93	133.25	102.65
3	151.19	142.08	151.88	155.23	157.15	135.58	130.71	119.43	132.22	122.10
4	135.03	145.25	157.82	149.62	157.49	145.02	125.95	126.93	128.33	123.24
5	136.31	120.99	165.78	159.33	135.59	153.70	133.80	146.81	127.16	109.78
6	146.97	120.57	148.79	153.00	142.09	159.49	130.23	116.05	134.62	125.50
7	160.51	132.78	149.62	140.23	161.08	152.86	135.78	128.25	127.53	118.24
8	152.54	147.18	163.85	164.64	167.95	147.70	138.66	134.85	133.38	115.53
9	131.73	112.97	157.82	139.73	132.20	127.36	117.84	82.77	110.68	91.37
10	171.10	162.35	165.78	175.93	177.33	169.74	154.93	147.84	152.79	138.76
σ_{Avg}	148.44	136.39	157.15	153.22	155.24	149.33	131.63	124.84	131.24	116.09
STDEV	9.70	12.37	6.73	7.36	10.86	7.05	4.15	13.51	3.04	7.75

Appendix Table C2 The Vickers microhardness of glass-ceramics.

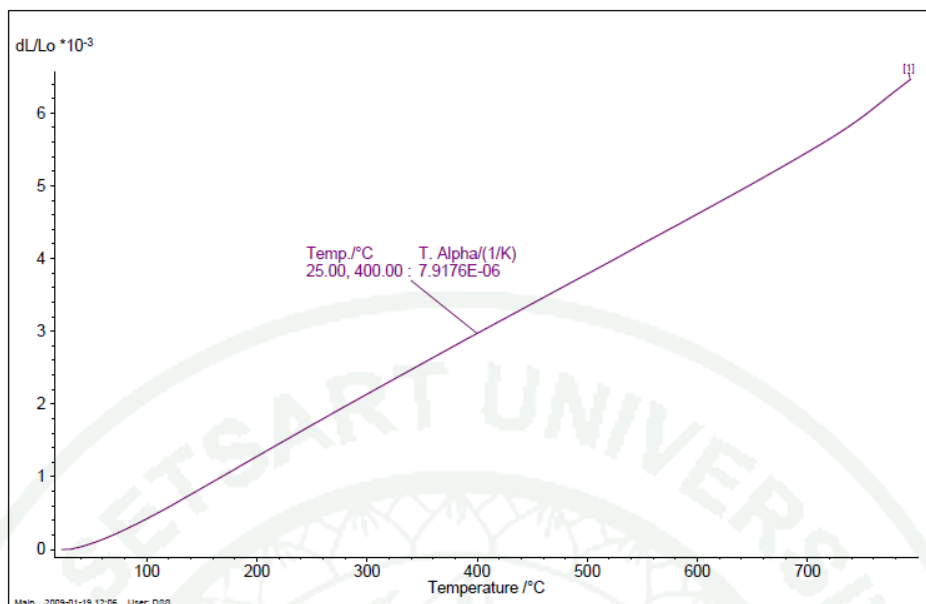
Sample No.	Vickers microhardness (GPa)									
	GCF3.0		GCF3.5		GCF4.0		GCF4.5		GCF5.0	
	T _{p1}	T _{p2}	T _{p1}	T _{p2}	T _{p1}	T _{p2}	T _{p1}	T _{p2}	T _{p1}	T _{p2}
1	2.44	3.06	3.50	2.33	2.80	2.75	3.12	2.57	2.80	2.61
2	3.01	2.8	3.50	2.44	3.18	3.01	3.18	2.95	3.01	2.33
3	3.06	3.43	3.36	3.12	3.18	3.01	3.01	2.80	2.80	2.26
4	3.24	3.3	3.06	3.12	3.30	3.50	3.18	2.90	3.30	3.01
5	2.61	3.5	2.95	2.70	3.43	2.80	3.24	2.70	3.18	2.29
6	3.36	2.75	4.12	3.24	3.95	2.57	2.85	3.24	2.95	3.06
7	3.06	2.75	3.79	3.01	3.12	2.53	3.24	2.90	2.75	2.95
8	2.75	2.9	3.18	2.95	3.36	2.70	3.12	2.90	2.61	2.95
9	3.24	2.29	3.50	2.90	3.18	3.06	3.06	2.57	2.85	3.12
10	3.43	2.52	4.12	2.75	3.43	2.61	3.30	2.70	2.75	2.80
σ_{Avg}	3.02	2.93	3.51	2.86	3.29	2.85	3.13	2.84	2.90	2.74
STDEV	0.33	0.39	0.40	0.30	0.30	0.30	0.13	0.20	0.21	0.34

Appendix Table C3 The fracture toughness of glass-ceramics.

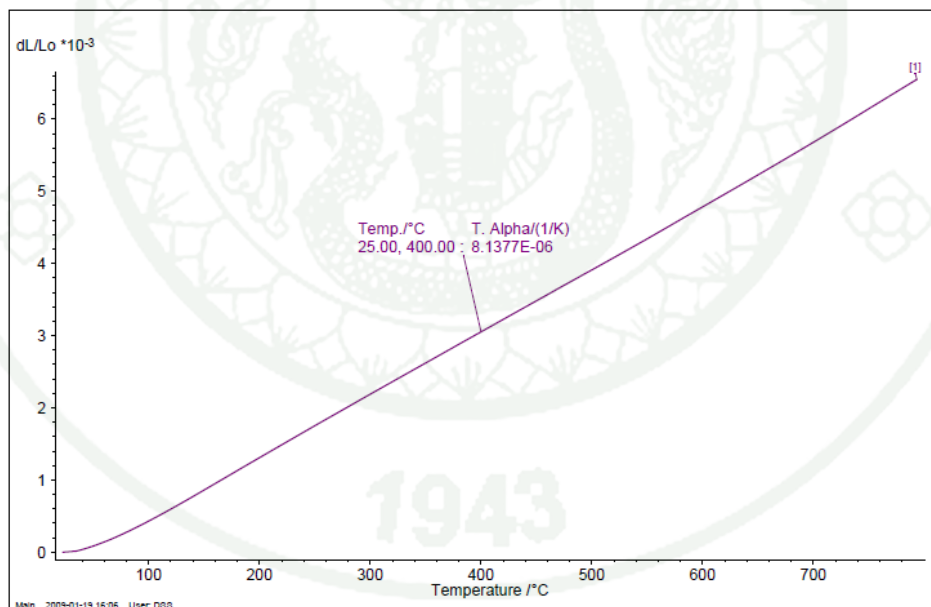
Sample No.	Fracture toughness (MPa.m ^{1/2})									
	GCF3.0		GCF3.5		GCF4.0		GCF4.5		GCF5.0	
	T _{p1}	T _{p2}	T _{p1}	T _{p2}	T _{p1}	T _{p2}	T _{p1}	T _{p2}	T _{p1}	T _{p2}
1	1.34	1.59	1.6	1.1	0.9	1.29	1.27	1.64	1.27	1.09
2	1.58	1.48	1.59	1.34	0.95	0.83	1.04	1.24	0.64	1.58
3	1.12	1.24	1.09	1.05	1.2	1.38	1.36	1.48	1.07	1.05
4	1.12	1.64	1.29	1.18	1.71	1.23	0.95	1.59	1.05	1.6
5	1.02	0.83	1.18	1.58	1.27	1.42	1.36	1.26	0.82	1.34
6	1.22	1.34	2.57	1.62	1.28	1.32	1.36	1.32	1.27	0.67
7	0.93	1.32	1.73	1.76	1.81	0.78	1.69	1.34	0.94	1.03
8	1.6	1.26	0.97	1.37	1.19	1.29	1.03	0.83	0.94	1.79
9	1.61	1.31	1.54	1.5	1.65	1.63	0.68	1.44	1.3	1.64
10	1.47	1.27	1.32	1.36	0.9	2.38	2.00	0.97	1.35	1.04
σ_{Avg}	1.30	1.33	1.49	1.39	1.35	1.35	1.27	1.31	1.06	1.28
STDEV	0.25	0.22	0.45	0.23	0.32	0.44	0.38	0.25	0.23	0.36



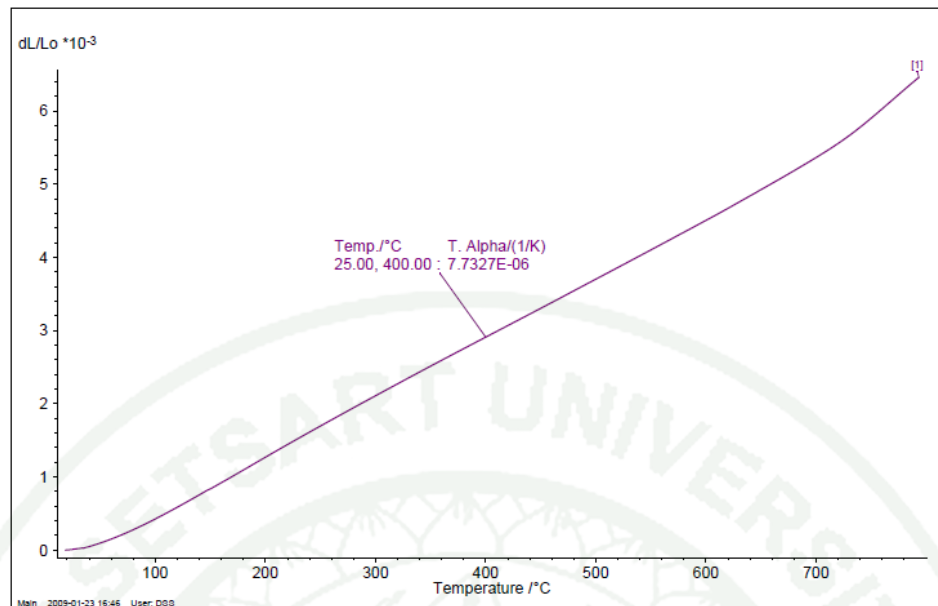
Appendix D
Coefficient of thermal expansion results



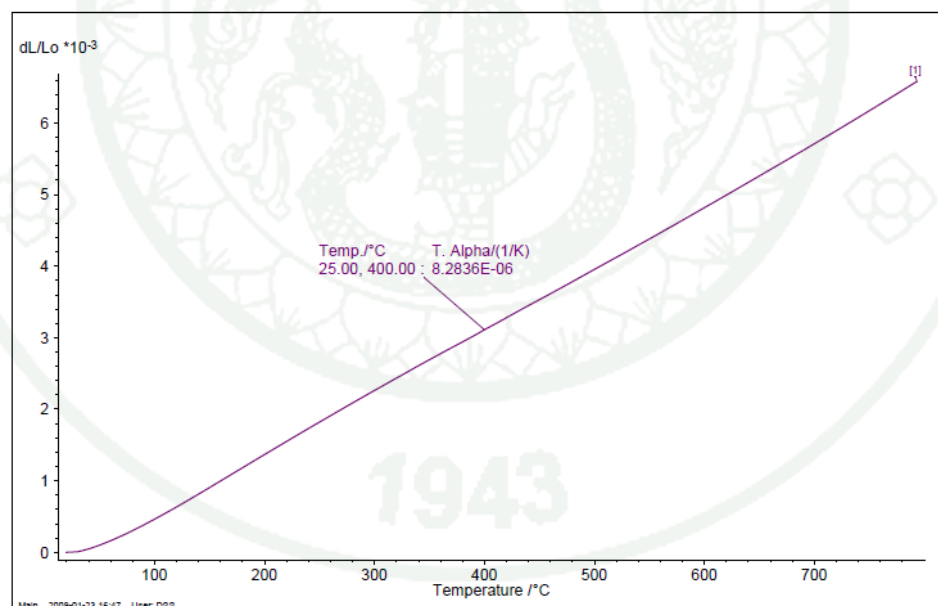
Appendix Figure D1 Coefficient of thermal expansion of heat-treated GCF3.0 at T_{p1} by dilatometer.



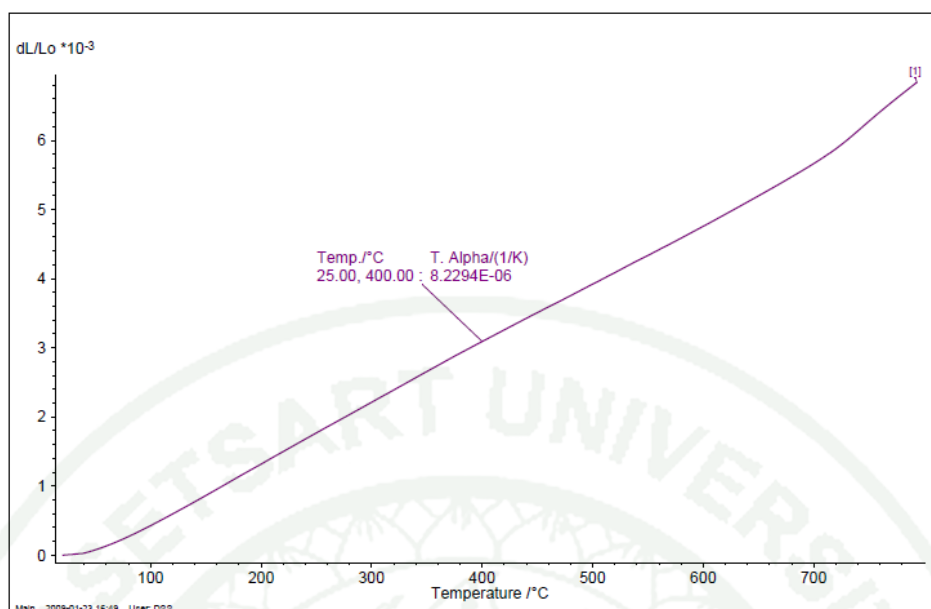
Appendix Figure D2 Coefficient of thermal expansion of heat-treated GCF3.0 at T_{p2} by dilatometer.



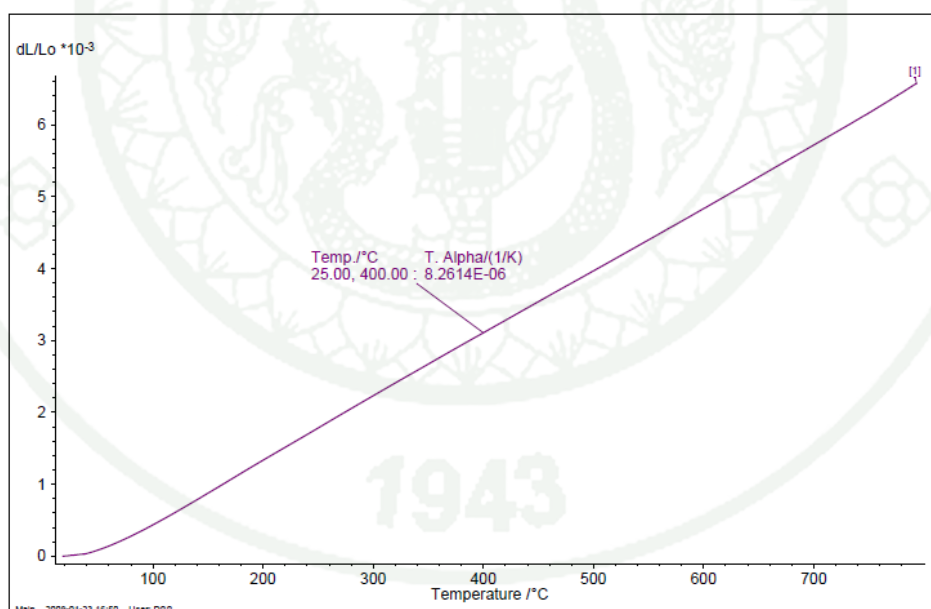
Appendix Figure D3 Coefficient of thermal expansion of heat-treated GCF3.5 at T_{p1} by dilatometer.



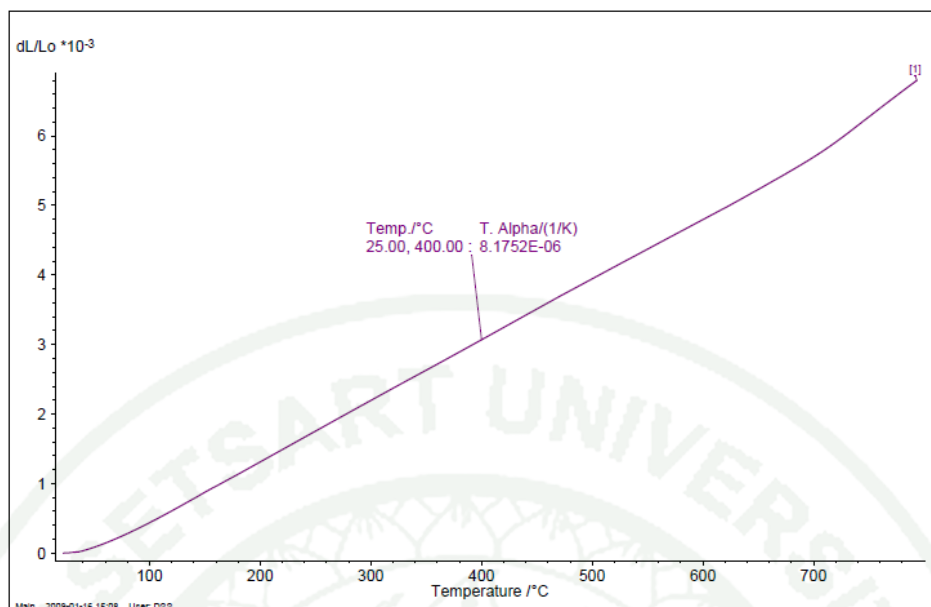
Appendix Figure D4 Coefficient of thermal expansion of heat-treated GCF3.5 at T_{p2} by dilatometer



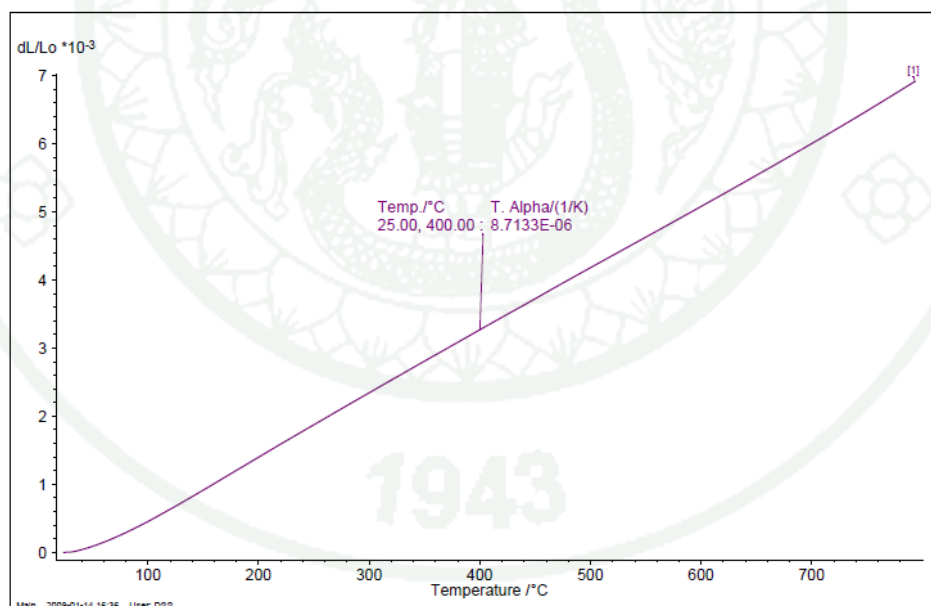
Appendix Figure D5 Coefficient of thermal expansion of heat-treated GCF4.0 at T_{p1} by dilatometer.



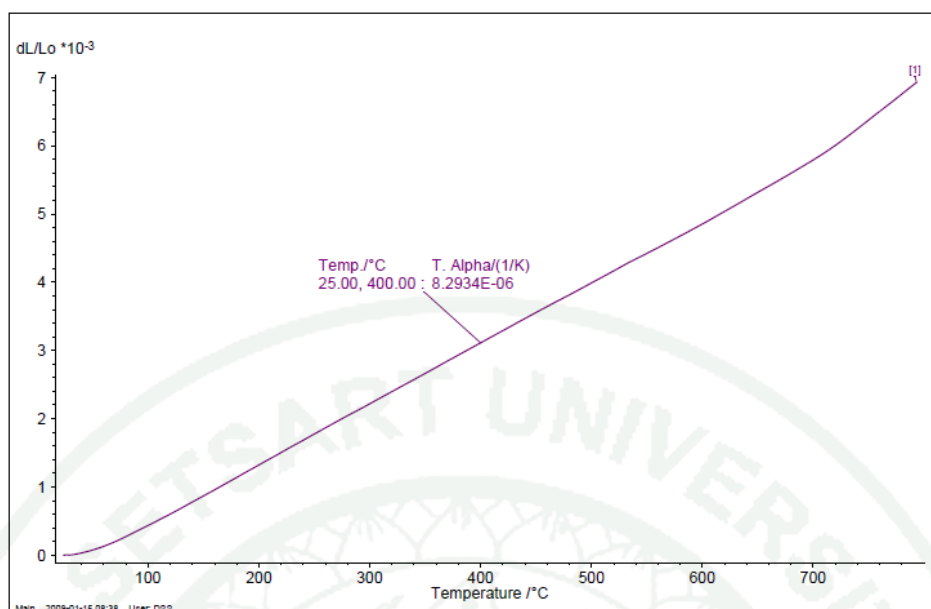
Appendix Figure D6 Coefficient of thermal expansion of heat-treated GCF4.0 at T_{p2} by dilatometer.



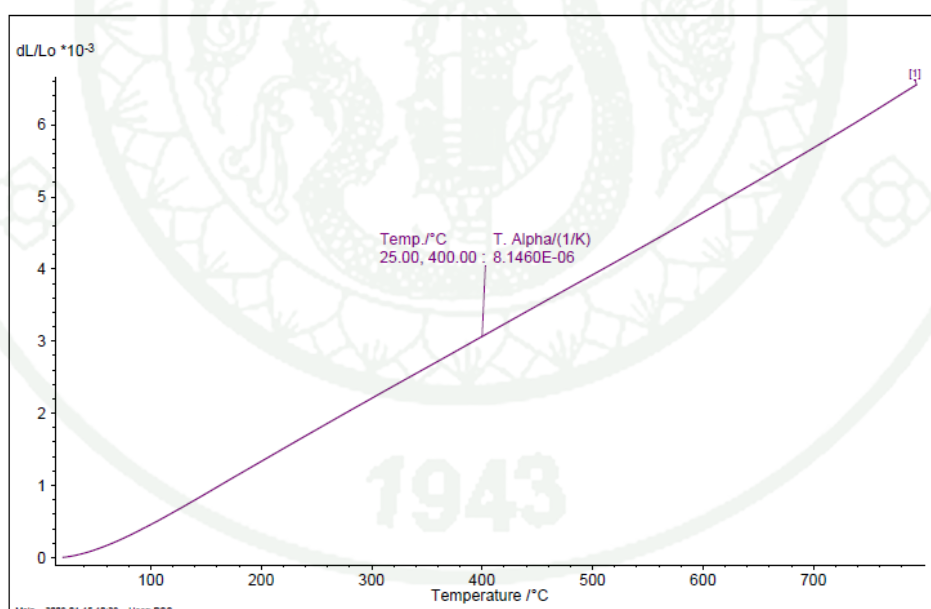
Appendix Figure D7 Coefficient of thermal expansion of heat-treated GCF4.5 at T_{p1} by dilatometer.



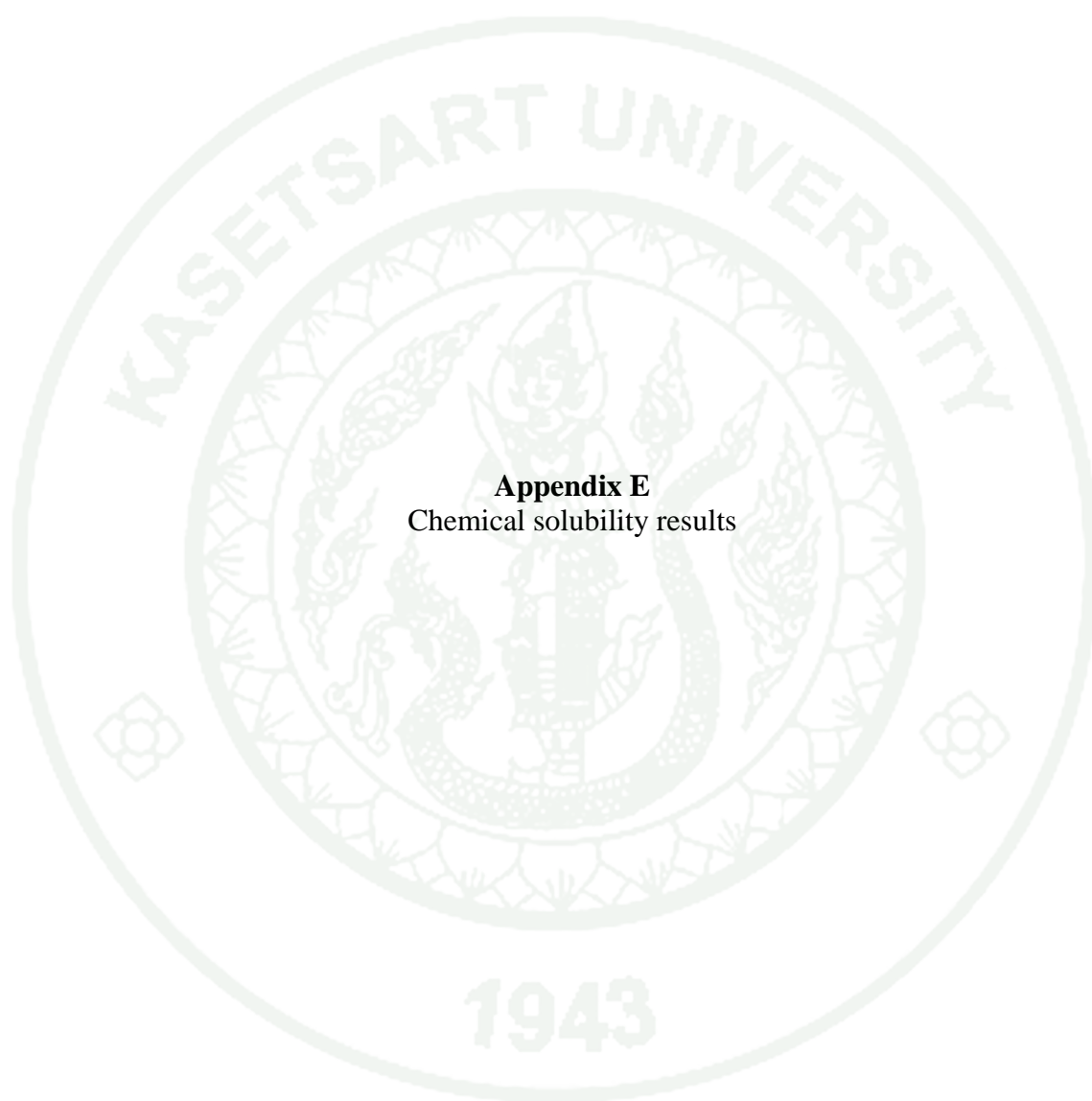
Appendix Figure D8 Coefficient of thermal expansion of heat-treated GCF4.5 at T_{p2} by dilatometer.



Appendix Figure D9 Coefficient of thermal expansion of heat-treated GCF5.0 at T_{p1} by dilatometer.



Appendix Figure D10 Coefficient of thermal expansion of heat-treated GCF5.0 at T_{p2} by dilatometer.



Appendix E
Chemical solubility results

Appendix Table E1 Chemical solubility of all glass-ceramics in 4%(v/v) acetic acid.

Sample No.	Chemical solubility in 4%(v/v) acetic acid ($\mu\text{g}\cdot\text{cm}^{-2}$)									
	GCF3.0		GCF3.5		GCF4.0		GCF4.5		GCF5.0	
	T _{p1}	T _{p2}	T _{p1}	T _{p2}	T _{p1}	T _{p2}	T _{p1}	T _{p2}	T _{p1}	T _{p2}
1	376	1697	1839	813	1824	916	1699	440	617	475
2	349	1685	1842	898	1753	964	1683	428	617	433
3	335	1632	1799	825	1705	979	1703	411	665	429
4	316	1644	1928	873	1829	942	1678	483	632	422
5	321	1699	1772	863	1728	971	1733	442	648	421
Avg	339	1671	1836	854	1768	954	1699	441	636	436
STDEV	24	31	59	35	56	25	22	27	21	22

Appendix Table E2 Chemical solubility of all glass-ceramics in distilled water.

Sample No.	Chemical solubility in water ($\mu\text{g}\cdot\text{cm}^{-2}$)									
	GCF3.0		GCF3.5		GCF4.0		GCF4.5		GCF5.0	
	T _{p1}	T _{p2}	T _{p1}	T _{p2}	T _{p1}	T _{p2}	T _{p1}	T _{p2}	T _{p1}	T _{p2}
1	50	50	47	32	31	18	28	19	24	12
2	58	42	66	52	32	28	33	22	36	5
3	70	30	51	39	42	49	29	31	21	1
4	71	40	50	26	25	39	40	42	28	11
5	67	44	41	34	31	30	24	34	19	2
Avg	63	41	51	36	32	33	31	30	25	6
STDEV	9	7	9	10	6	12	6	9	7	5

Appendix Table E3 Chemical solubility of all glass-ceramics in 0.1M sodium hydroxide.

Sample No.	Chemical solubility in 0.1M sodium hydroxide ($\mu\text{g}\cdot\text{cm}^{-2}$)									
	GCF3.0		GCF3.5		GCF4.0		GCF4.5		GCF5.0	
	T _{p1}	T _{p2}	T _{p1}	T _{p2}	T _{p1}	T _{p2}	T _{p1}	T _{p2}	T _{p1}	T _{p2}
1	275	41	51	23	68	83	86	17	42	13
2	343	28	220	96	39	39	46	31	30	14
3	325	65	117	28	89	13	28	24	15	23
4	267	52	174	18	54	14	9	29	22	32
5	283	48	197	29	64	25	62	35	11	10
Avg	298	47	152	39	63	35	46	27	24	19
STDEV	33	14	68	32	19	29	30	7	12	9

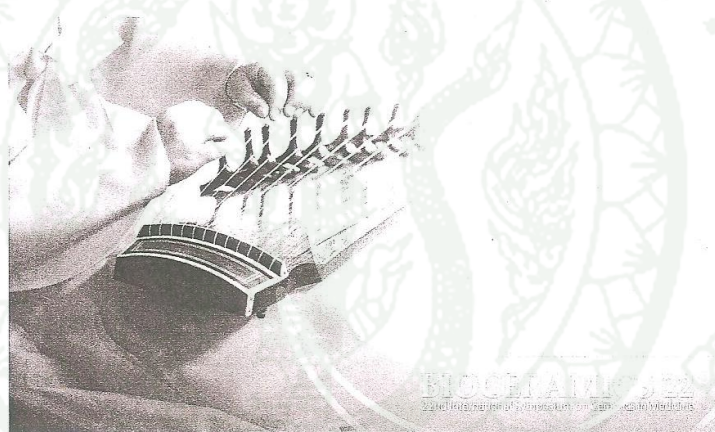


Appendix F
Conferences

Sukyoung Kim

BIOCERAMICS 22
22nd International Symposium on Ceramics in Medicine

Volume 22



Daegu, Korea

The Korean Society for Biomaterials

Bioceramics 22

Chairman
Sukyoung Kim, Ph. D.

Co-Chair
Inn-Kyu Kang, Ph. D.

Honorary Chair
Cheol Young Kim, Ph. D.

Executive Committee (2009)**International Society for Ceramics in Medicine (ISCM)**

President:	Sukyoung Kim (Korea)	
Secretary General:	Guy Daculsi (France)	
Treasurer:	Takashi Nakamura (Japan)	
Members:	Besim Ben-Nissan (Australia)	Antonio Moroni (Italy)
	Ian C. Clake (USA)	Hajime Ohgushi (Japan)
	Paul Duchene (USA)	Marcelo Prado (Brazil)
	Tadashi Kokubo (Japan)	Antti Yli-Urpo (Finland)
	Racquel LeGeros (USA)	Xingdong Zhang (China)
	Panjian Li (USA)	
Honorary Members:	William Bonfield (UK)	Larry L. Hench (UK)
	Mario Barbarosa (Portugal)	Hironobu Oonishi (Japan)
	K. de Groot (Netherlands)	Laurant Sedel (France)

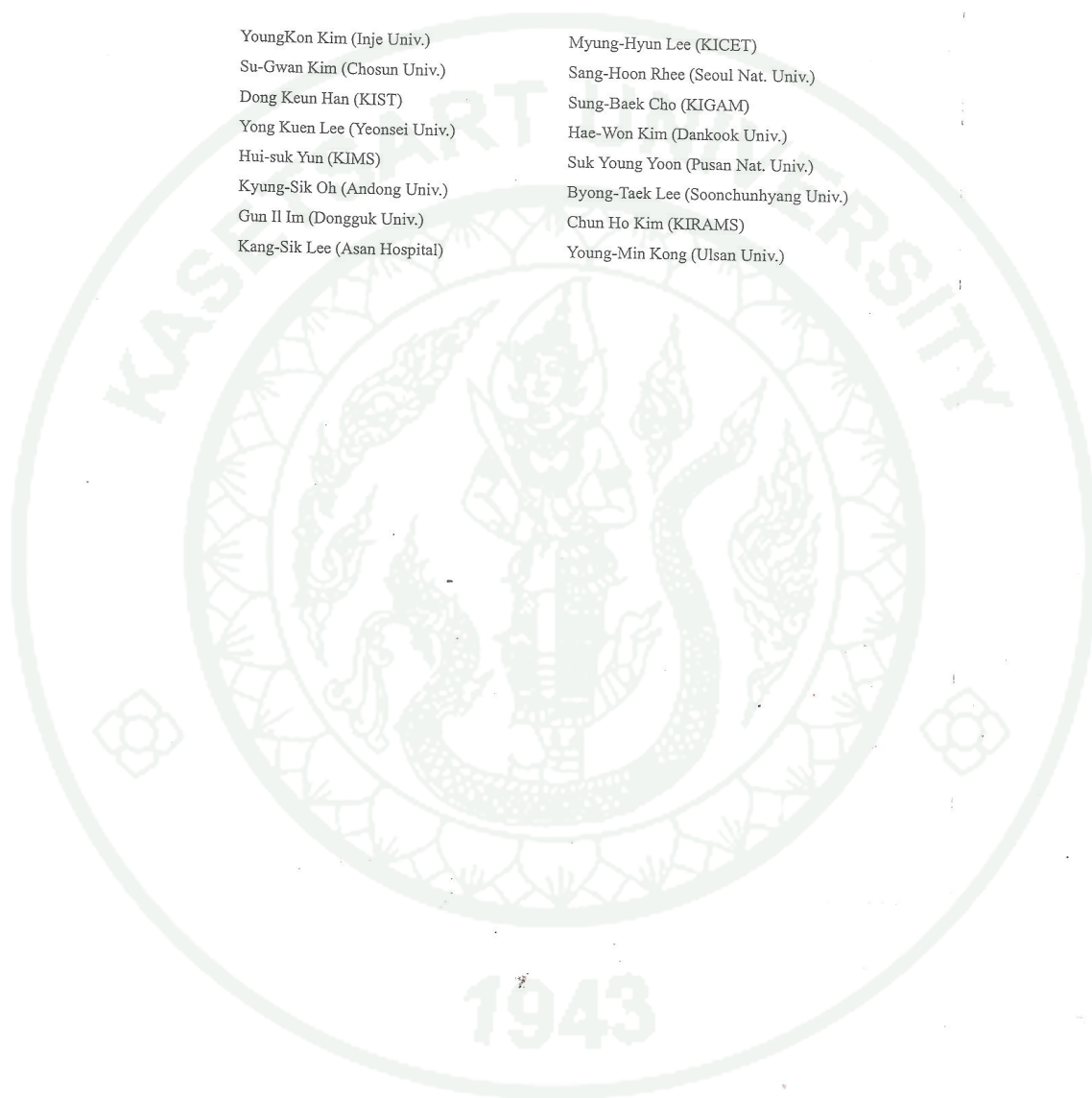
International Scientific Committee

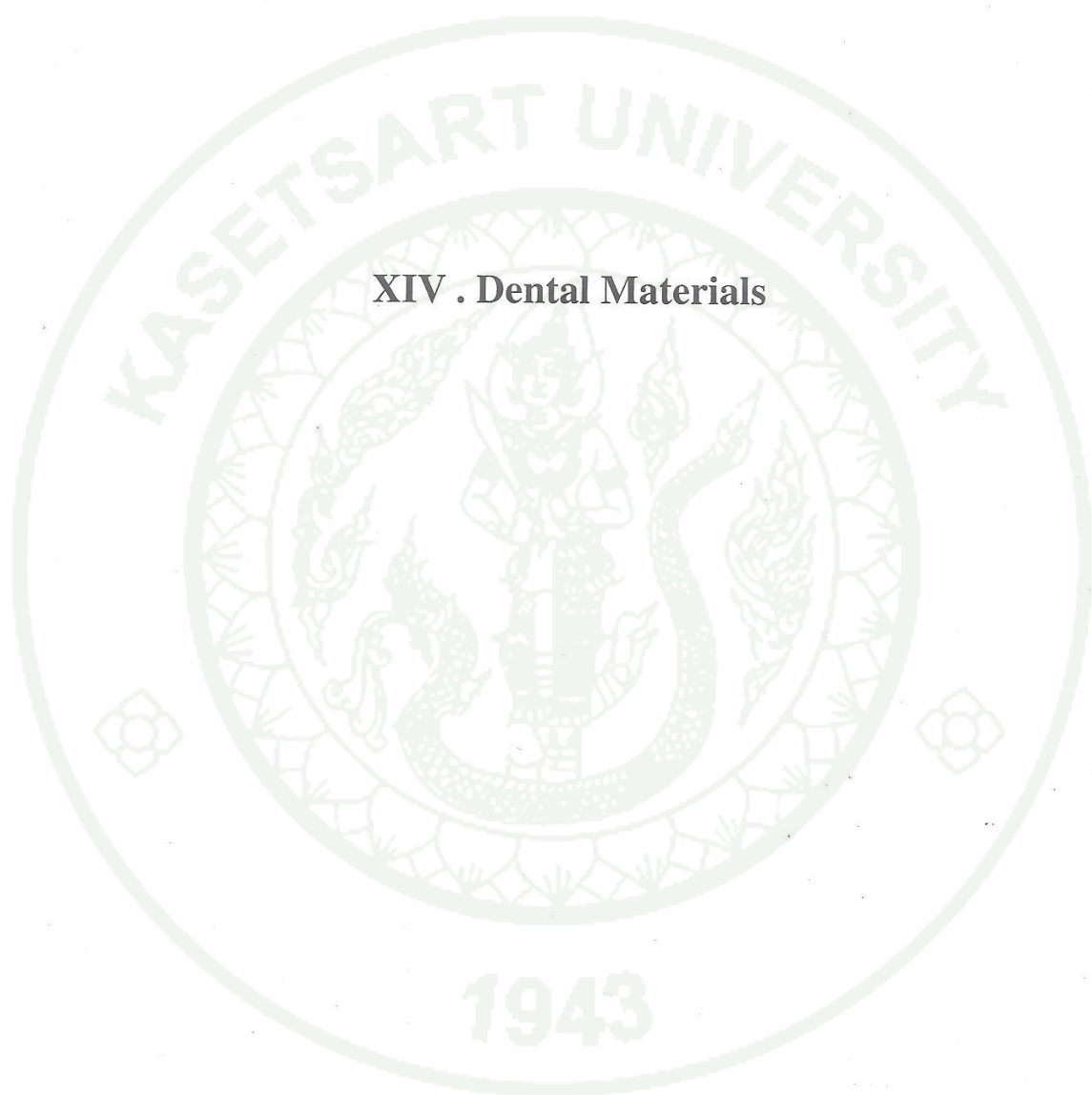
A. Osaka (Japan)	K. Ishikawa (Japan)	R. Pilliar (Canada)
C. Ohtsuki (Japan)	A. Ito (Japan)	S. J. Ding (Taiwan)
K. Ioku (Japan)	H. Fan (China)	D. J. Kim (Korea)
T. Kasuga (Japan)	S. Li (China)	P. Layrolle (France)
M. Kikuchi (Japan)	M. Wang (Hong Kong)	J. LeGeros (USA)
S. M. Best (UK)	F. Monteiro (Portugal)	E. S. Kayali (Turkey)
J. de Bruijn (UK)	H.E. Kim (Korea)	K. M. Paraskevopoulos (Greece)
U. Gross (Germany)	I. S. Lee (Korea)	K. H. Kim (Korea)
Y. Leng (Hong Kong)	D. Oh (USA)	

1943

Local Organizing Committee

YoungKon Kim (Inje Univ.)	Myung-Hyun Lee (KICET)
Su-Gwan Kim (Chosun Univ.)	Sang-Hoon Rhee (Seoul Nat. Univ.)
Dong Keun Han (KIST)	Sung-Baek Cho (KIGAM)
Yong Kuen Lee (Yeonsei Univ.)	Hae-Won Kim (Dankook Univ.)
Hui-suk Yun (KIMS)	Suk Young Yoon (Pusan Nat. Univ.)
Kyung-Sik Oh (Andong Univ.)	Byong-Taek Lee (Soonchunhyang Univ.)
Gun Il Im (Dongguk Univ.)	Chun Ho Kim (KIRAMS)
Kang-Sik Lee (Asan Hospital)	Young-Min Kong (Ulsan Univ.)





XIV . Dental Materials

Effect of osteoconductive HA on RA of mutilance type with extremely low ability of osteoconduction in cemented total joint arthroplasty with HA (IBBC) -In Histological studies- S. C. Kim, H. Oonishi Jr., H. Oonishi, R. Iwata	721
Long Term Outcomes of HAp Ceramic and Dental Implants in Atrophic Posterior Maxilla G. Salms, A. Skagers, I. Salma, J. Locs, L. Berzina-Cimdina, L. Feldmane	725
Effect of osteoconductive HA on defense against radiolucent line and osteolysis in cemented total joint arthroplasty with HA (IBBC) -In histological studies- H. Oonishi Jr., H. Oonishi, S. C. Kim, R. Iwata	729
Osteogenic potential of a porous uncalcined hydroxyapatite/poly-DL-lactide (u-HA/PDLLA) composite with bone marrow aspirate K. Tanaka, M. Takemoto, S. Fujibayashi, M. Neo, Y. Shikinami, and T. Nakamura	733
Transplantation of Human Tooth and Dentin by using newly developed machines J. Tazaki, M. Murata, T. Yuasa, T. Akazawa, K. Ito, J. Hino, A. Niida, M. Arisue, T. Shibata	737
Blood compatibility of a Newly Developed Ceramic Scaffold K. Ito, M. Murata, T. Akazawa, S. Yodogawa, T. Hanawa, J. Tazaki, M. Arisue	741
Human Dentin Autograft for Bone Regeneration - Automatic Pulverizing Machine and Biopsy M. Murata, T. Akazawa, J. Tazaki, K. Ito, J. Hino, Y. Kamiura, R. Kumazawa, M. Arisue	745
Anterior Aesthetic Implant Using CAD/CAM Manufactured Zirconia Restoration : A Case Report G. B. Choi, J. S Yang, S. J. Oh, J. S. Song	749
Canine critical bone defect regeneration using unidirectional porous Hydroxyapatite/Collagen device K. Aoki, K. Edamura, Y. Koyama, M. Kikuchi, S. Tanaka	753
Bone Reconstruction with beta-TCP/PLGC membranes Y. Koyama, M. Kikuchi, K. Edamura, S. Tanaka, O. K. Kweon, K. Takakuda	757
Novel Unidirectional Porous Hydroxyapatite used as a Bone Substitute for Canine Tibial Wedge Osteotomy A. Watanabe, M. Sakane, T. Funayama, M. Iwasashi, A. Kanamori, N. Ochiai	761
Histological Study of Newly Formed Bone with the use of a Novel Hydroxyapatite with Unidirectional Pores as Spacers in Spine Surgery T. Funayama, M. Sakane, A. Watanabe, T. Abe, M. Iwasashi, Y. Suetsugu, N. Ochiai	765
Bone generation in porous hydroxyapatite scaffolds with Leucine coating M. Yoshikawa, T. Yabuuchi, N. Tsuji, H. Hayashi, H. Ohgushi	769
Tumor growing potential of the mice implanted with 15%paclitaxel coated thermo-rods Y. K. Kim, H. W. Choo, E. M. Hwang, S. M. Choi	773

XIV . Dental Materials

Surface Oxide Film Formation on Titanium Alloys Immersed in Acidic Saline Solutions Containing Hydrogen Peroxide S. Takemoto, M. Hattori, M. Yoshinari, E. Kawada, and Y. Oda	779
Development of Mica-Based Glass-Ceramics with Fluorapatite Variation for Restorative Dental Applications K. Keawsupsak, P. Tucksanont, T. Supanaraj, J. Bai, T. Chitwatcharakomol and D. Chaysuwan	783
Bonding Strengths of Dental Zirconia Ceramics to Resin Cements with Surface Treatments H. Sato, Y. Yamasaki and S. Ban	787
Ageing of Dental Zirconia in the Oral Cavity: First Results after Six Months T. Kosmac, P. Jevnikar	791
In vitro bioactivity studies of sol-gel derived dental ceramics/bioactive glass composites in periodically renewed biomimetic solution O. M. Goudouri, E. Kontonasaki, A. Theocharidou, L. Papadopoulou, X. Chatzistavrou, P. Koidis, K. M. Paraskevopoulos	795

Development of Mica-Based Glass-Ceramics with Fluorapatite Variation for Restorative Dental Applications

Kanungnuch Keawsupsak¹, P. Tucksanont¹, T. Supanaroj¹,
 J. Bai², T. Chitwatcharakomol³ and D. Chaysuwan^{1,4}

¹Dept of Materials Engineering, Fac. of Engineering, Kasetsart Univ., Bangkok 10900, Thailand

²Scientifique, Ecole Nationale Supérieure de Chimie de Lille, 59652-Villeneuve D'ASCQ, France

³Department of Science Service, Bangkok 10400, Thailand

⁴Materials Innovation Center, Fac. of Engineering, Kasetsart Univ., Bangkok 10900, Thailand
 nonedon_27@hotmail.com

Keywords: Fluorapatite, Mica, Glass-ceramics, Machinability, Dental applications

Abstract Glass-ceramics are materials which are widely used in dentistry especially mica-based glass-ceramics because of their machinability. Fluorapatite is found also in bones and teeth so it has good biocompatibility. Thus, the aim of this research is to study the effect of fluorapatite variation on thermal and mechanical properties and microstructures of the mica-based glass-ceramics.

Five glass-ceramics in the glass system of $\text{SiO}_2\text{-Al}_2\text{O}_3\text{-MgO-MgF}_2\text{-SrCO}_3\text{-CaCO}_3\text{-CaF}_2$ and P_2O_5 were produced by variation of fluorapatite content between 3.0-5.0 mol% and called GCF3.0-5.0, respectively. The glass chemicals were melted in an alumina crucible at 1420 °C for 1 h and quenched in cold water to form frits. Glass frits were ground and sieved in order to use for subsequent experiments. The optimum nucleation temperatures and times were analysed by using differential thermal analysis (DTA). The frit was re-melted and poured into a carbon mould to obtain glass rods. The glass rods were annealed and heated for nucleation and crystallization in order to transform to glass-ceramic rods. Crystalline phases in the glass-ceramics were determined by X-ray diffraction (XRD) and microstructures of both bulk and surface nucleations were observed by a scanning electron microscope (SEM). The biaxial flexural strength of the glass-ceramics was examined by a universal testing machine (UTM). The Vickers hardness and fracture toughness were determined by the indentation method.

The resultant glass-ceramics revealed crystalline phases of calcium-mica, fluorapatite and other phases. The microstructures of surface nucleation in the glass-ceramics presented partly needle-like structures whereas bulk nucleation showed plate-like and feather-like structures. The fluorapatite content has affected on the glass transition, peak crystallization and melting temperatures. The higher the fluorapatite content, the lower all temperatures. Moreover, mechanical properties such as biaxial flexural strength and hardness increased at first and significantly decreased with higher than 3.5 mol% fluorapatite while fracture toughness was even better.

Introduction

Dental materials have been widely developed to carry out for suitability on applications such as in-lays, on-lays and crowns. New materials which are of interest to restorative dentistry now are glass-ceramics because of their mechanical properties, biochemical compatibility with the oral environment, aesthetic similar to natural human teeth and appreciated fabrication techniques [1]. One of the most popular crystalline phases of glass-ceramics for dental applications is mica-based glass-ceramics. Although they have the plate-like structure

arrangement affected on excellent machinability and high fracture toughness, but low mechanical strength [1,2]. Thus, the production of mica-based glass-ceramics for restorative dentistry needs to improve their mechanical properties such as biaxial flexural strength and fracture toughness. Natural teeth contain hydroxyapatite, fluorapatite and fluorite [3]. Because fluorapatite is one of the crystalline structures in the teeth, therefore, it is good biocompatible, moreover, has high strength. Aim of this study is to study the effect of fluorapatite variation on thermal and mechanical properties as well as microstructures of the mica-based glass-ceramics.

Materials and Methods

Compositions of the glass consisted of MgO, SiO₂, Al₂O₃, SrCO₃, CaCO₃, CaF₂, MgF₂ and P₂O₅ which were varied fluorapatite contents 3.0, 3.5, 4.0, 4.5 and 5.0 mol% and called GCF3.0, GCF3.5, GCF4.0, GCF4.5 and GCF5.0, respectively. Varied chemical compositions are shown in Table 1. All the weighed chemicals were rolling mixed for 2 h, melted in an alumina crucible at 1420 °C for 1 h and quenched in water at room temperature to form glass frits. The frits were ground and sieved in order to use for subsequent experiments. Optimum nucleation temperatures and times were analyzed by a differential thermal analysis [4]. The frits were re-melted at 1420 °C for 1 h, poured into a carbon mould to form glass rods and then they were heated at their annealing temperatures determined by using a DTA, that is, about 50 °C lower than their glass transition temperatures. To form glass-ceramics, the rods were heated for nucleation at 630-650 °C and crystallization at 880-900 °C, respectively.

Table 1 Varied chemical compositions of the glass-ceramics by weight (g)

Type of the glass-ceramics	CaF ₂	CaCO ₃	P ₂ O ₅
GCF3.0	0.52	5.97	2.82
GCF3.5	0.60	6.87	3.25
GCF4.0	0.67	7.76	3.67
GCF4.5	0.75	8.62	4.07
GCF5.0	0.82	9.46	4.47

Crystalline phases in the glass-ceramics were characterized by X-rays diffraction. Both surface and bulk microstructures of the samples were sputtered with Au and observed by a scanning electron microscope. Perfectly polished specimens were used for mechanical testing. Biaxial flexural strength of the specimens were examined by a universal testing machine followed ISO 6872:1995(E). Hardness of the glass-ceramics were measured by a Vickers hardness that was conducted under a load of 0.5 kg for 15 s. Calculated data of fracture toughness was obtained by using the full Charles and Evans equation as following:

$$K_{Ic} = 0.0732 \left(\frac{E}{H_v} \right)^{0.4} H_v a^{1/2} \left(\frac{c}{a} \right)^{-3/2}$$

Where E is Young's modulus (MPa), H_v is Vickers hardness (MPa), a is the half diagonal of the indentation (m) and c is the half distance between the opposite crack tips (m).

Results and Discussion

Temperature data, e.g., T_g , T_p and T_m of the glasses are shown in Figure 1. The higher fluorapatite content in the glass-ceramics is, the lower those temperatures are. Because incorporation of F in the glasses results in the substitution of strong Si-O-Si linkages by weak Si-F linkages, consequently, viscosity of the glasses decreases [5].

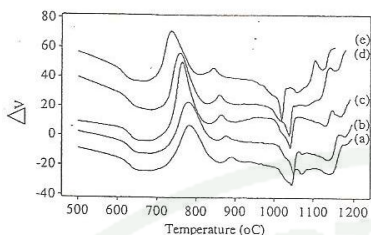


Figure 1 DTA curves of the five glasses: (a) GCF3.0, (b) GCF3.5, (c) GCF4.0, (d) GCF4.5, (e) GCF5.0.

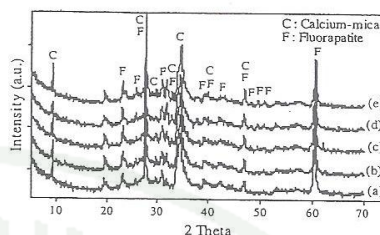


Figure 2 XRD patterns of the five glass-ceramics: (a) GCF3.0, (b) GCF3.5, (c) GCF4.0, (d) GCF4.5, (e) GCF5.0.

Suitable heat treatments lead to crystallization in glass-ceramics examined with the XRD and presented patterns in Figure 2. The major crystals possess calcium-mica ($\text{Ca}_{0.5}\text{Mg}_3\text{AlSi}_3\text{O}_{10}\text{F}_2$) and fluorapatite ($\text{Ca}_5(\text{PO}_4)_3\text{F}$). For CaCO_3 , CaF_2 and P_2O_5 , they influence to increase not only fluorapatite but also calcium-mica structures. It is observed that the intensity of peaks of the former slightly increase while those of the latter significantly do.

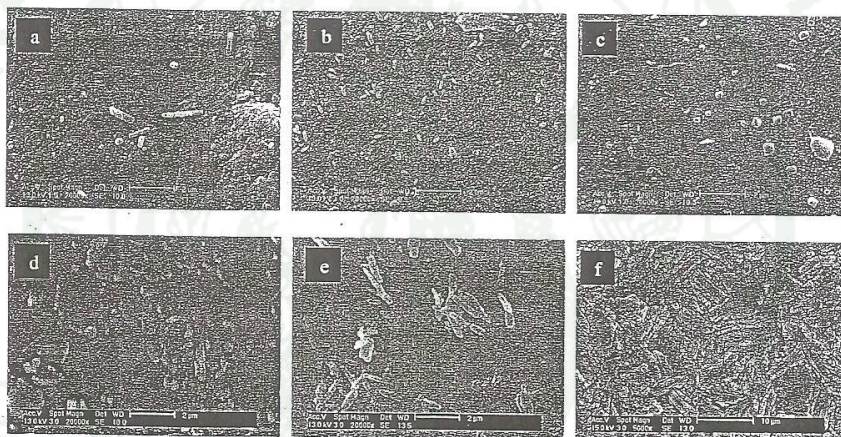


Figure 3 SEM micrographs on the surfaces of the glass ceramics: (a) GCF3.0, (b) GCF3.5, (c) GCF4.0, (d) GCF4.5, (e) GCF5.0 and (f) SEM micrographs on the bulk of GCF4.0.

In the bulk of all specimens, it is found that plate-like structures of the mica crystals formed highly interlocking as shown in Figure 3(f). There are needle-like and angular crystals, known as fluorapatite and likely calcium-mica, sparsely clustered on surface in Figure 3(a)-(e). CaF_2 and P_2O_5 play the role as nucleating agents to accelerate and induce the formation of fluorapatite phases [5,6]. Therefore, there are the amounts of needle-like fluorapatite crystals in GCF3.0 less than those of other glass-ceramics as presented intensity in Figure 2 and micrographs in Figure 3. In addition, crystalline size of bulk structure is greater than that of surface structure.

Increase of fluorapatite contents from 3.0 to 3.5 mol% influences to higher biaxial flexural strength, hardness and fracture toughness. Consequently, the flexural strength and hardness

Bioceramics 22

decreased with the higher than 3.5 mol% fluorapatite, but fracture toughness is slightly increased.

Table 2 Biaxial flexural strength, Vickers hardness and fracture toughness of the glass-ceramics.

Type of the glass-ceramics	Biaxial flexural strength (MPa) (S.D.)	Vickers hardness (GPa) (S.D.)	Fracture toughness (MPam ^{1/2}) (S.D.)
GCF3.0	136.39 (12.37)	3.09 (15.28)	0.09 (0.01)
GCF3.5	153.22 (7.36)	3.44 (27.18)	0.10 (0.02)
GCF4.0	149.34 (7.58)	3.01 (19.67)	0.12 (0.01)
GCF4.5	124.84 (13.51)	2.89 (31.00)	0.12 (0.03)
GCF5.0	116.10 (8.37)	2.70 (23.11)	0.12 (0.03)

However, both strength and hardness of the glass-ceramics are accepted but the fracture toughness is too low for dental applications following ISO/CD 6872:1999. Therefore, the mica-based glass-ceramics with fluorapatite variation need more development in fracture toughness.

Conclusions

The resultant glass-ceramics reveal plate-like calcium-mica crystals in bulk and needle-like fluorapatite crystals on surface. The more contents of CaCO₃, CaF₂ and P₂O₅ which are as the composition of fluoapatite crystals, the higher fluorapatite and mica. This reason causes decreasing in the strength and hardness and increasing in the fracture toughness. The optimum contents of fluorapatite should be not more than 4 mol% fluorapatite.

Acknowledgements

This work is supported by Department of Science Service, Ministry of Science and Technology and Kasetsart University Research and Development Institute, Kasetsart University.

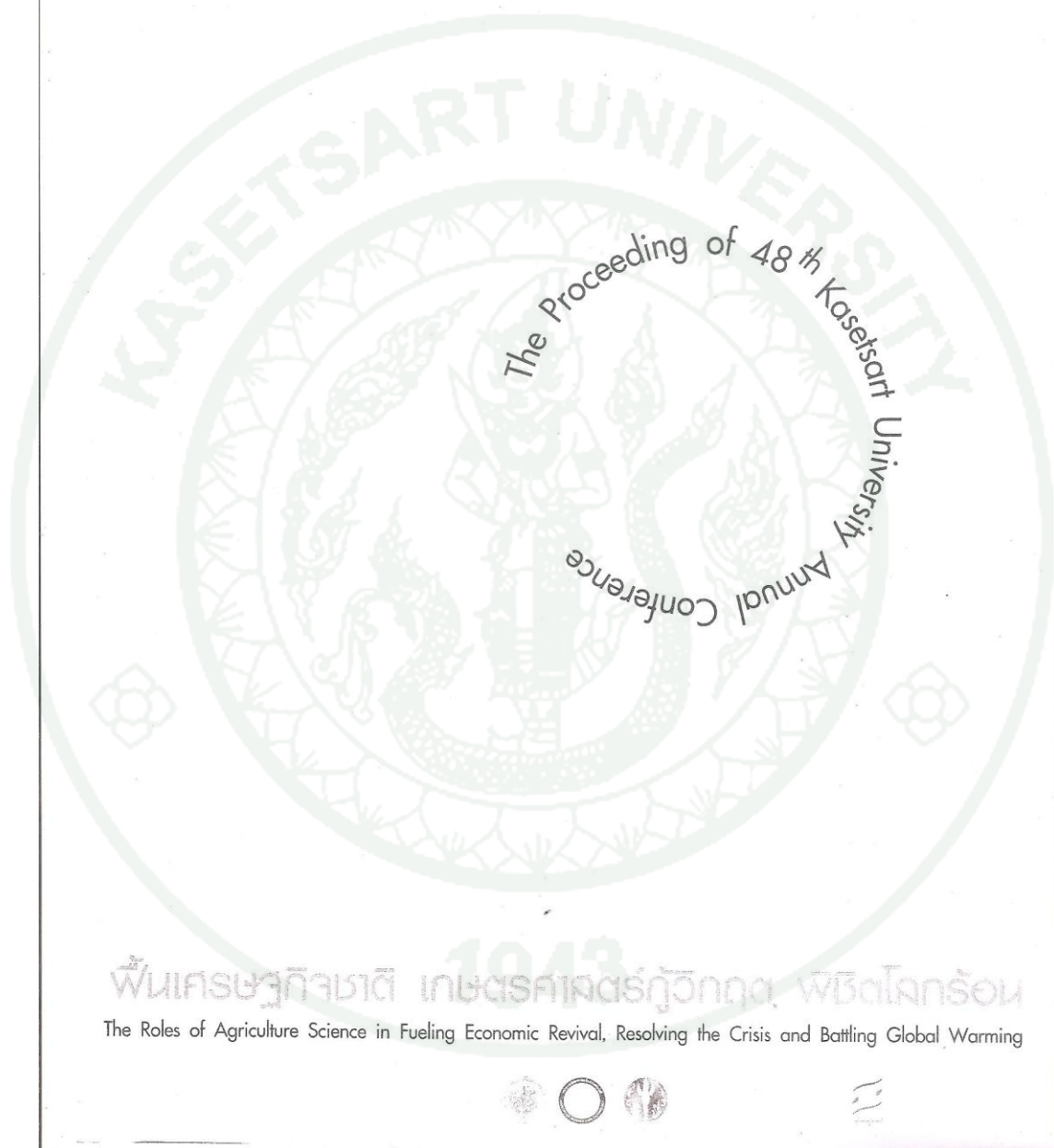
- [1] W. Höland, G. Beall. Glass-Ceramic Technology. The American Ceramic Society, United States of America. (2002) p277-279
- [2] R.G. Hill, A. Stamboulis, R.V. Law, A. Clifford, M.R. Towler, C. Crowley. J. Non-Cryst. Solids. 336 (2004) p223-229
- [3] A.P. Barth, C. Kropf, T. Poth. U.S. Pat. (2007) No. 20070154411
- [4] A. Marotta, A. Buri, F. Branda. J. Mater. Sci. 16 (1981) p341-344
- [5] P.W. McMillan. Glass-Ceramics. Academic Press Inc., London, (1979) p84-87
- [6] X. Zheng, G. Wen, L. Song, X.X. Huang. Acta Mater. 56 (2008) p549-558

1943

เรื่องได้มีการประชุมทางวิชาการ ครั้งที่ ๔๘ มหาวิทยาลัยเกษตรศาสตร์

เล่มที่ 7 สาขาสถาปัตยกรรมศาสตร์และวิศวกรรมศาสตร์

(Subject: Architecture and Engineering)



- 43 สท.วศ.72/O215 การศึกษาและการวิเคราะห์ผลกระทบของภาวะโลกร้อนต่อกิจกรรมฟ้าผ่าในประเทศไทย.....351
A Study and Analysis of Impact of Global Warming on Lightning Activity in Thailand
โดย โชคชัย เดชโยธิน และวินัย พงศ์ชะวัน
- 44 สท.วศ.73/O301 การออกแบบและศึกษาคุณสมบัติของปั๊มไดอะแฟรมสำหรับการสูบน้ำ..... 359
Design & Study Characteristics of Diaphragm Pump for Water Pumping
โดย อนุรักษ์ ครองทรัพย์
- ภาคโปสเตอร์ (Poster Presentation)**
1. สท.วศ.3/P7 Effect of Fluorapatite on Chemical Solubility of Glass-Ceramics for Dental Restoration.....373
By Kanungnuch Keawsupsak Palida Tucksanont
Theerapa Supanaraj Tepiwan Jitwatcharakomol
and Duangrudee Chaysuwan
- 2 สท.วศ.7/P16 การศึกษาองค์ประกอบของลูกถ้วยที่เปราะเปื้อนในระบบสายส่ง 69, 115 เควี.บริเวณ ถ.เพชรเกษม และ ถ.กาญจนาภิเษกของการไฟฟ้านครหลวง..... 379
A Study to Correction Factor of Contaminated Insulators in Transmission Line 69, 115 kV. At Petchkasem Road and Karnjanapisek Road for Metropolitan Electricity Authority
โดย กมล พะเทพ และวินัย พงศ์ชะวัน
- 3 สท.วศ.8/P19 ศึกษาและพัฒนากระบวนการนำกลับมาใช้ใหม่ของเมทานอลจากกลีเซอรินดิบที่ได้จากกระบวนการผลิตน้ำมันไบโอดีเซล..... 387
The Study and Development of Methanol Recovery Process from Crude Glycerol by Product of Biodiesel Production
โดย เดช เหมือนขาว และยงยุทธ ดุลยกุล

สาขาสถาปัตยกรรมศาสตร์
และวิศวกรรมศาสตร์

Subject: Architecture and Engineering

ภาคโปสเตอร์

Poster Presentation

อิทธิพลของฟลูอออะพาไทต์ที่มีต่อความสามารถในการละลายสารเคมีของกลาสเซรามิก
สำหรับการซ่อมแซมทางทันตกรรม

Effect of Fluorapatite on Chemical Solubility of Glass-Ceramics for Dental Restoration

คณิงนุช แก้วทรัพย์ศักดิ์¹ ปาลิดา ทักชนนท์¹ ซีราภา สุพรรณโรจน์¹ เทพีวรรณ จิตวัชรโกมล³ และ

ดวงฤดี ฉายสุวรรณ^{1,2}

Kanungnuch Keawsupsak¹, Palida Tucksanont¹, Theerapa Supanaraj¹, Tepiwan Jitwatcharakomol³, and

Duangrudee Chaysuwan^{1,2}

บทคัดย่อ

กลาสเซรามิกในระบบ $\text{SiO}_2\text{-Al}_2\text{O}_3\text{-MgO-MgF}_2\text{-SrCO}_3\text{-CaCO}_3\text{-CaF}_2\text{-P}_2\text{O}_5$ ที่มีสารเปลี่ยนแปลงปริมาณฟลูอออะพาไทต์ 3.0-5.0 mol% เฟสผลึกหลักของกลาสเซรามิกนี้ คือ แคลเซียมไมก้าและฟลูอออะพาไทต์ โดยผลึกแคลเซียมไมก้าและฟลูอออะพาไทต์กระจายตัวบนพื้นผิว ในขณะที่ผลึกแคลเซียมไมก้า เท่านั้นปกคลุมอยู่ในเนื้อในของกลาสเซรามิก ผลการศึกษาข้างต้นตรวจโดย X-Rays Diffraction (XRD) และ Scanning Electron Microscope (SEM) การทดสอบความสามารถการละลายสารเคมีสำหรับเซรามิกทางทันตกรรมอ้างอิงตามมาตรฐาน International Standard ISO 6872:1995 จากการศึกษาพบว่าการเพิ่มของปริมาณฟลูอออะพาไทต์เป็นผลทำให้ทั้งผลึกแคลเซียมไมก้าและฟลูอออะพาไทต์เพิ่มขึ้น ความสามารถในการทนต่อสารเคมีของกลาสเซรามิกเพิ่มขึ้น นอกจากนั้นค่าความสามารถในการละลายสารเคมีของกลาสเซรามิกน้อยกว่า $2000 \mu\text{g}\cdot\text{cm}^{-2}$ จึงเหมาะสำหรับใช้เป็นวัสดุแกนชนิดเซรามิกสำหรับการซ่อมแซมทางทันตกรรมที่เรียกว่า Core Ceramics

ABSTRACT

Glass-ceramics of the $\text{SiO}_2\text{-Al}_2\text{O}_3\text{-MgO-MgF}_2\text{-SrCO}_3\text{-CaCO}_3\text{-CaF}_2\text{-P}_2\text{O}_5$ system were varied between 3.0 and 5.0 mol% fluorapatite. The main crystalline phases of glass-ceramics are calcium-mica and fluorapatite. Calcium-mica and fluorapatite crystals were shown dispersed on surfaces whereas calcium-mica crystals only revealed in bulks. These results were investigated by X-Rays Diffraction (XRD) and Scanning Electron Microscope (SEM). Chemical solubility testing for dental ceramics was carried out according to International Standard ISO 6872:1995. It was found that the more fluorapatite compositions, the higher both calcium-mica and fluorapatite crystals. Those increased crystalline structures led to the induction of chemical durability. In addition, the chemical solubility values which were less than $2000 \mu\text{g}\cdot\text{cm}^{-2}$ would be suitable as core ceramics for dental restorations.

Key Words: glass-ceramics, fluorapatite, chemical solubility, dental restoration

nonedon_27@hotmail.com

¹ภาควิชาวิศวกรรมวัสดุ คณะวิศวกรรมศาสตร์ มหาวิทยาลัยเกษตรศาสตร์

Department of Materials Engineering, Faculty of Engineering, Kasetsart University.

²ศูนย์นวัตกรรมวัสดุ คณะวิศวกรรมศาสตร์ มหาวิทยาลัยเกษตรศาสตร์

Materials Innovation Center, Faculty of Engineering, Kasetsart University.

³กรมวิทยาศาสตร์บริการ กระทรวงวิทยาศาสตร์และเทคโนโลยี

Department of Science Service, Ministry of Science and Technology

Introduction

Glass-ceramics are becoming the materials which are very interesting for dental restorations such as inlay, onlays, crowns and bridges. They possess the strength, aestheticism similar to human teeth, biocompatibility due to direct contact with oral environment and ease to adjust dimension (Höland and Beall, 2006). Especially, mica-based glass-ceramics are machinable which is conspicuous character.

The application of computer aided design and computer aided machining (CAD/CAM) technology is used to improve the dimension of the glass-ceramics to a patient's need and to reduce the time consuming. However, there are disadvantages of glass-ceramics which are low mechanical properties (Hill *et al.*, 2004). Due to strength and biocompatibility of needle-like fluorapatite, one of the phases of bones and teeth (Barth, 2007), it improves mica-based glass-ceramics to increase mechanical properties (Liu, 2008). Although, glass-ceramics, in general, possess good chemical stability (McMillan, 1979), it is still necessary for glass-ceramics to be tested the chemical resistance. Therefore, this research concentrates on the effect of fluorapatite on chemical solubility of mica-based glass-ceramics for restorative dental applications.

Materials and Methods

Five series of glass contained SiO_2 ($\geq 99.865\%$, Fluka), Al_2O_3 ($\geq 99.695\%$, Fluka), MgF_2 (Granules about 1.25 mm, Merck), MgCO_3 ($\geq 98\%$, Merck), SrCO_3 ($\geq 98.4\%$ Aldrich), CaF_2 ($\geq 97\%$, BDH), CaCO_3 (99.0%, BDH) and P_2O_5 ($>97\%$, Fluka) were varied 3.0-5.0 mol% fluorapatite which resulted from combination of CaF_2 , CaCO_3 and P_2O_5 . They were called GCF3.0, GCF3.5, GCF4.0, GCF4.5 and GCF5.0, respectively. The codes and varied chemicals were shown in Table 1. All chemicals were weighed, rolled to homogenize powders and transferred into a concealed alumina crucible in order to avoid volatile components such as fluorine (McMillan, 1979) in forms of silicon tetrafluoride (SiF_4). Then, they were melted in an electric furnace with a heating rate of $10^\circ\text{C}/\text{min}$ and soaking temperature at 1420°C for 1h. At complete melting, the liquid were quenched in water to receive glass frits. The frits were dried, ground and sieved in order to use for subsequent experiments.

The determination of optimum nucleation temperature and time was developed by Marotta's method (Marotta *et al.*, 1981) with Differential Thermal Analysis (DTA, Perkin Elmer Series DTA7). The frits were remelted as the previous condition, poured into a carbon mould and annealed for 2 h in

order to release internal stress before cooling in the furnace to room temperature. For transformation from a glass into a glass-ceramic, the glass rod was heat-treated to nucleation and crystallization temperatures.

Table 1 Varied chemical compositions of each glass-ceramic by weight (g).

Codes	CaF ₂	CaCO ₃	P ₂ O ₅
GCF3.0	0.52	5.97	2.82
GCF3.5	0.60	6.87	3.25
GCF4.0	0.67	7.76	3.67
GCF4.5	0.75	8.62	4.07
GCF5.0	0.82	9.46	4.47

Crystalline phases of glass-ceramics were examined by X-Rays Diffraction (XRD, Phillips series X'Pert) and observed by Scanning Electron Microscope (SEM, Phillips Series XL30). For SEM, the sample were etched by 10 % (V/V) hydrofluoric acid solution for 25 s. International Standard ISO 6872, dental ceramics, was referred for chemical solubility testing (ISO 6872, 1995). Reagent for this testing was 4% (V/V) acetic acid solution.

Results and Discussion

XRD patterns of the prepared glass-ceramics investigated both surface and bulk are given in Figure 1. The main crystalline phases identified are calcium-mica (Ca_{0.5}Mg₃AlSi₃O₁₀F₂, 25-0155) and fluorapatite (Ca₅(PO₄)₃F, 15-0876). Moreover, Magnesium oxide (MgO, 02-1207), forsterite (Mg₂SiO₄, 71-1083), silicon oxide (SiO₂, 82-1556), strontium oxide (SrO, 48-1477) were the minor crystalline structures of those. Increasing of fluorapatite compositions, CaF₂, CaCO₃ and P₂O₅, affects the stronger intensity of the identified peaks because CaF₂ and P₂O₅ play the role nucleating agents of fluorapatite crystals and CaCO₃ and CaF₂ were component formed calcium-mica crystals. The furthermore they resulted in increase of significantly unknown peaks. Therefore, the crystallinity of these glass-ceramics increases (McMillan, 1979).

The microstructures of plate-like calcium-mica crystals formed interlocking in bulk are shown in Figure 2(a) which is the representative of all samples while angular crystals of calcium-mica and needle-like crystals of fluorapatite are embedding and dispersing on the surface in Figure 2(b)-(f). The increasing chemical compositions of fluorapatite forming affect the tendency to form clusters of crystal of fluorapatite.

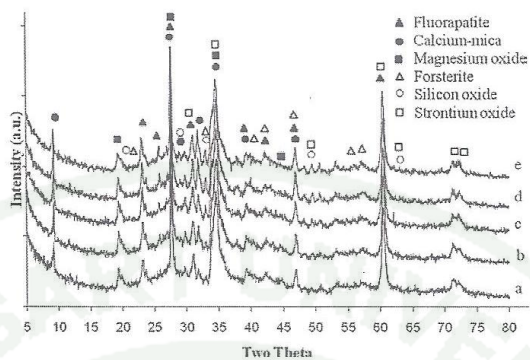


Figure 1 XRD patterns of glass-ceramics GCF (a) 3.0, (b) 3.5, (c) 4.0, (d) 4.5, (e) 5.0.

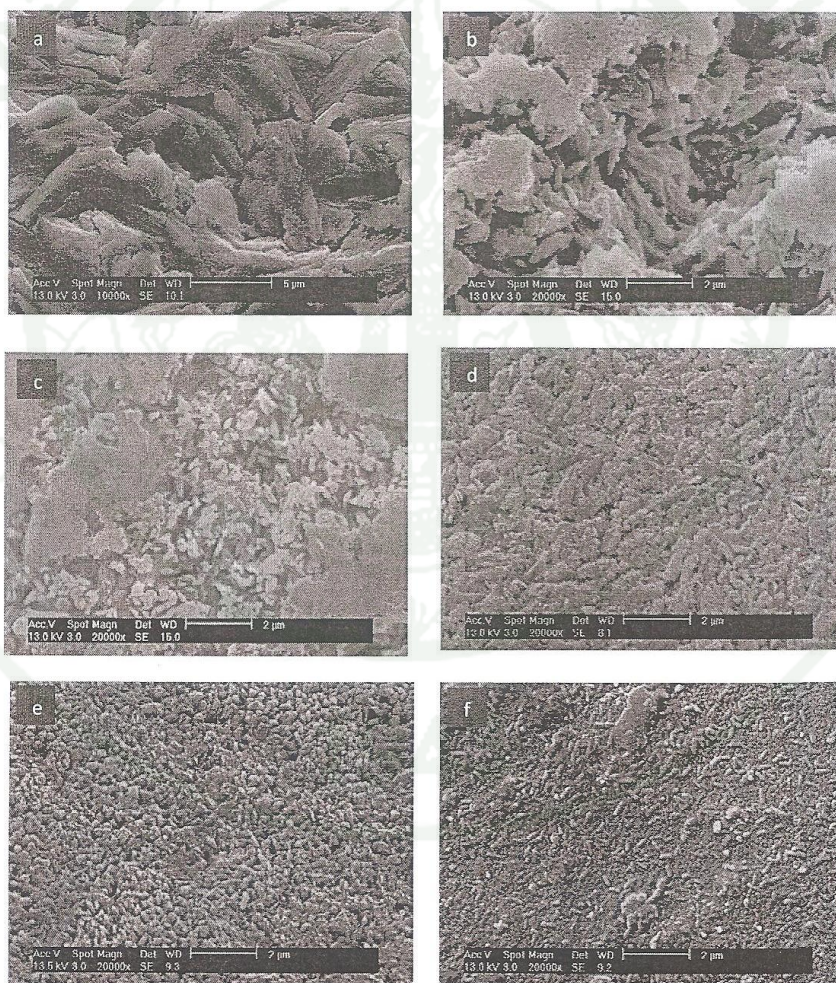


Figure 2 SEM micrographs in bulk of GCF (a) 3.5 and on surface of GCF (b) 3.0, (c) 3.5, (d) 4.0, (e) 4.5, (f) 5.0.

In Table 2, it is found that the chemical solubility of the glass-ceramics depend upon the fluorapatite contents. The alkaline earth oxides such as MgO and CaO increase chemical stability in glass-ceramics due to the increased volume of crystalline phase (McMillan, 1979). In this study, CaO resulted from thermal decompose of CaCO_3 is one of the components of varied fluorapatite content in glass-ceramics; therefore, the more the added content increase, the higher chemical durability get. This results were related to the research of Taruta (Taruta *et al.*, 2001) discovered in 2001. Normally, the chemical solubility of the core ceramic materials must be less than $2000 \mu\text{g}\cdot\text{cm}^{-2}$ and that of the body ceramic materials contacting directly with the oral environment should be less than $100 \mu\text{g}\cdot\text{cm}^{-2}$ (ISO 6872, 2008) as in Table 3. Therefore, all glass-ceramics in this research are acceptable by ISO 6872 to be used as core ceramics. Considering chemical solubility, the most of adequate glass-ceramic for dental restorative material was GCF5.0. However, they need to test mechanical properties such as strength, hardness and toughness in order to compare with the standard.

Table 2 Chemical solubility of glass-ceramics ($\mu\text{g}\cdot\text{cm}^{-2}$)

Codes	Chemical Solubility ($\mu\text{g}\cdot\text{cm}^{-2}$, (S.D.))
GCF3.0	1776 (179)
GCF3.5	973 (285)
GCF4.0	862 (152)
GCF4.5	591 (267)
GCF5.0	450 (74)

Table 3 Chemical properties of dental ceramic (ISO 6872:2008)

Materials	Chemical Solubility ($\mu\text{g}\cdot\text{cm}^{-2}$)(Maximum)
Core ceramic	2000
Dentine/body ceramic	100

Conclusions

Fluorapatite crystals in glass-ceramics affect to the chemical solubility, the more fluorapatite content, the higher chemical solubility. The resulting glass-ceramics are all acceptable to be used as core ceramics for dental restorations.

Acknowledgement

This work was supported by funding grants of Department of Science Service, Ministry of Science and Technology and Kasetsart University Research and Development Institute, Kasetsart University, Thailand.

References

- Barth, A.P., Kropf, C., and T. Poth. 2007. Oral and Dental Care Product. U.S. Patent 20070154411 A1.
- Hill, R.G., Stamboulis, A., Law, R.V., Clifford, A., Towler, M.R., and C. Crowley. 2004. The influence of Strontium Substitution in Fluorapatite Glasses and Glass-ceramics. *J. Non-Cryst. Solids*. 336: 223-229.
- Höland, W. and G. Beall. 2006. *Glass-Ceramic Technology*. American Ceramic Society, United Stated of America.
- International Organization for Standardization. ISO 6872. 2008. Dental ceramics. Switzerland.
- Liu, Y., Xiang, Q., Sheng, X. and X. Dan. 2008. Nucleation and Growth of Needle-Like Fluorapatite Crystals in Bioactive Glass-Ceramics. *J. Non-Cry. Sol*. 354: 938-944.
- Marotta, A., Buri, A., and F. Branda. 1981. Nucleation in Glass and Differential Thermal Analysis. *J. Mater. Sci*. 16: 341-344.
- McMillan, P.W. 1979. *Glass-Ceramics*. Academic Press Inc., London.
- Taruta, S., Mukoyama, K., Suzuki, S.S., Kitajima, K., and N. Takusagawa. 2001. Crystallization Process and Some Properties of Calcium Mica-Apatite Glass-Ceramics. *J. Non-Cryst. Solids*. 296: 201-211.

CIRRICULUM VITAE

NAME : Ms.Kanungnuch Keawsupsak

BIRTH DATE : May 25, 1984

BIRTH PLACE : Bangkok, Thailand

EDUCATION	: <u>YEAR</u>	<u>INSTITUTE</u>	<u>DEGREE/DIPLOMA</u>
	2007	King Mongkut's University of Technology Thonburi	B. Sc.(Chemistry)

SCHOLARSHIP/AWARDS : The King Prajadhipok and Queen Rambhai
Barni memorial Foundation of years 2009